Appendix

数値的合成手法を用いた断層変位評価に関する研究

Report for NRA Project: "Study on fault displacement evaluation using numerical simulation methods."

Summary

This project is subdivided in two tasks:

1) Dynamic rupture simulations for a characterized asperity source model of 1999 Chi-chi earthquake: In this sub-task we have developed a suite of dynamic rupture models for a characterized kinematic asperity source model of the 1999 Chi-chi Taiwan earthquake developed by the KKE group. The geometrical dimension and dip angle of the fault are the same as the asperity model developed in the fiscal year 2013. The dip angle is 30 degree and the locations and dimensions of the asperities are the same as proposed by the KKE group. The kinematic fault model proposed by the KKE group is composed of five asperities named and distributed from north to south as SMGA1a, SMGA1b, SMGA2, SMGA3 and SMGA4, with a respective average slip 20m, 7m, 3m, 3m and 2m. The goal of this task is to develop a dynamic rupture model, so that the average slip at each asperity be consistent with the ones from kinematic model. We used the trial and error approach to estimate the stress drop at each asperity. The background stress drop in the seismogenic zone is assumed to be zero, and a weak shallow layer (SL) zone of the first 2km depth is assumed to operate during rupture with enhanced energy absorption mechanism, as such it is parameterized with negative stress drop. We have developed a total of 9 asperity models. Our final dynamic model results in an earthquake of Mw 7.52 and predicts average slip for each asperity, respectively from north to south, of 16.8m, 7.0m, 4.4m, 3.3m and 2m, corresponding to stress drops of 17.0MPa, 3.0MPa, 2.5MPa, 2.5MPa and 2.5MPa. Comparison of fault displacement with observed data shows relative consistency along the fault, but with larger values than observed ones at the very north of the fault. Low frequency ground motion compared with observed is also good in some stations, but final displacement at the northern zone is over-predicted in the near source. The model can still be improved by reducing the stress drop of the last asperity located at the north (SMGA1a)

2) Preliminary study of dynamic rupture simulations for strike-slip model with uniform stress drop.

In this sub-task we have developed sets of dynamic rupture models for vertical strike slip faults with uniform stress drop, as a preliminary work for the next fiscal year project, in which strike slip fault will be evaluated. The goal of this study is to estimate a scaling relation of stress drop consistent with the seismic moment-rupture area empirical scaling model proposed by Murotani et al (2015), and to evaluate the fault displacement. The set of dynamic models consists of fault models with width 20km and fault length L=20km, 40km, 60km, 80km, 100km, 120km, 200km, 300km and 400km and uniform stress drop values of 2.0MPa, 2.5MPa, 3.0MPa, 3.5MPa, 5.0MPa and 7.5MPa. In order to evaluate the effect of the weak shallow layer (SL) zone, we have also considered two additional set of models assuming that the SL zone has 2km width of stress drop 0.0MPa and -2.0 MPa. Our results show that the stress drop at the seismogenic zone is approximately constant for the source scaling relation of Murotani et al (2015). In this study, the amplitude of the constant stress drop range from 3.0 to 3.7 MPa (static stress drop from 3.4 to 4.1 MPa) depending on the characterization of the weak SL zone. If stress drop at SL zone is the same as the seismogenic zone, the dynamic stress drop is around 3.0MPa (static stress drop around 3.4MPa). For weak SL with zero stress drop, the dynamic stress drop is around 3.5MPa (static stress drop around 3.9MPa). For weak SL with stress drop -2.0MPa, the dynamic stress drop is around 3.7MPa (static stress drop around 4.1MPa). These results show that the value of the constant stress drop in the source scaling model of Murotani et al (2015) depends on the definition of the SL. The SL also plays an important role on the prediction of final slip and fault displacement.

Introduction

Since the fiscal year 2013, we have started to work on dynamic rupture models based on characterized kinematic source asperity models. We have initiated with dip-slip faults and planning to continue the next fiscal year of 2016 with strike-slip faults. For the dip-slip fault, the 1999 Chi-chi, Taiwan, earthquake has been used as case study. For the strike-slip fault, the 2010 Darfield, New Zealand, earthquake is planned for 2016 fiscal year. Therefore, this report has two parts. The first part corresponds to the simulations of the 1999 Chi-chi earthquake, and the second part are simulations of strike-slip faults with uniform stress drop as a preliminary work for the next fiscal year project.

First part: The dynamic rupture simulation of the 1999 Chi-chi earthquake based on asperity characterization has been initiated during the fiscal year of 2013 and reported by Dalguer, (2014). The parameterization of the asperity models proposed in Dalguer (2014) has its basis on the proposed source model of Kamae and Irikura (1998) and the empirical kinematic source characterization proposed by Somerville et al (1999). The stress drop ration between asperity and background has been guided by the proposed model of Dalguer et al (2004, 2008) and initial parameterization was constrained by the kinematic source inversion results of Iwata et al (2000) and stress drop distribution of Zhang et al (2003). For the present fiscal year 2015, reported in this document, the dynamic rupture model is fully based on the characterized kinematic asperity source model developed by the KKE group (see table 1 and Figure 1). Final results of near-source ground motion compared to observed data (see Appendix A), indicate that the dynamic rupture model for this fiscal year produces similar ground motion pattern at the ones from the 2013 fiscal year model. In general, the dynamic rupture model from the 2013 fiscal year predict more consistent ground motion at the northern area than the present model of 2015 fiscal year. On the other hand, fault displacement is better for the 2015 model, except also at the end of the fault (north part) in which amplitudes are over-predicted. The prediction of fault displacement at the northern part can be improved with better characterization of the weak shallow zone that controls the surface rupture as well as reducing the stress drop amplitude from the last northern asperity.
In appendix B is shown the final slip and stress drop distribution from all asperity models.

Second part: As preliminary study for strike slip fault that will be tackled next fiscal year of 2016, we have started to develop strike slip fault dynamic rupture models that break the free-surface with uniform stress drop. The goal of this preliminary study is to estimate stress drop values for the seismic moment-rupture area empirical scaling model proposed by Murotani et al (2015). These authors examined 11 large crustal earthquakes occurred on inland crustal mega-fault systems that include earthquakes with magnitudes larger than Mw7.4. The main conclusion of Murotani et al (2015) is that scaling relations between rupture area (S) and seismic moment (Mo) have three stages. For the first stage, S is proportional to $Mo^{2/3}$ for earthquakes smaller than $Mo = 7.5x10^{18}$ Nm. For the second stage, S is proportional to a ranges from $Mo^{1/2}$ to $Mo^{2/3}$, depending on the thickness of the seismogenic zone. For the third stage, S is proportional to Mo because of the saturation of the slip on the fault. From the compiled data of 11 earthquakes, they derived the third scaling relation: S (km^2) = 1.0 x 10^{-17}Mo (Nm), for Mo larger than1.8 x 10^{20} (Nm). In the present study we focus on this third stage to estimate stress drop based on dynamic rupture models. Our main finding indicate that stress drop is constant for this third stage. The value of the dynamic stress drop range from 3.0 to 3.7 MPa (static stress drop from 3.4 to 4.1 MPa) depending on the characterization of the weak shallow layer zone. This study indicates that the definition of the shallow zone in the numerical simulations play an important role for the prediction of the slip.
In appendix C and D is shown the shown the final slip and fault displacement distribution from all the set of models

First Part: Dynamic rupture simulations for a characterized asperity source model of 1999 Chi-chi earthquake.

The dynamic rupture model developed in this task is constrained by the kinematic asperity model developed by the KKE group. Table 1 shows the general characteristics of the KKE asperity model, and figure 1 shows the geometric location of the asperities on the fault. In the dynamic rupture model, the dip angle of the fault has been assumed to be 30^0 over all the fault due to the limitations of the numerical model. So the dip angles of asperities SMGA2 and SMGA3 are not the same as the KKE model. The initial rake angle, controlled by the initial stress, is assumed to be 90^0 for all the fault. The shallow layer (SL) of the first 2km depth is assumed to operate during rupture with enhanced energy absorption mechanism, as such it is parameterized with negative stress drop (e.g., Dalguer et al, 2008, Pitarka, et al, 2009) as also done in the 2013 fiscal year (Dalguer, 2014). Fault area (79km length, 39km width) and velocity structure are the same used in 2013 fiscal year (Dalguer, 2014). The Numerical technique used for dynamic rupture simulation is the Support Operator Rupture Dynamics code developed by Ely et al., (2008, 2009), as described in Dalguer (2014).

Table 1: Parameters for kinematic characterized source model by KKE group

Parameter	Unit	SMGA1a	SMGA1b	SMGA2	SMGA3	SMGA4	Total
Strike	deg.	N3°E	N3°E	N3°E	N3°E	N3°E	
Dip	deg.	30	30	30	30	30	
Length	km	15	12	12	12	10	
Width	km	10	21	12	10	20	
Area	km^2	150	252	144	120	200	866
Average Slip	m	20	7	3	3	2	
Seismic moment	Nm	5.33E+19	3.96E+19	9.09E+18	7.06E+18	8.86E+18	1.18E+20
Moment magnitude	—	7.08	7.00	6.57	6.50	6.56	7.31
Rupture velocity	km/s	2.5	2.5	2.5	2.5	2.5	
Rise time	s	7.0	7.0	3.0	3.0	3.0	
Rake	deg.	75	75	90	90	75	
Upper depth	km	2.0	2.0	2.0	2.0	2.0	
Rupture delay time	s	15.8	10.8	2.8	0.0	8.4	
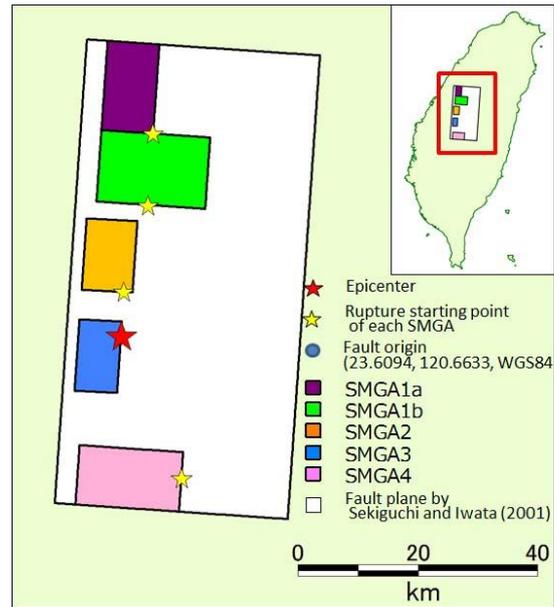
Figure 1. Asperity source model for the 1999 Chi-chi, Taiwan, earthquake proposed by the KKE group.

We use the simple slip weakening friction model in the form given by Andrews (1976) for the dynamic rupture simulation. The fault rupture of the first 2 km of the shallow zone is assumed that operates in a distinctive manner from the rest of the fault. This is due to the formation of incompetent fault gouge, cracking (e.g. Marone, 1998; Marone and Scholz, 1988), presence of thick surface deposits of sediments, fissured rocks and other forms of brittle rock damage. This damage zone can be accumulated during the lifetime of a fault, either as the result of dynamic stress change induced by rupture during an earthquake (e.g., Dalguer et al., 2003a,b) or from quasi-static deformation during the life of a shear fault (e.g., Vermilye and Scholz, 1998). The main feature of this shallow depth zone is that it operates during rupture with an enhanced energy absorption mechanism. To mimic this mechanism, we parameterized this zone with negative stress drop. And to account for the fault strength depth dependent in this shallow zone, strength excess reduces as approach to the free-surface.

Following the trial and error procedure for the parameterization of the asperity model, we have developed a total of 9 asperity models. The target of the trial and error procedure is to approximately fit the slip of kinematic asperity model from KKE group (Table 1 and Figure 1) in term of average slip at each asperity. Figure 2 shows the stress drop, strength excess and critical slip distance (Dc) distribution of the preferred model (Masp8) that fits approximately the kinematic model. Dc is assumed to be larger at the northern asperities than those at the southern. The largest Dc is at the shallow weak zone with 2km depth. Strength excess at the shallow zone decrease when approaching the free-surface, stress drop is negative in this zone with the largest values at the northern. This asperity model predicts an earthquake of Mw 7.52 with average slip for each asperity, respectively from north to south, of 16.8m, 7.0m, 4.4m, 3.3m and 2m, corresponding to stress drops of 17.0MPa, 3.0MPa, 2.5MPa, 2.5MPa and 2.5MPa. The back ground stress drop in the rest of the fault is assumed to be zero, except between the zone of asperities SMGA3 and SMGA4, in which stress drop is 0.15MPa. Large strength excess was necessary at the right side of the asperity SMGA4. This particular stress parameterization between asperities SMGA3 and SMGA4 ensures rupture between them and produce rupture initiation propagation from bottom to top at the SMGA4 asperity. Simulation results are now presented in a similar way as the 2013 fiscal year report (Dalguer, 2014)
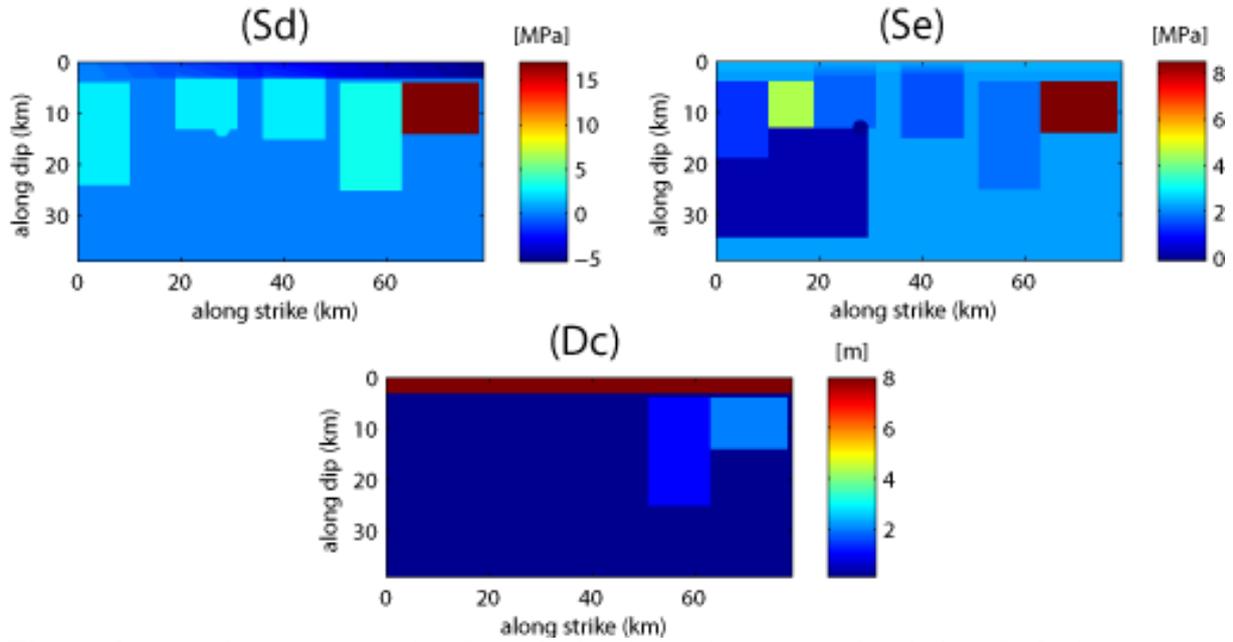
Figure 2. Asperity source model (Masp8) for dynamic rupture simulation. Left shows stress drop distribution, right strength excess and bottom critical slip distance (Dc)

Source rupture solution

Figure 3 shows the dynamic rupture solution represented by the final slip, peak slip velocity, rupture speed and rupture time distribution along the fault. Sip distribution shows large slip at the northern asperity. Rupture breaks the free-surface with the largest slip at the northern side. Peak slip velocity (obtained directly from the simulation without filtering) is also dominated by the asperities, suggesting that most of the seismic radiation energy come from the asperities. Notice that at the shallow zone large slip velocities is observed, specially at the northern site. A close looks of the slip velocity function at different points on the fault is shown in Figure 4. These slip velocity waveforms are low pass filtered with a frequency cut of 3.0Hz (the maximum frequency resolvable in our simulation is (2.0Hz). Even though the shallow zone is dominated by negative stress drop, seismic radiation is maybe considerable from this zone due to the large slip velocity (as also reported in Dalguer, 2014), particularly at eth northern zone. The rupture speed distribution is very complex with acceleration and decelerations due to the stress heterogeneity introduced at the asperities, back ground and shallow zone. The rupture reaches the northern part after about 26 seconds.
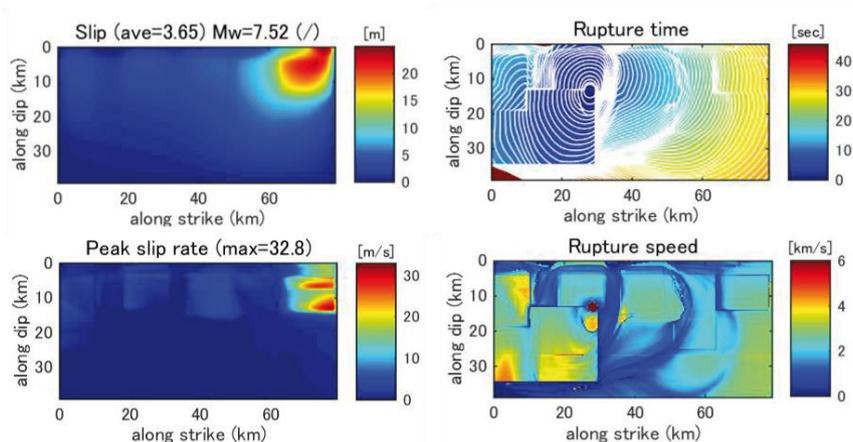
Figure 3. Dynamic rupture solution of Masp8 model represented by the final slip distribution (top left), peak slip velocity (bottom left), rupture time (top right) and rupture speed (bottom right). Contour lines on the rupture time images are also the rupture time each 0.5 seconds.
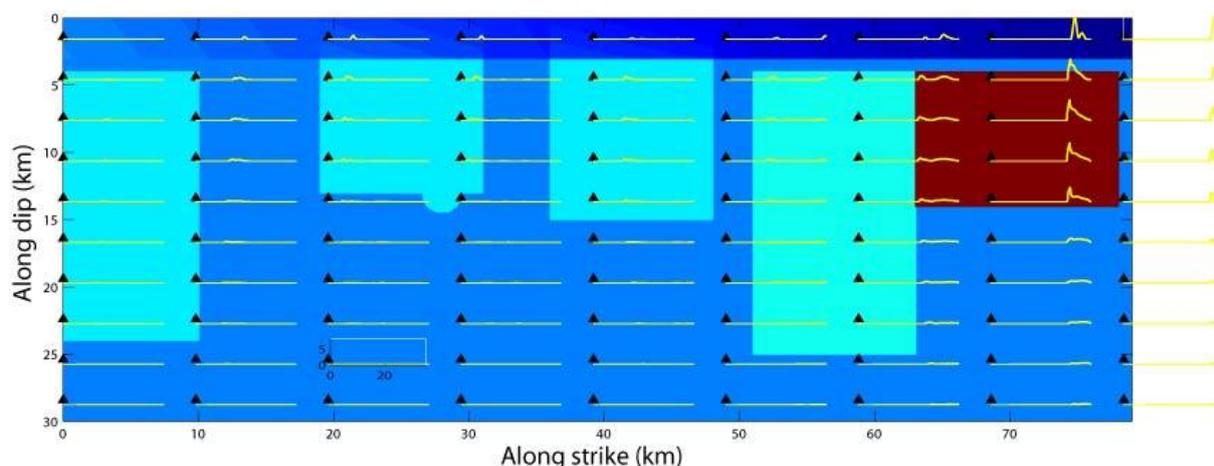
Figure 4. Slip velocity functions resulted from the dynamic rupture simulation of Masp8 model at selected points on the fault. These slip velocity waveforms are low pass filtered with a frequency cut of 3.0Hz.

Ground motion velocity and displacement
Ground motion is calculated at the free-surface in an area of 150m x 120 km. Figure 5 shows the peak ground velocity (PGV) and peak ground displacement (PGD) of the fault parallel, fault normal and vertical component. The PGV shown in the figure is from the raw data directly obtained from the calculation, i.e, no filter has been applied. For further application, this data need to pass a low pass filter with a frequency cut of 3.0Hz. Overall, as also reported in the fiscal year 2013 (Dalguer, 2014), the ground motion distribution shows that PGV and PGD are larger in the northern site and there are large differences between the near source ground motions on the hanging wall and on the footwall. It is also notice (as in Dalguer, 2014) that the fault parallel component of PGV and PGD are considerable large at the northern site, it is because during rupture propagation a long strike, the horizontal ground motion exhibit rotation. This phenomenon becomes significance at large propagation distance (e.g. Oglesby et al, 2000).
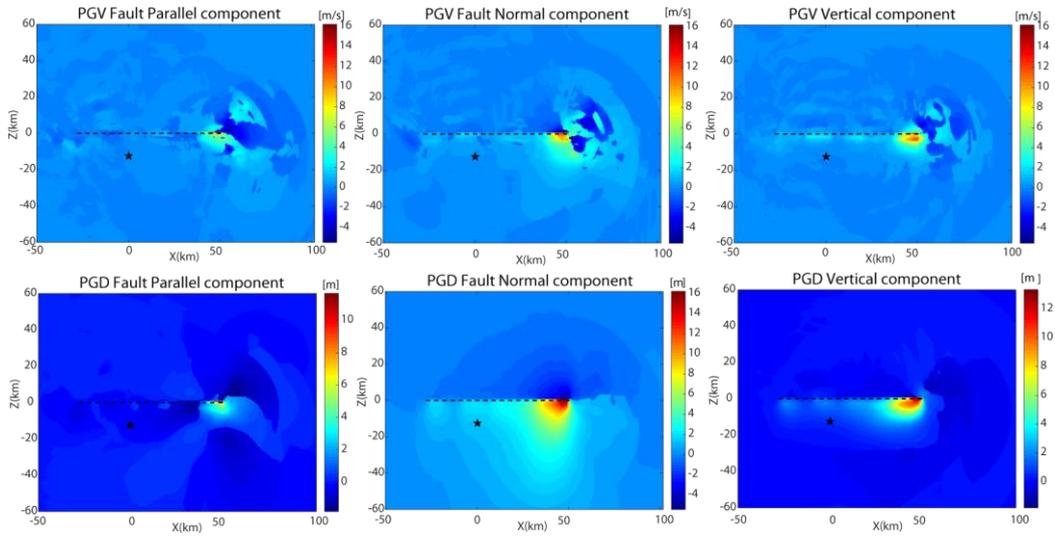
Figure 5. Peak ground velocity (PGV) at the top and peak ground displacement (PGD) at the bottom calculated from the dynamic rupture simulation (Masp8). Left shows fault parallel component, middle fault normal component and right vertical component. Dashed black line is the trace of the fault intersecting the free-surface. Black star is the epicenter. Right side is the northern. The PGV shown in this figure is from the raw data directly obtained from the calculation, i.e, no filter has been applied.

Fault displacement and ground motion compared with observed data.

Left side of Figure 6 shows the fault displacement of our preferred model (Masp8) compared with the observed one. As a reference the results of the fiscal year 2013 is also plotted. Overall the shape of the fault displacement along the fault is consistent with the observed data, nevertheless the amplitude at the end of the northern side is over-predicted. At the end of the southern side observed data suggest zero fault displacement, while the model predicts some offset. These results can be improved by tuning the weak shallow zone. For this purpose we developed a new asperity model (Masp9) tuning the negative stress drop in the shallow zone. Right side of Figure 6 shows the comparison of the results from Masp9. We succeeded to improve the fault displacement at the southern site. Further tuning can be done for the norther site, but this will be for future work.
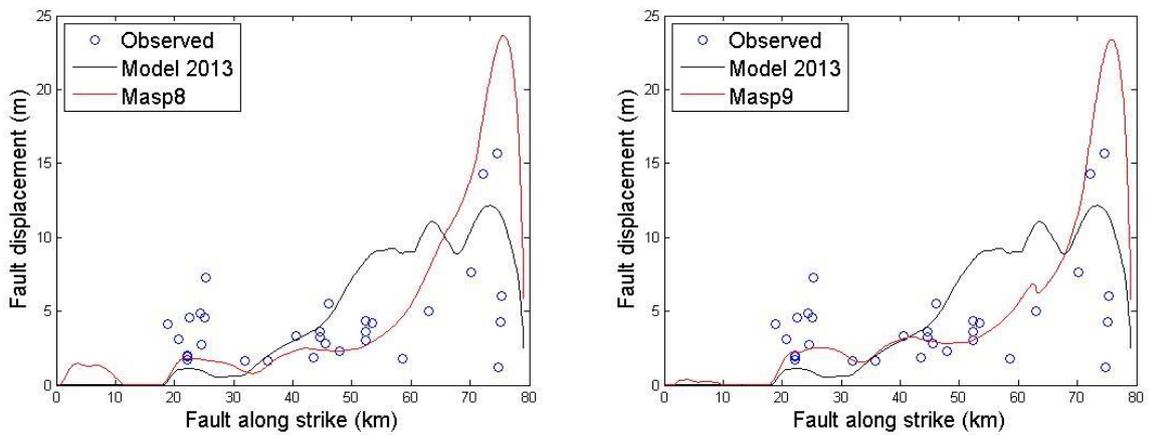
Figure 6. Fault displacement compared with observed data, [left] Masp8 model: [right] Masp9 Model. In both cases the results of the 2013 fiscal year is included as reference

A-7

The 3 components of velocity and displacement compared with observed data at several stations are shown in Appendix A. Results of the 2013 fiscal year are also included in the comparison. Seismograms passed a low pass filter with frequency cut off of 0.5Hz. In all the figures, left column are velocity and right column displacement of three components (EW, NS and UD). Observed velocity and displacement has been obtained respectively by integration and double integration from recorded acceleration. The recorded accelerations were corrected by KKE group using quadratic fit to velocity following Boore et al.(2002). In general synthetics ground motion follow the general pattern of observation. The results are similar to those from the 2013 fiscal year. Nevertheless, the results from the 2013 fiscal year better predicts displacement ground motion than the one from this year at the northern side.

Second part: Preliminary study of dynamic rupture simulations for strike-slip model with uniform stress drop.

We have developed sets of dynamic rupture models that beak the free-surface with fault width 20km and fault length L=20km, 40km, 60km, 80km, 100km, 120km, 200km, 300km, 400km. These models have uniform stress drop values at the seismogenic zone (assumed 18km) of 2.0MPa, 2.5MPa, 3.0MPa, 3.5MPa, 5.0MPa and 7.5MPa. In order to evaluate the effect of the weak shallow layer (SL) zone assumed to have 2km width, three cases have been considered: 1) stress drop is the same as the seismogeneic zone (so it can be considered as no weak SL zone models); 2) the SL zone has tress drop 0.0MPa; and 3) the SL zone has tress drop -2.0 MPa. The goal of this study is to estimate stress drop values for the empirical source scaling model proposed by Murotani et al (2015). Therefore, the output value of interest from the dynamic rupture simulations is the final slip. So the transient feature of the rupture propagation may not play an important role, as long as the rupture breaks the whole fault. We use the simple slip weakening friction model in the form given by Andrews (1976) for the dynamic rupture simulation. Critical slip distance is assumed to be 0.2m. The S parameter (Strength excess/ stress drop ratio) is 0.5. This value has been used to ensure rupture propagation along the fault. The implication of assuming this S value is that rupture goes predominantly with supershear speed. Since we are only interested in the final slip, this is not an issue. However, supershear rupture can be justified for surface rupture in long faults as it accepted by the community. In order to prevent the effect of overloading at the nucleation zone (that produce large slip), rupture initiation at the nucleation area (assumed a patch of 5km x5km) has been triggered by reducing the static frictional strength slightly below the initial stress, so that stress drop at the nucleation zone will be the same at the rest of the seismogenic zone, ensuring a complete homogeneous stress drop at the seismogenic zone.

Figure 7 shows the slip distribution of three models for the case of fault length 120km and stress drop 3.0MPa. The model shown in the top figure does not consider a weak shallow zone, but the middle and the bottom models consider weak shallow zone with stress drop of 0.0Mpa and 2.0Mpa respectively. The average slips predicted by these three models are respectively from top to bottom 3.1m, 2.7m and 2.4m. The three models break the free-surface along the whole fault length. Figure 8 shows the fault displacement (free-surface slip) distribution along the fault length with maximum fault displacement for each model (from top to bottom) respectively of 4.6m, 3.5m and 2.7m. This results show that the shallow zone plays an important role on the prediction of final slip and fault displacement. A summary of average and maximum slip overall the fault and fault displacement for all the suite of dynamic rupture models are shown in Figure 9, 10 and 11, respectively for the three SL zone models without weak zone, with 0.0Mpa and -2.0MPa of stress drop. The results reveal that saturation of average slip and maximum slip starts for models with fault length of 100km. This is more remarkable ate the average values.
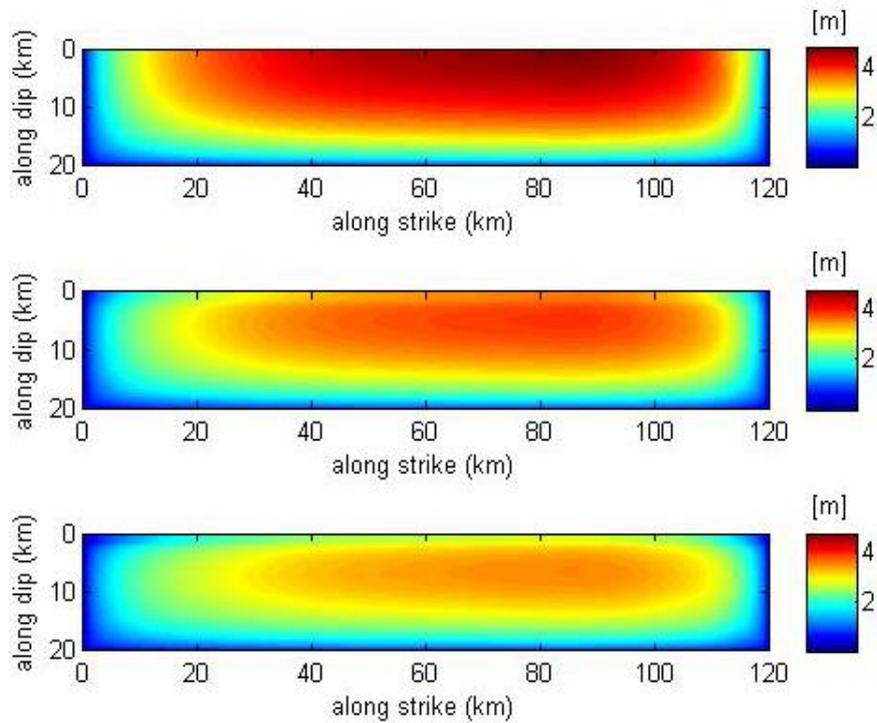
Figure 7. Final slip distribution predicted by dynamic rupture model for a fault with fault length 120km and stress drop 3.0Mpa. [Top] no shallow zone model; [middle] weak shallow zone stress drop 0.0MPa; [bottom] weak shallow zone stress drop -2.0MPa.
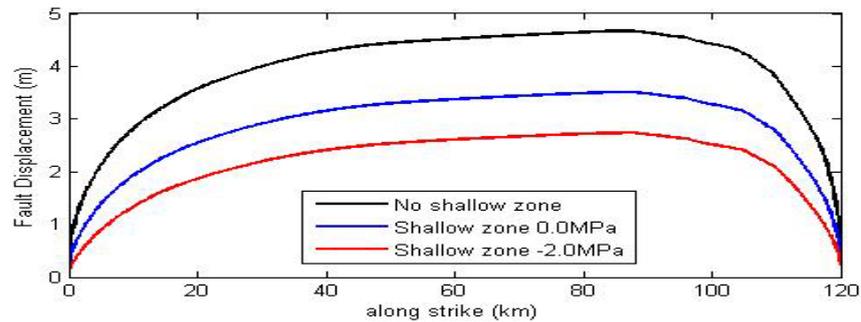
Figure 8. Fault displacement (surface rupture slip) distribution predicted by dynamic rupture
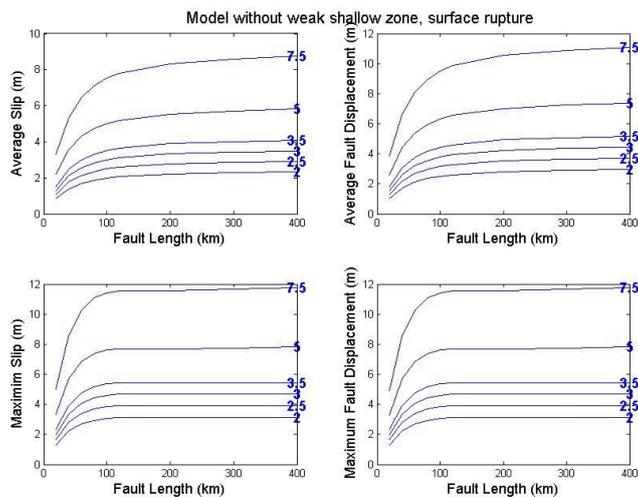
model for a fault with fault length 120km and stress drop 3.0MPa.

Figure 9. Models without weak shallow zone: Average slip and maximum slip (left) and average fault displacement and maximum fault displacement (right) as a function of fault

A-9

length for all the set of models. Each curve is indicated by a level of the corresponding dynamic stress drop at the end of each curve.

Model with 2km weak shallow zone (stress drop=0.0MPa), surface rupture
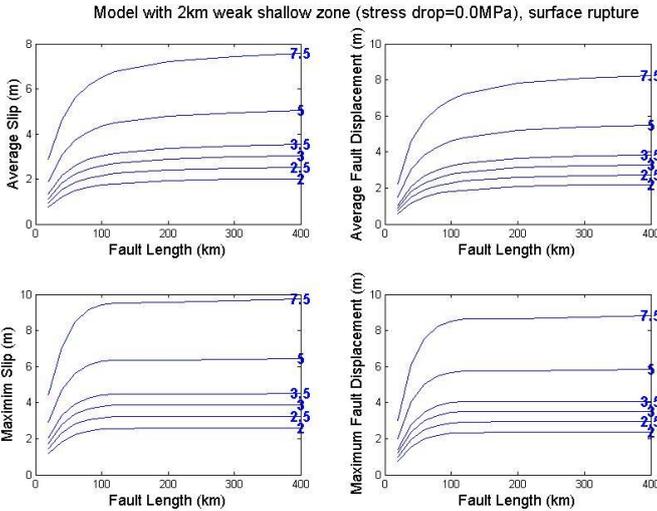
Figure 10. Models with weak shallow zone characterized with 0.0 MPa of stress drop: Average slip and maximum slip (left) and average fault displacement and maximum fault displacement (right) as a function of fault length for all the set of models. Each curve is indicated by a level of the corresponding dynamic stress drop at the end of each curve.

Model with 2km weak shallow zone (stress drop=-2.0MPa), surface rupture
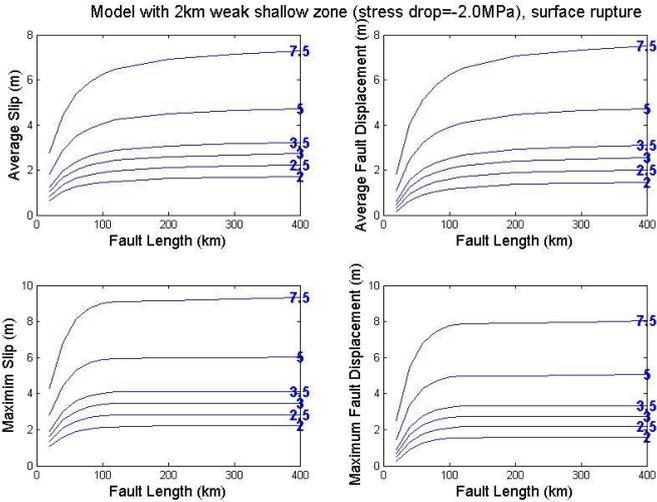
Figure 11. Models with weak shallow zone characterized with -2.0 MPa of stress drop: Average slip and maximum slip (left) and average fault displacement and maximum fault displacement (right) as a function of fault length for all the set of models. Each curve is indicated by a level of the corresponding dynamic stress drop at the end of each curve.

Figures 12, 13 and 14 shows the Seismic moment Vs rupture area respectively for the three SL zone models without weak zone, with 0.0Mpa and -2.0MPa of stress drop. The source scaling relation of Murotani et al (2015) is plotted on the top. As reference the source scaling relation from Irikura and Miyake (2001, 2011) is also shown in the figure. These figures shown that the models that fit the Murotani et al (2015) empirical model suggest that stress drop at the seismogenic zone is approximately constant. In this study, the amplitude of the constant stress drop range from 3.0 to 3.7 MPa (static stress drop from 3.4 to 4.1 MPa)

depending on the characterization of the weak SL zone. If stress drop at SL zone is the same as the seismogenic zone, the dynamic stress drop is around 3.0MPa (static stress drop around 3.4MPa). For weak SL with zero stress drop, the dynamic stress drop is around 3.5MPa (static stress drop around 3.9MPa). For weak SL with stress drop -2.0MPa, the dynamic stress drop is around 3.7MPa (static stress drop around 4.1MPa). These results show that the value of the constant stress drop in the source scaling model of Murotani et al (2015) depends on the definition of the SL.

Figure 12. Models without weak shallow zone: Rupture area vs seismic moment for all the dynamic stress drop models and empirical models of Murotani et al (2015) and Irikura and Miyake (2001, 2011). The blue level at the end of each curve is the corresponding dynamic stress drop. The black number at each point is the static stress drop corresponding to each individual model.
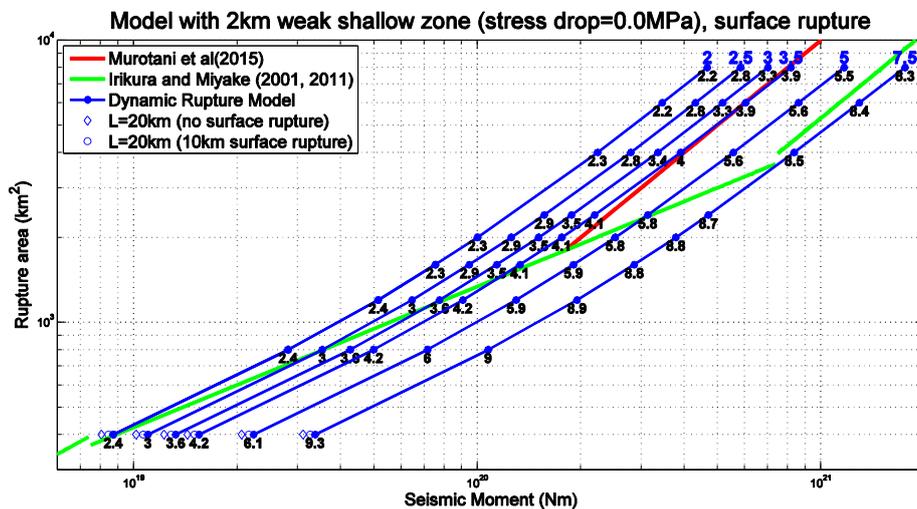
Figure 13. Models with weak shallow zone characterized with 0.0 MPa of stress drop:: Rupture area vs seismic moment for all the dynamic stress drop models and empirical models of Murotani et al (2015) and Irikura and Miyake (2001, 2011). The blue level at the end of each curve is the corresponding dynamic stress drop. The black number at each point is the static stress drop corresponding to each individual model.
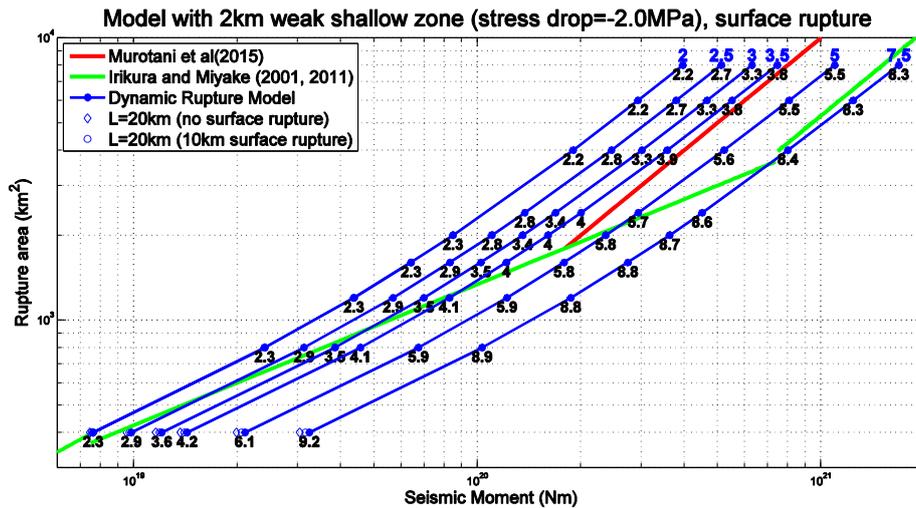
Figure 14. Models with weak shallow zone characterized with -2.0 MPa of stress drop:: Rupture area vs seismic moment for all the dynamic stress drop models and empirical models of Murotani et al (2015) and Irikura and Miyake (2001, 2011). The blue level at the end of each curve is the corresponding dynamic stress drop. The black number at each point is the static stress drop corresponding to each individual model.

References:
Andrews, D.J (1976). Rupture velocity of plane-strain shear cracks, J. Geophys. Res., 81, 5679-5687.

Dalguer (2014). "Study on fault displacement evaluation using numerical simulation methods", Report for JNES Project fiscal year 2013

Dalguer L.A; Irikura K; Riera J. And Chiu H.C (2001). The Importance of the Dynamic Source Effects on Strong Ground Motion During the 1999 Chi-Chi (Taiwan) Earthquake: Brief Interpretation of the Damage Distribution on Buildings. Bull. Seismol. Soc. Am., 95, 1112-1127.

Dalguer, L.A; K. Irikura and J. Riera, (2003a). Generation of New Cracks Accompanied by the Dynamic Shear Rupture Propagation of the 2000 Tottori (Japan) Earthquake, Bull. Seismol. Soc. Am., 93, 2236-2252.

Dalguer, L.A; K. Irikura and J. Riera, (2003b). Simulation of Tensile Crack Generation by 3D Dynamic Shear Rupture Propagation During an Earthquake. J. Geophys. Res., 108(B3), 2144, doi:10.1029/2001JB001738.

Dalguer, L.A., H. Miyake, S.M. Day and K. Irikura (2008), Surface Rupturing and Buried Dynamic Rupture Models Calibrated with Statistical Observations of Past Earthquakes. Bull. Seismol. Soc. Am. 98, 1147-1161, doi: 10.1785/0120070134.

Dalguer, L. A., H. Miyake, and K. Irikura (2004). Characterization of dynamic asperity source models for simulating strong ground motion, Proceedings of the 13th World Conference on Earthquake Engineering (13WCEE), Vancouver, B.C., Canada, August 1-6, 2004, Paper No. 3286.

Ely, G. P., S. M. Day and J.-B. Minster (2008)., A support-operator method for viscoelastic wave modelling in 3-D heterogeneous media, Geophysical Journal International, 172(1) 331-344.

Ely, G., S. M. Day and J-B. Minster (2009). A support-operator method for 3D rupture dynamics, Geophysical Journal International, 177 1140-1150, DOI: 10.1111/j.1365 246X.2009.04117.x.

Irikura, K., and H. Miyake (2001). Prediction of strong ground motions for scenario earthquakes, *Journal of Geography*, 110, 849-875, doi:10.5026/jgeography.110.6_849 (in Japanese with English abstract)

Irikura, K., and H. Miyake (2011). Recipe for predicting strong ground motion from crustal earthquake scenarios, Pure Appl. Geophys., 168, 85-104, doi:10.1007/s00024-010-0150-9.

Iwata, T., H. Sekiguchi, and K. Irikura (2000), Rupture process of the 1999 Chi-Chi, Taiwan, earthquake and its near-source strong ground motions, Proc. International Workshop on Annual Commemoration of Chi-Chi earthquake, Taipei, Taiwan, Vol.1, 36-46, Sep. 2000.

Kamae, K. and K. Irikura "Source model of the 1995 Hyogo-ken Nanbu earthquake and simulation of near-source ground motion", BSSA, 88, 2, 400-412,1998.

Marone, C. (1998). Laboratory-derived friction laws and their application to seismic faulting, Ann. Revs. Earth Plan. Sci. 26, 643–696.

Marone, C., and C. H. Scholz (1988). The depth of seismic faulting and the upper transition from stable to unstable slip regimes, Geophys. Res. Lett. 15, 621–624.

Murotani, S.; S. Matsushima; T- Azuma; K. Irikura and S. Kitagawa (2015). Scaling Relations of Source Parameters of Earthquakes Occurring on Inland Crustal Mega-Fault Systems, Pure Appl. Geophys. 172, 1371–1381; DOI 10.1007/s00024-014-1010-9.

Oglesby, D. D., R. J. Archuleta, and S. B. Nielsen (2000). The threedimensional dynamics of dipping faults, Bull. Seism. Soc. Am. 90, 616–628.

Pitarka, A., L.A. Dalguer, S.M. Day, P. Somerville, and K. Dan (2009). Numerical study of ground motion differences between buried and surface-rupturing earthquakes, Bull. Seism. Soc. Am. , Vol. 99, No. 3, pp. 1521–1537, June 2009, doi:10.1785/0120080193

Somerville, P., K. Irikura, R. Graves, S. Sawada, D. Wald, N. Abrahamson, Y. Iwasaki, T. Kagawa, N. Smith, and A. Kowada (1999). Characterizing crustal earthquake slip models for the prediction of strong ground motion, Seism. Res. Lett. 70, 59–80.

Vermilye, J. M., and C. H. Scholz (1998). The process zone: a microstructural view of fault growth, J. Geophys. Res. 103, 12,223–12,237.

Zhang, W; Tomotaka Iwata; Kojiro Irikura; Haruko Sekiguchi and Michel Bouchon (2003). Heterogeneous distribution of the dynamic source parameters of the 1999 Chi-Chi, Taiwan, earthquake, J. Geophys. Res., 108, NO. B5, 2232, doi:10.1029/2002JB001889, 2003.

APPENDIX A: Comparison between observation and synthetic of velocity and displacement ground motion at 39 stations near the Chelongpu fault of the 1999 Chi-Chi, Taiwan, earthquake.

The figures below compare with observations the synthetic ground motion developed in this project (2015 fiscal year) and the ones from the 2013 fiscal year. Seismograms passed a low pass filter with frequency cut off of 0.5Hz. In all the figures, left column are velocity and right column displacement of three components (EW, NS and UD).
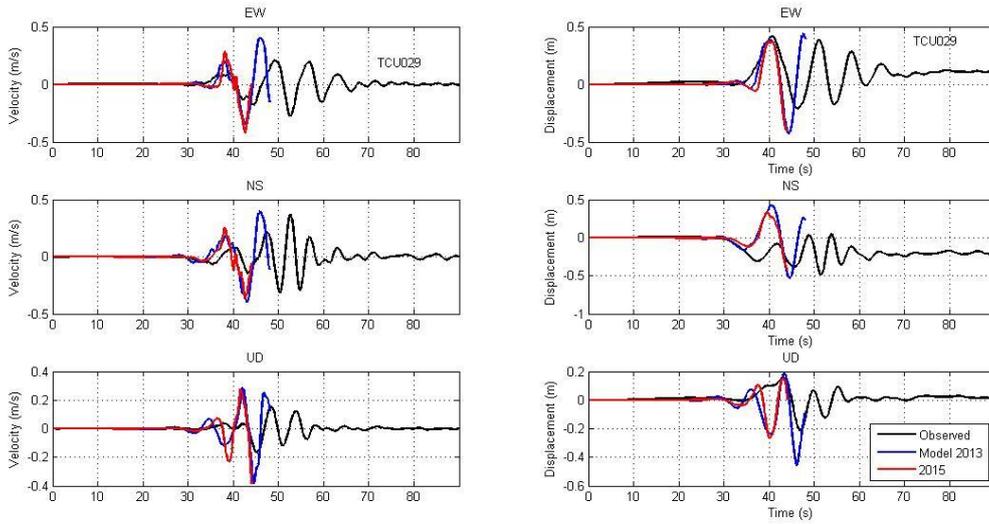
Figure A.1. Station TCU029
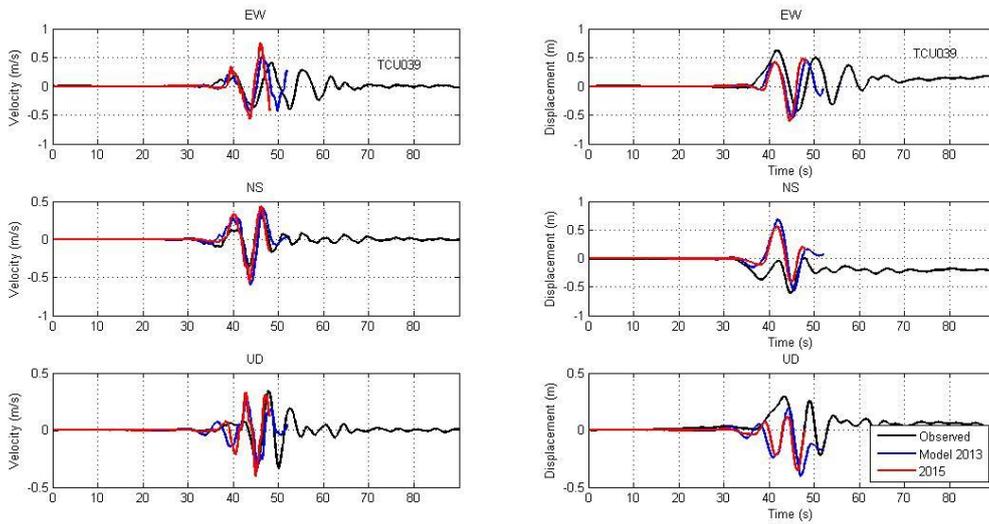
Figure A.2. Station TCU039
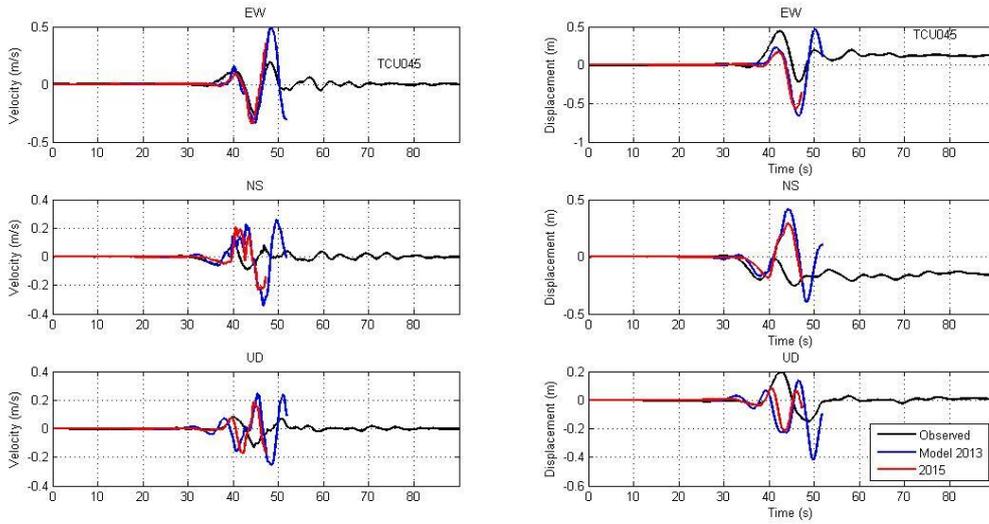
Figure A.3. Station TCU045
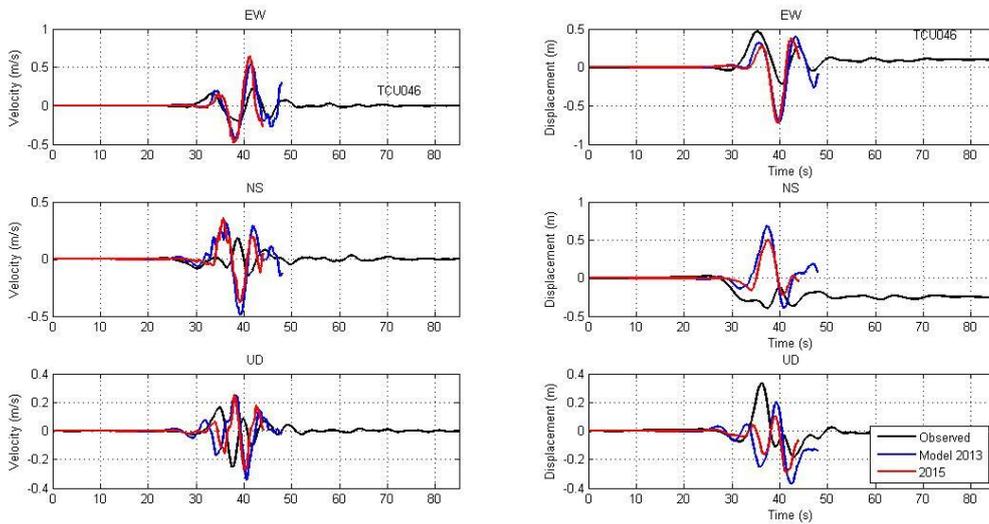
Figure A.4. Station TCU046
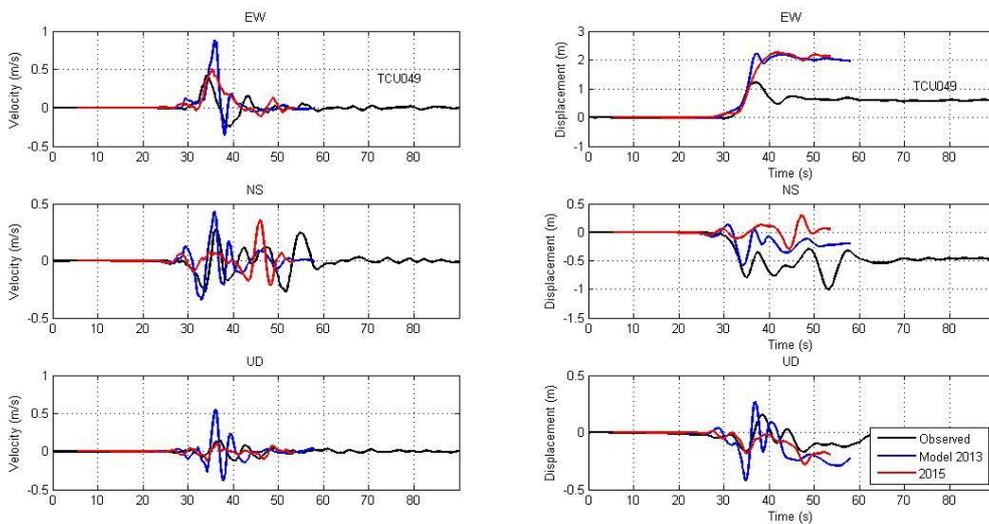
Figure A.5. Station TCU049
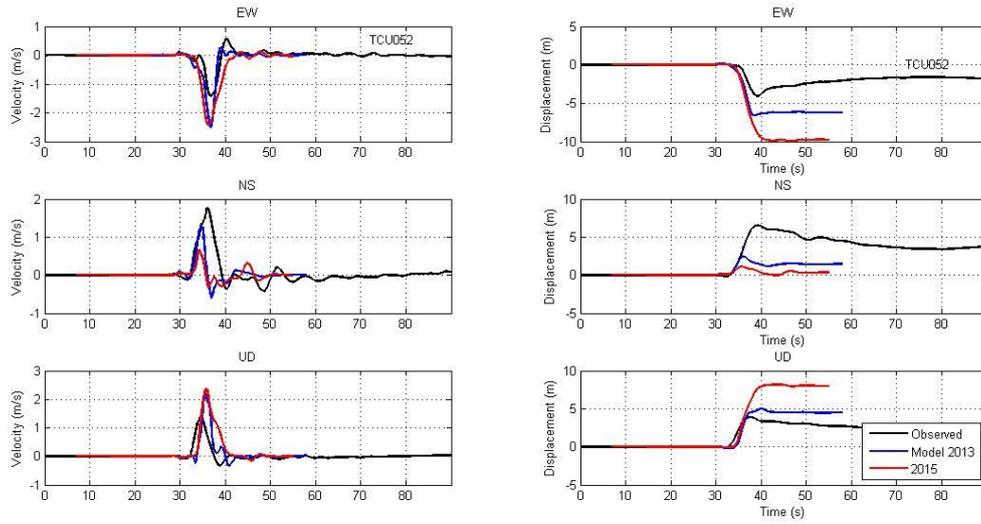
Figure A.6. Station TCU052
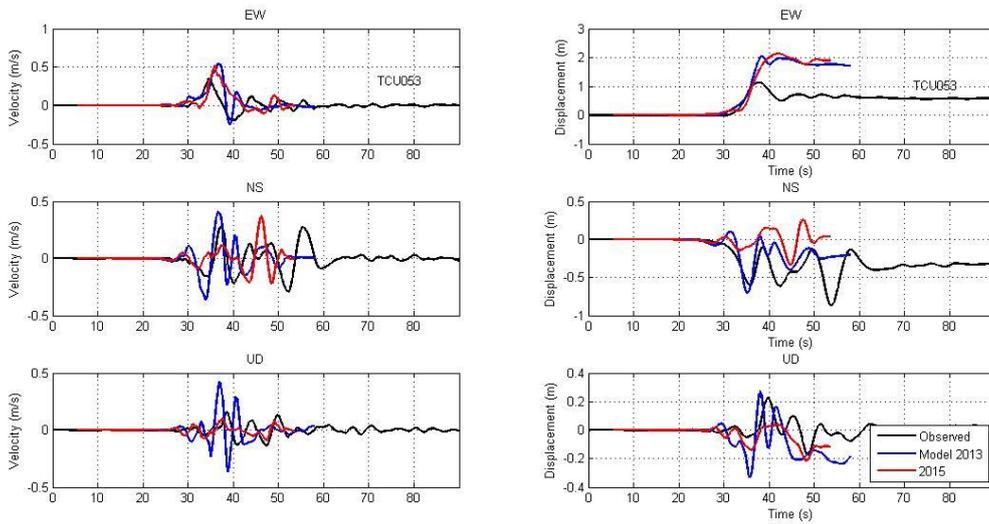
Figure A.7. Station TCU053
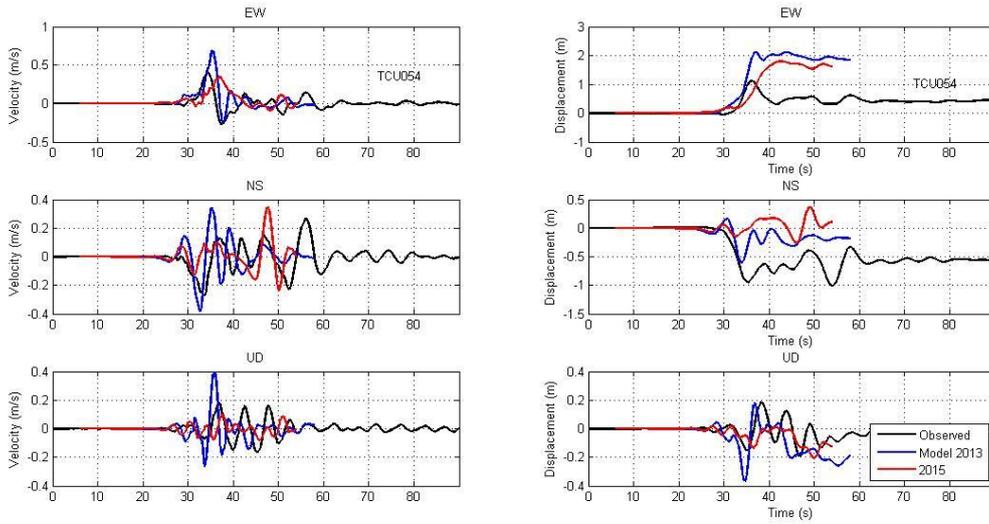
Figure A.8. Station TCU054
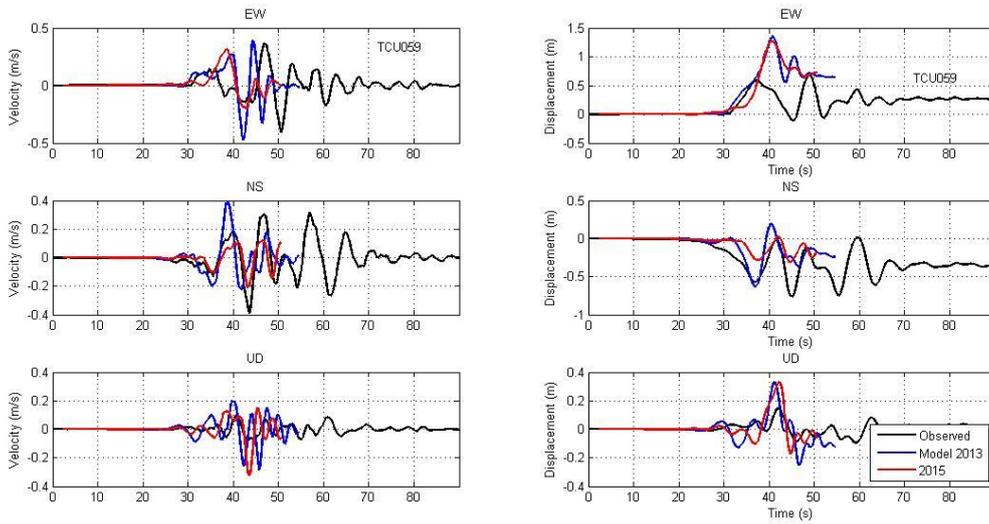
Figure A.9. Station TCU059
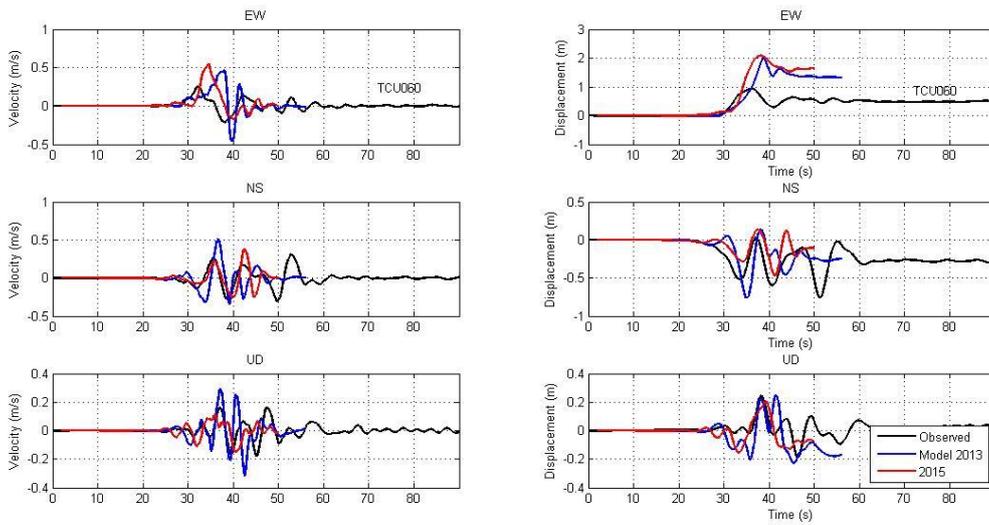
Figure A.10. Station TCU060

A-17
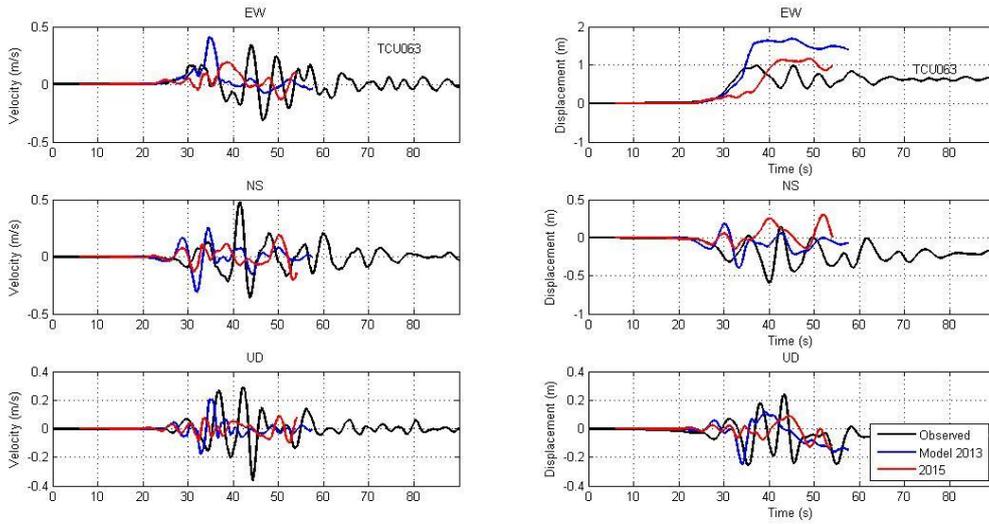
Figure A.11. Station TCU063
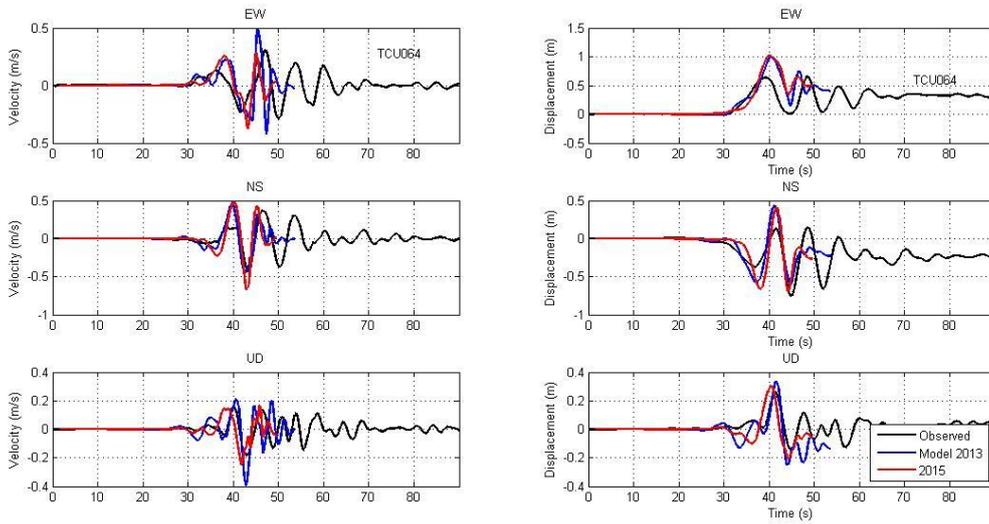
Figure A.12. Station TCU064
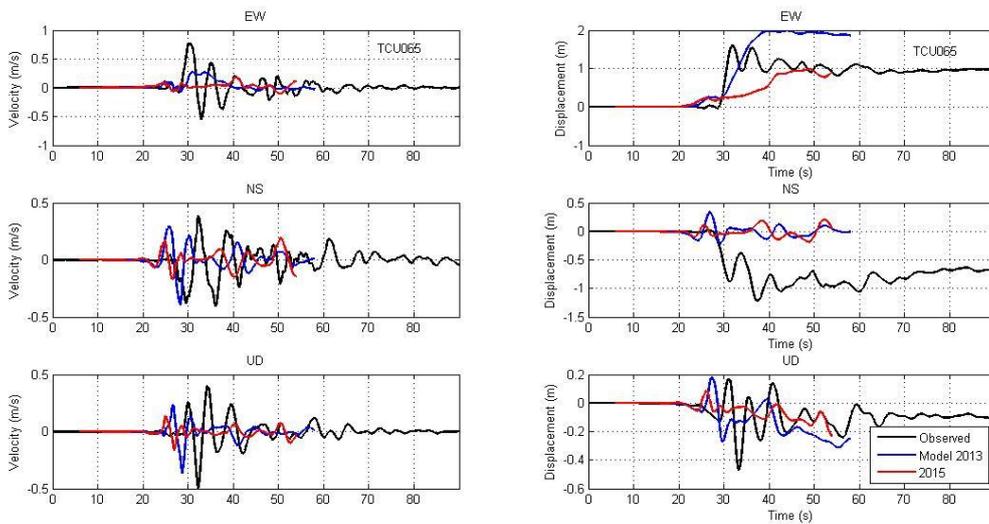
Figure A.13. Station TCU065

A-18
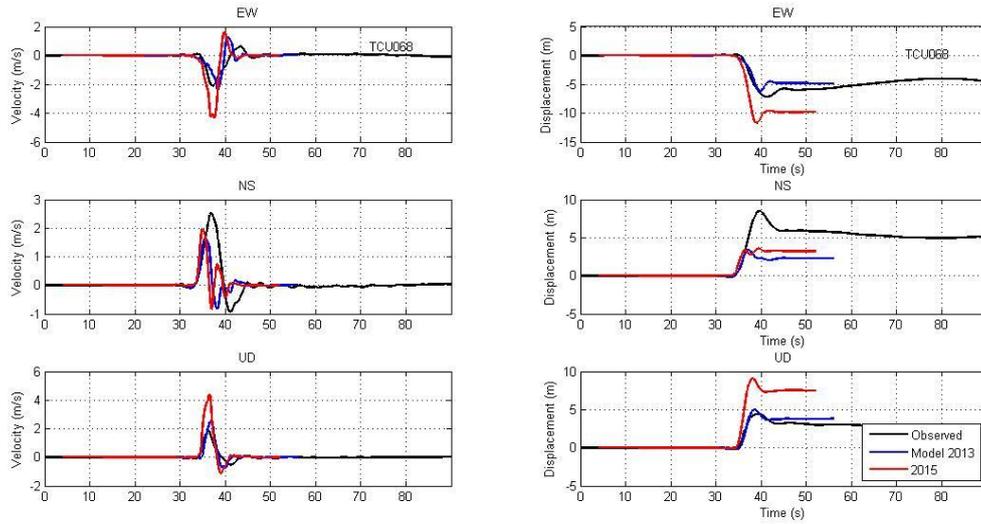
Figure A.14. Station TCU068
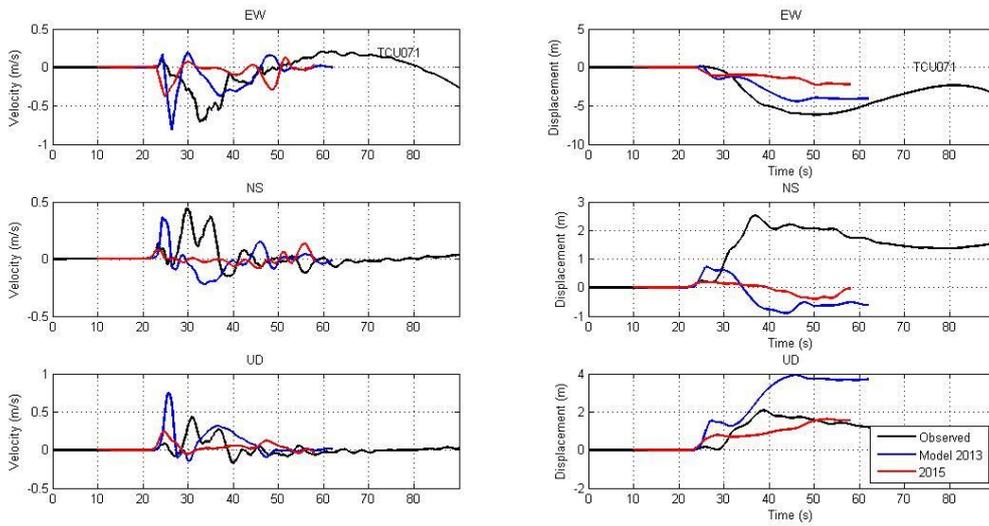
Figure A.15. Station TCU071

A-19
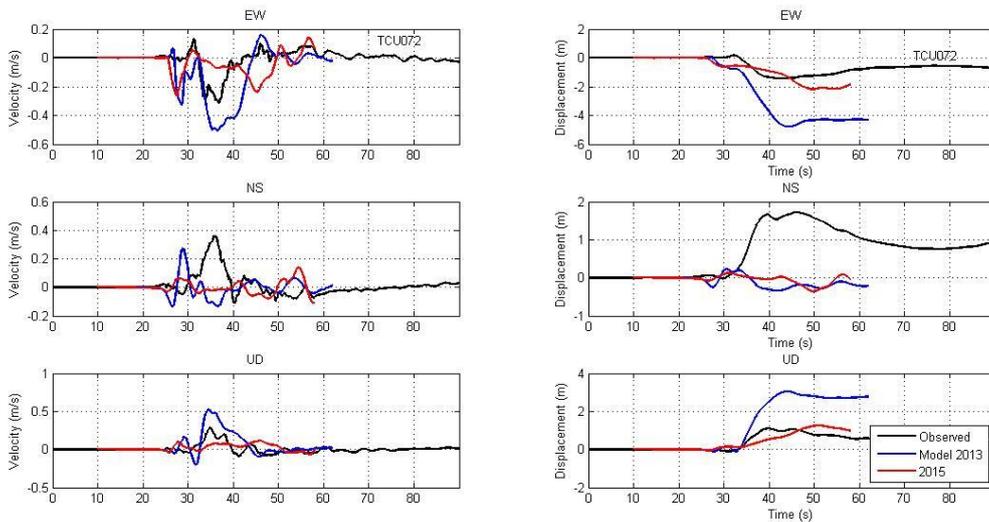
Figure A.16. Station TCU072
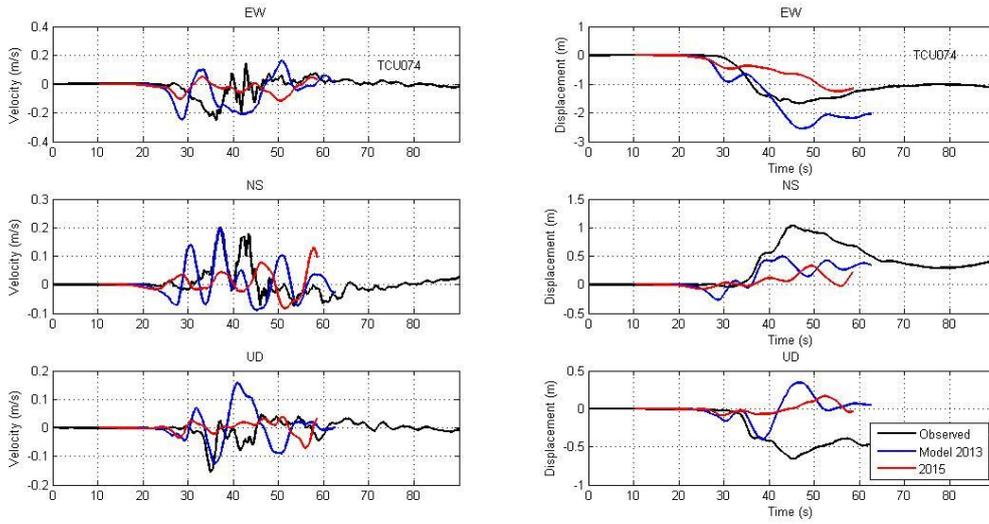
Figure A.17. Station TCU074
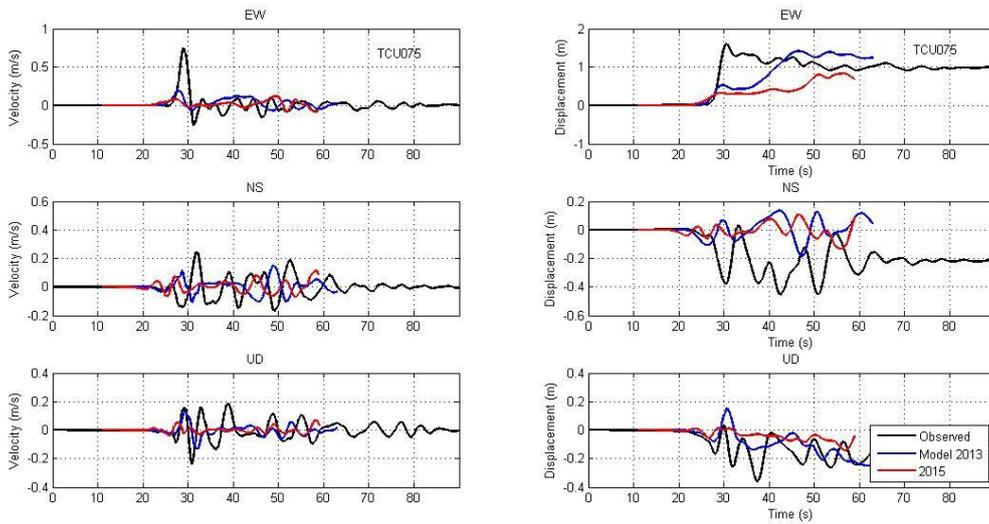
Figure A.18. Station TCU075
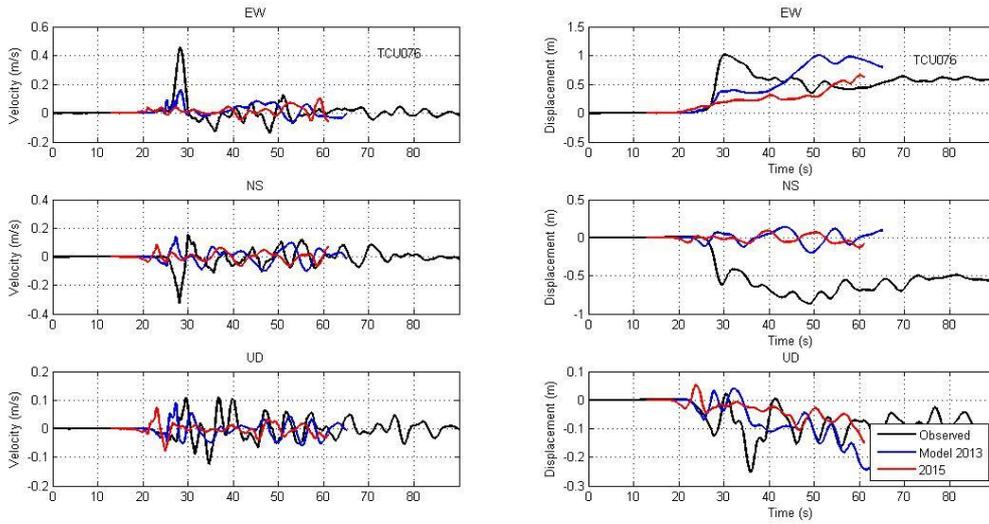
Figure A.19. Station TCU076
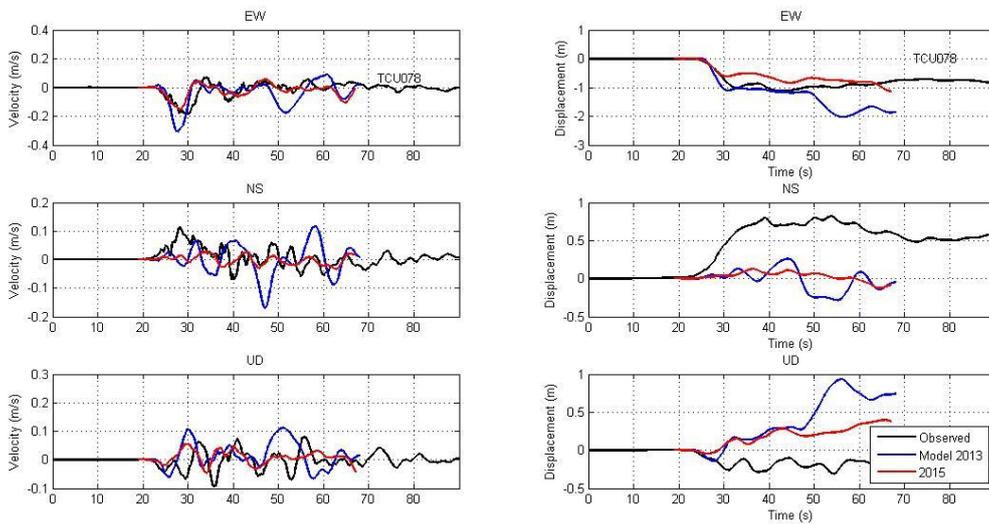
Figure A.20. Station TCU078
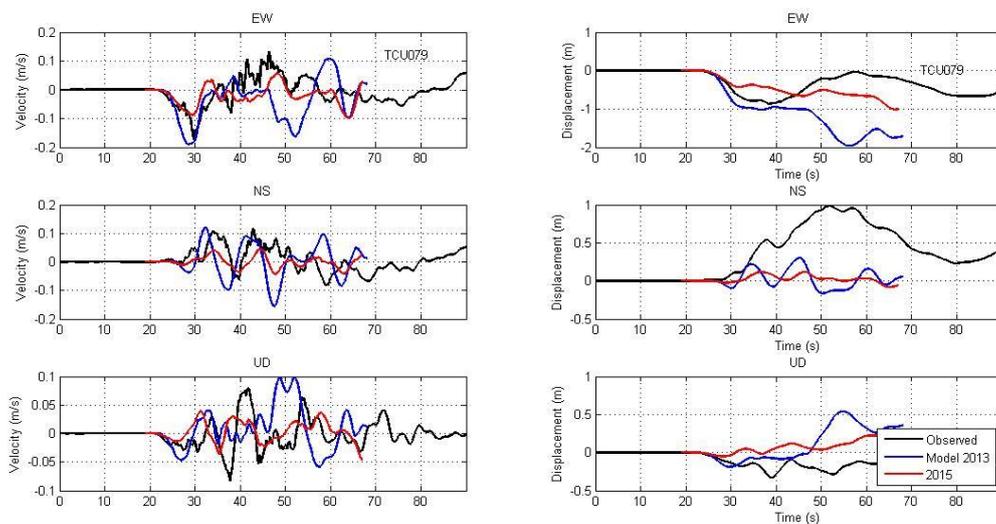
Figure A.21. Station TCU079

A-21
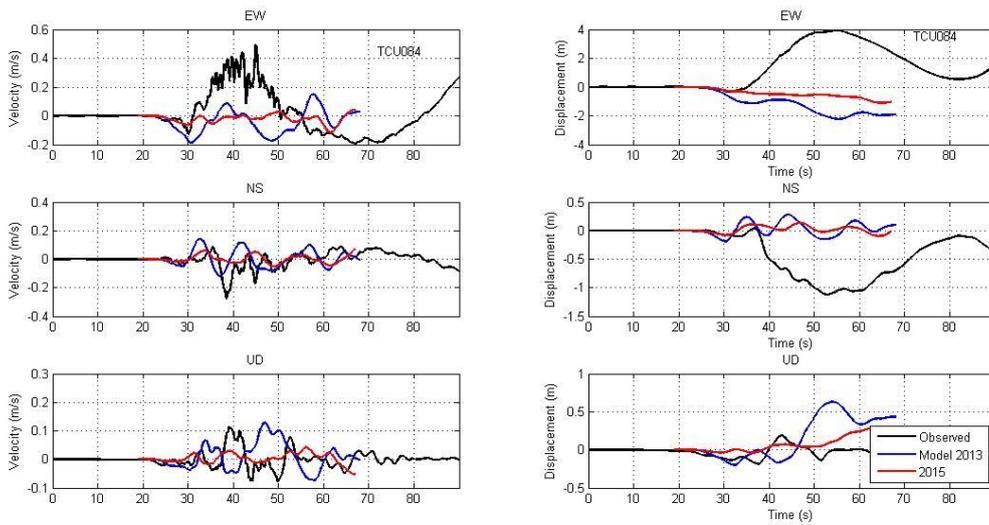
Figure A.22. Station TCU084
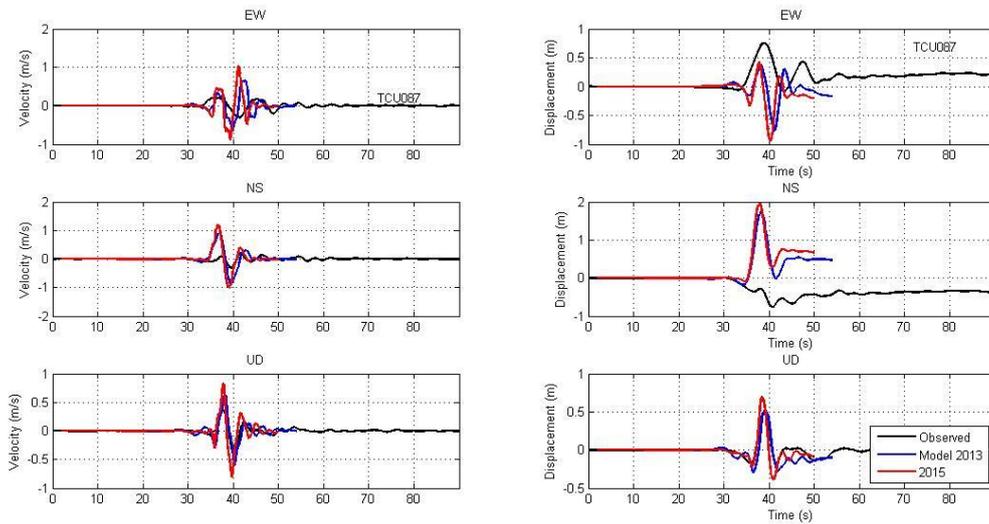
Figure A.23. Station TCU087
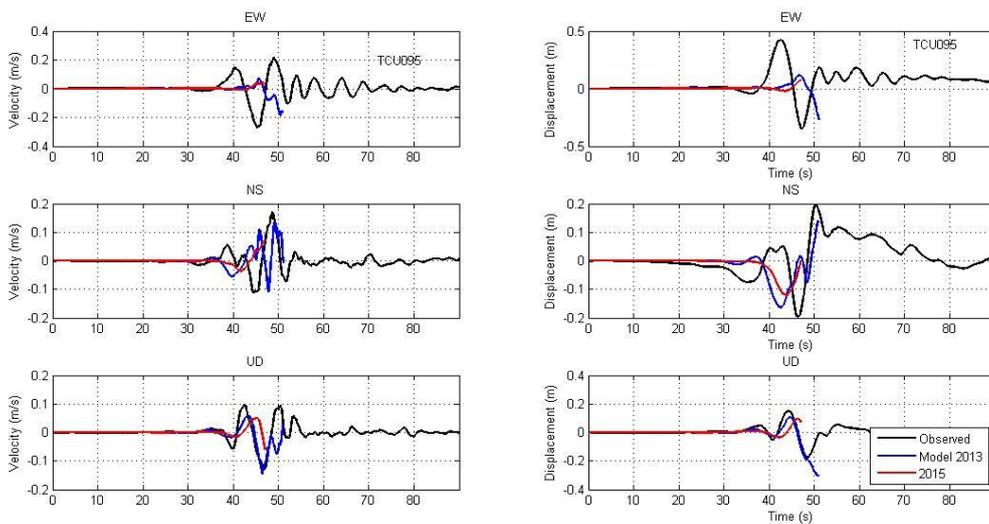
Figure A.24. Station TCU095
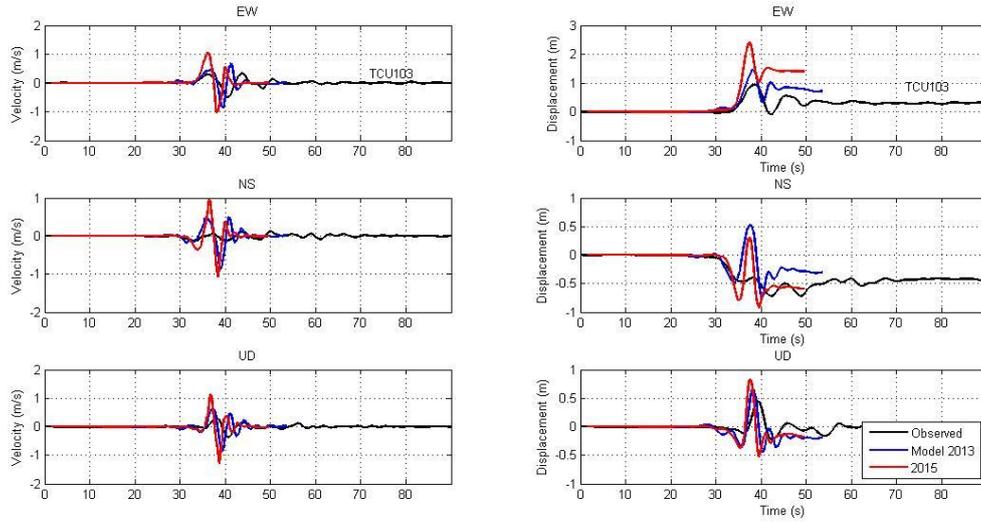
Figure A.25. Station TCU103
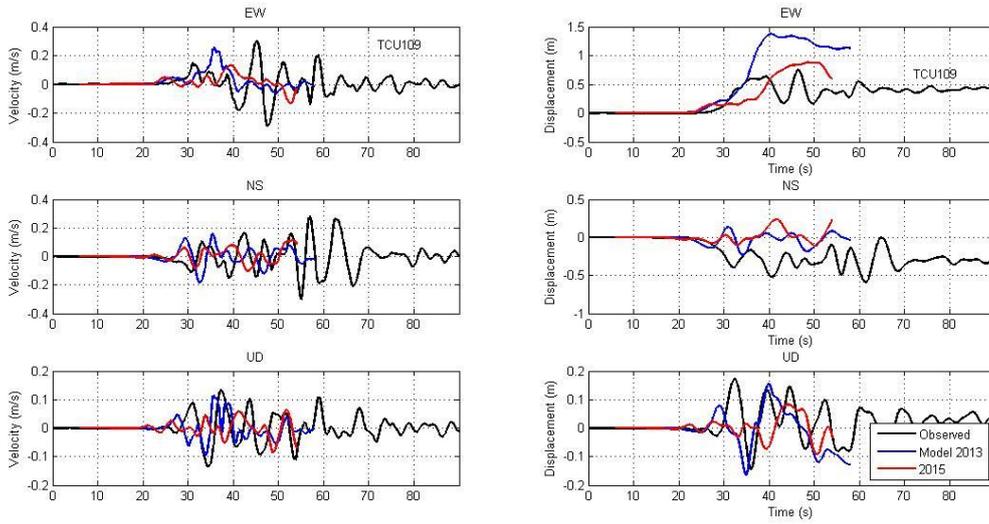
Figure A.26. Station TCU109
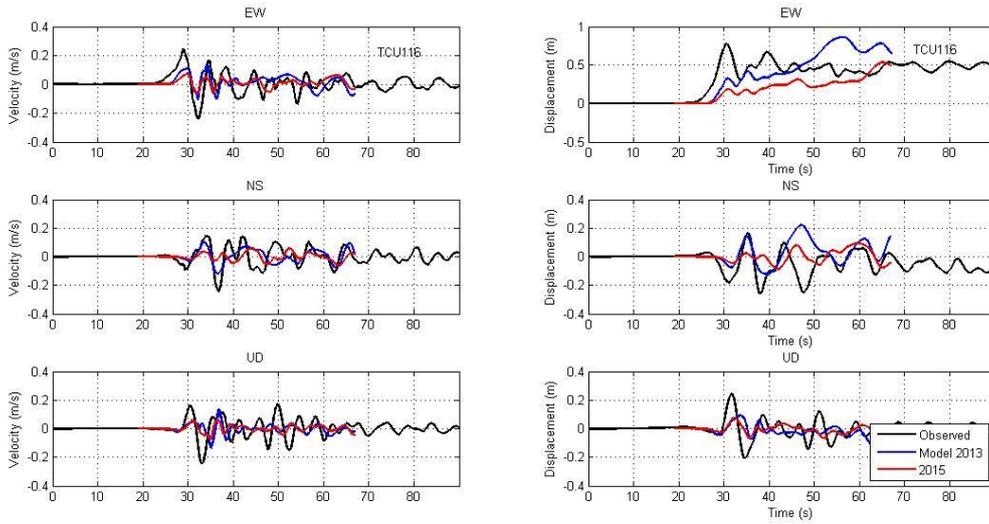
Figure A.27. Station TCU116
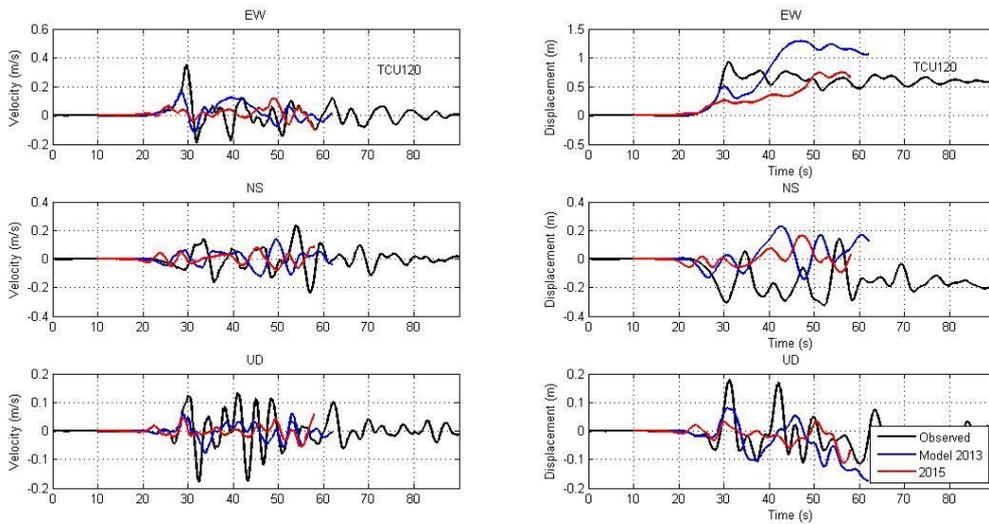
Figure A.28. Station TCU120
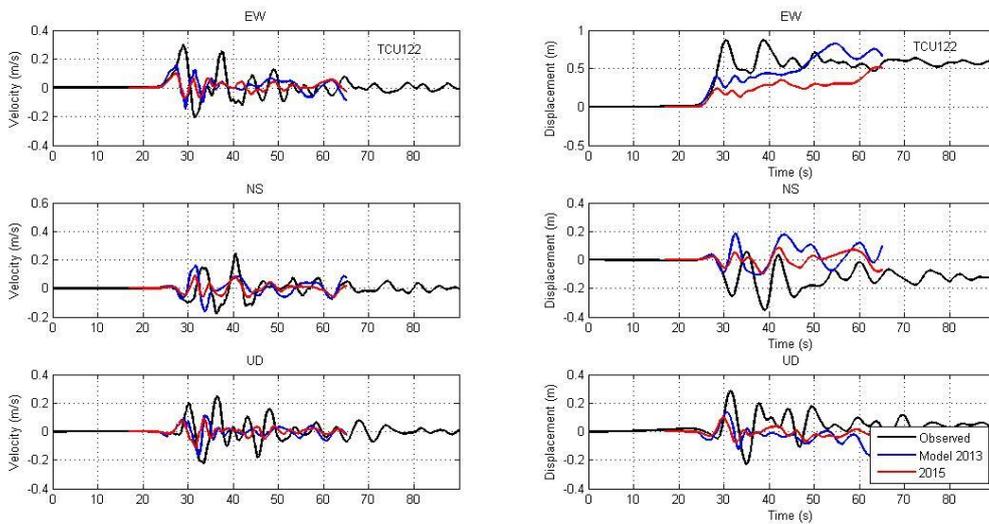
Figure A.29. Station TCU122

A-24
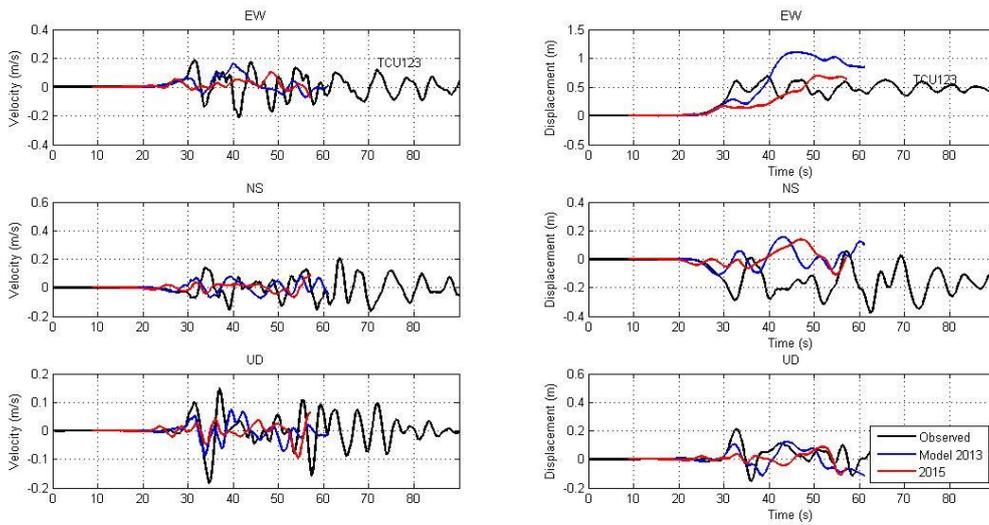
Figure A.30. Station TCU123
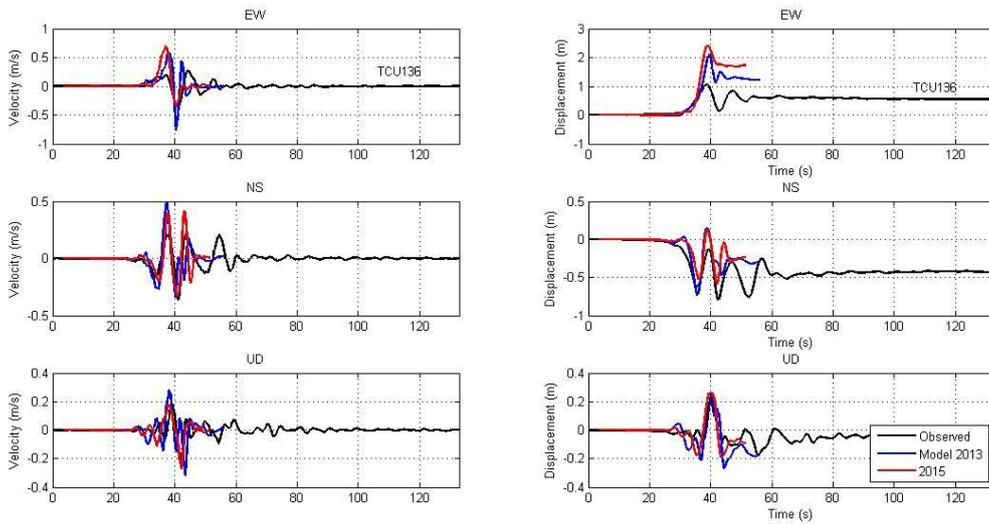
Figure A.31. Station TCU136

A-25
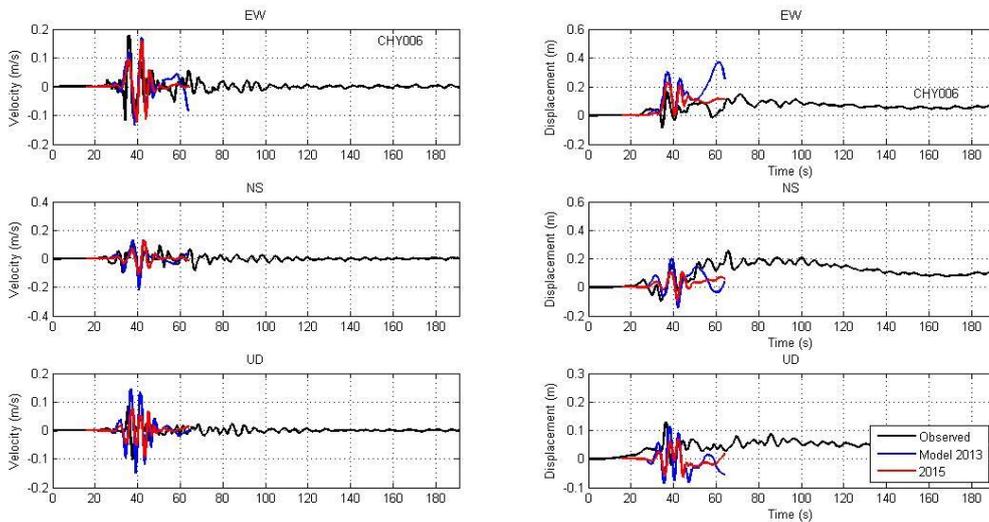
Figure A.32. Station CHY006
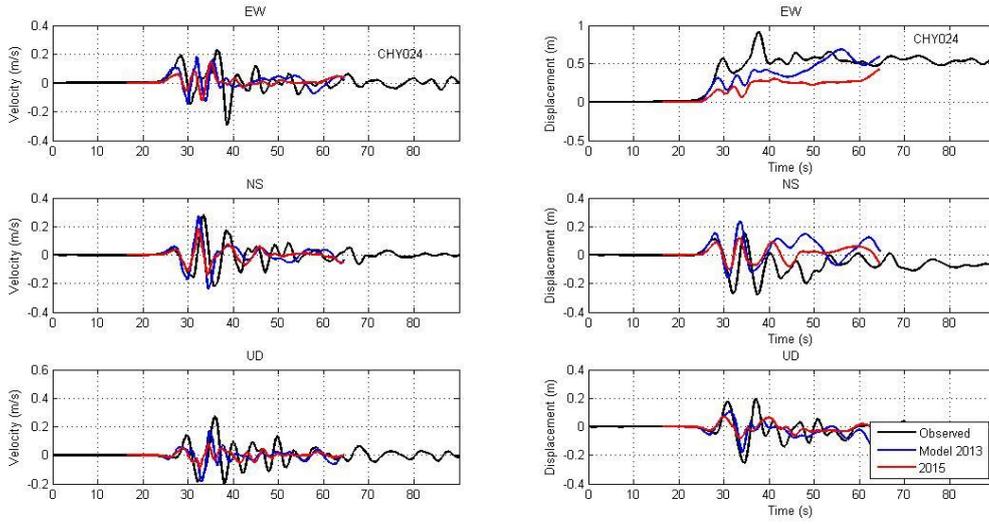
Figure A.33. Station CHY024
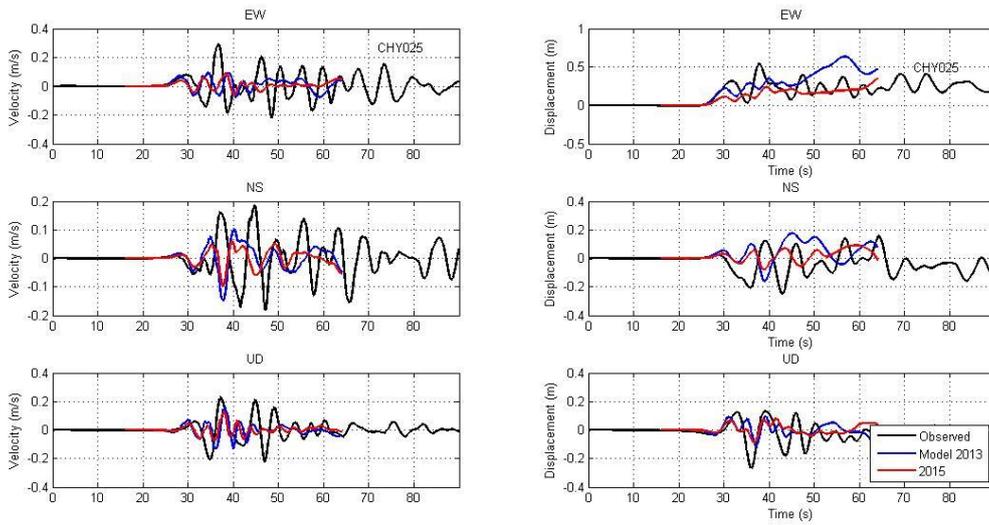
Figure A.34. Station CHY025
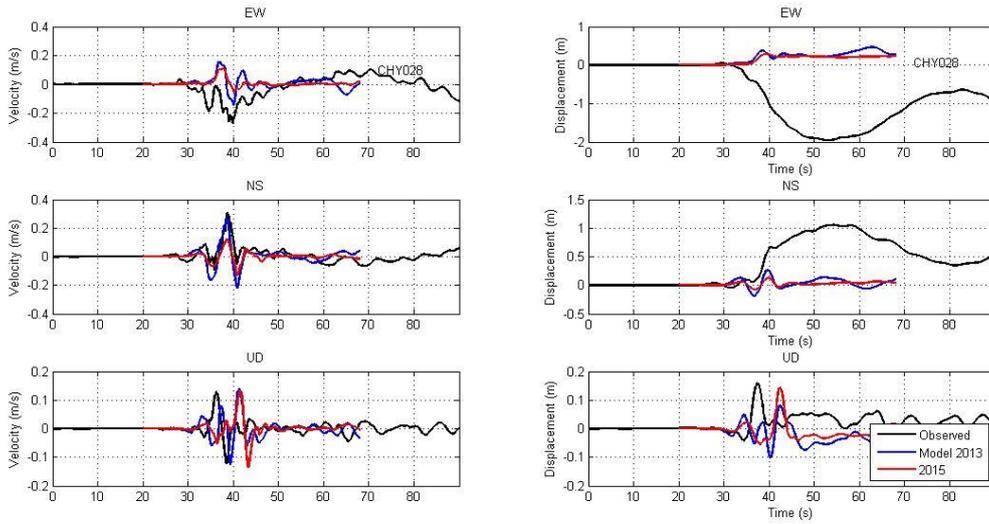
Figure A.35. Station CHY028
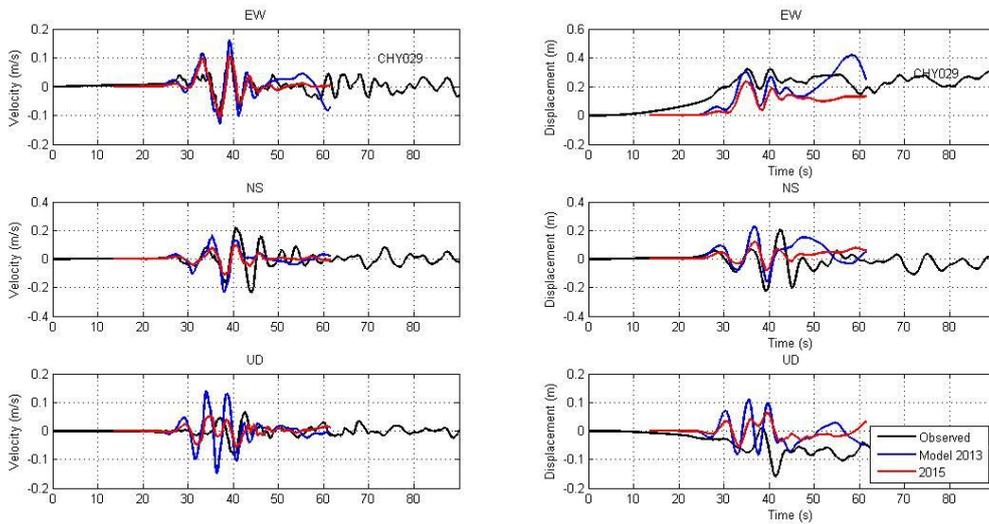
Figure A.36. Station CHY029
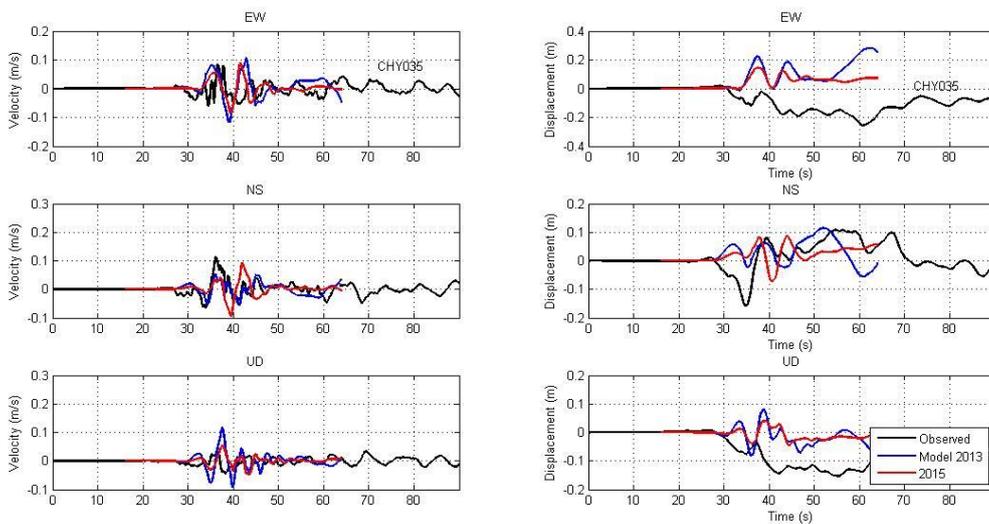
Figure A.37. Station CHY035
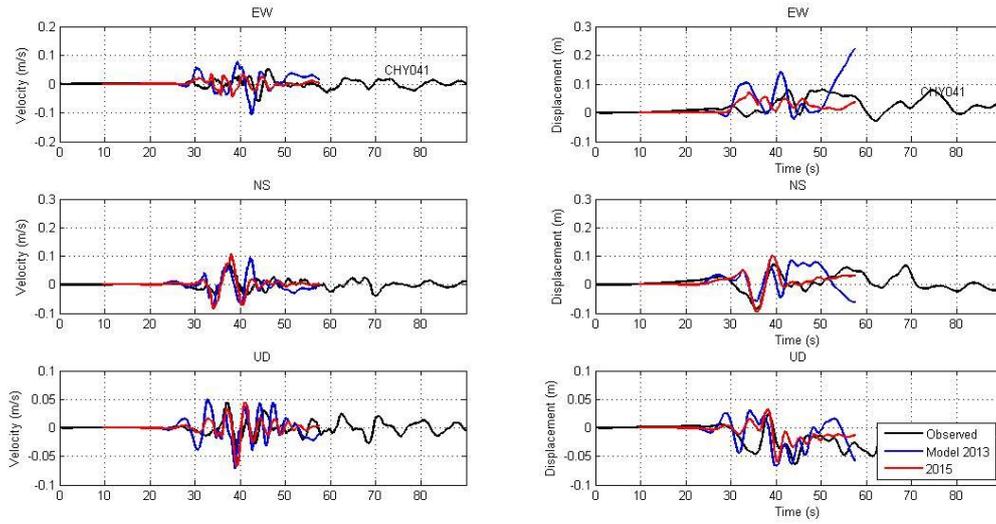
Figure A.38. Station CHY041
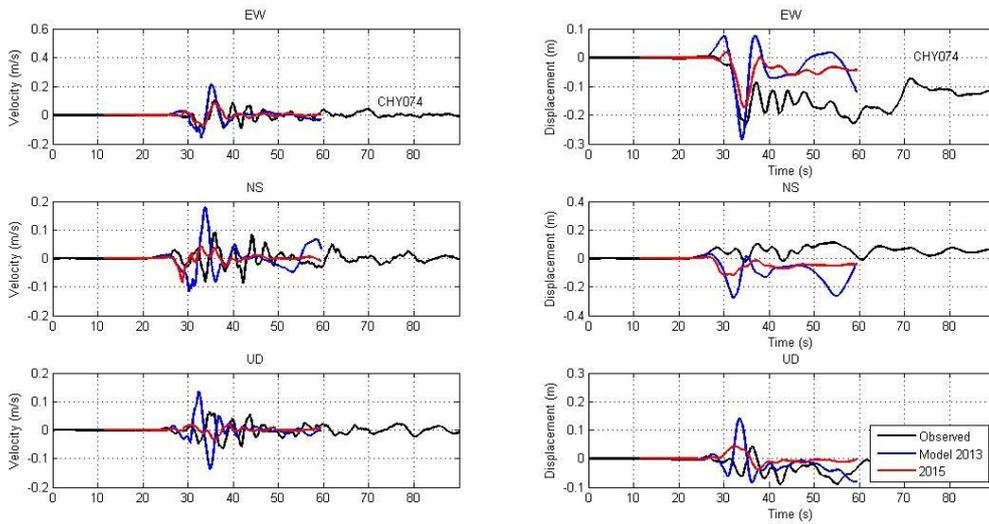
Figure A.39. Station CHY074

A-28

Appendix B, Slip distribution from other dynamic asperity models.
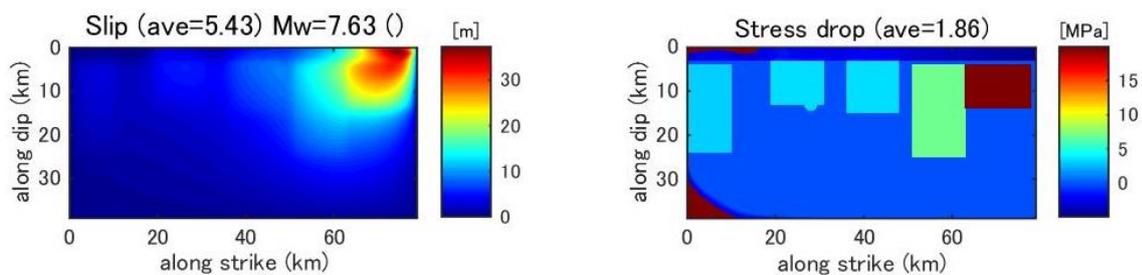
Figure B1. Slip distribution (left) from the dynamic asperity model (Masp1) that correspond to the stress drop distribution (right).
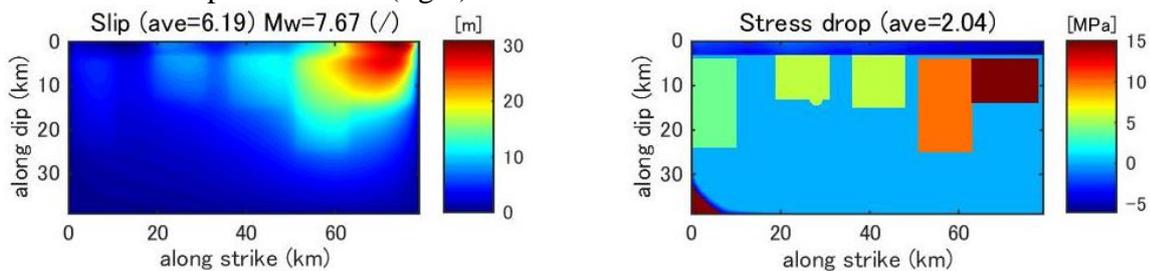
Figure B2. Slip distribution (left) from the dynamic asperity model (Masp2) that correspond to the stress drop distribution (right).
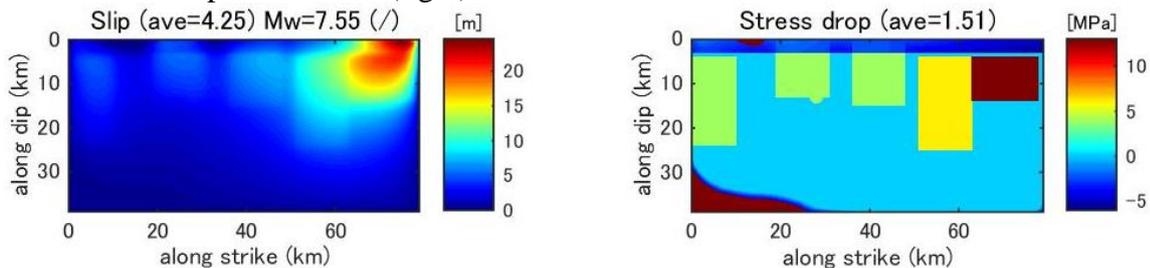
Figure B3. Slip distribution (left) from the dynamic asperity model (Masp3) that correspond to the stress drop distribution (right).
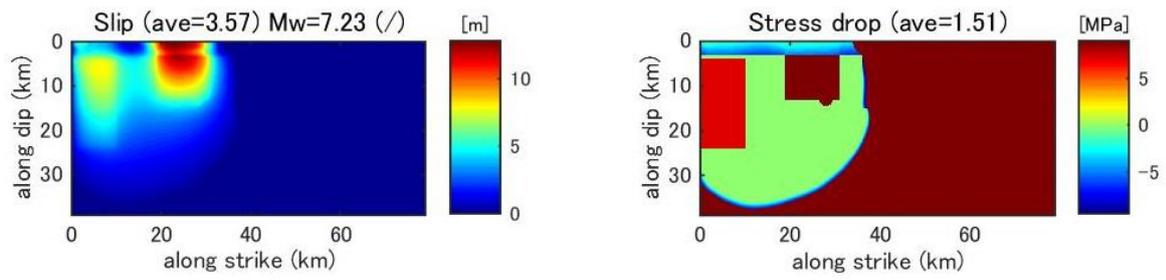
Figure B4. Slip distribution (left) from the dynamic asperity model (Masp4) that correspond to the stress drop distribution (right).
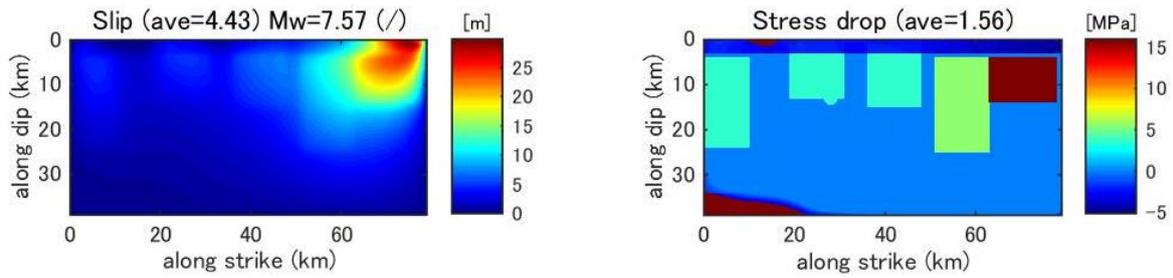
Figure B5. Slip distribution (left) from the dynamic asperity model (Masp5) that correspond to the stress drop distribution (right).
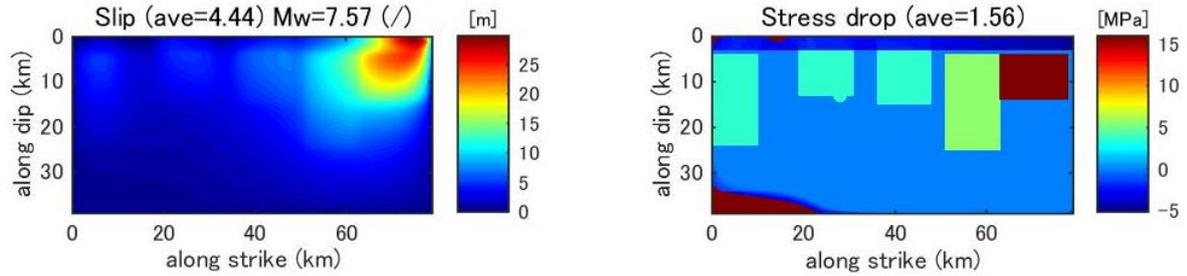
Figure B6. Slip distribution (left) from the dynamic asperity model (Masp6) that correspond to the stress drop distribution (right).
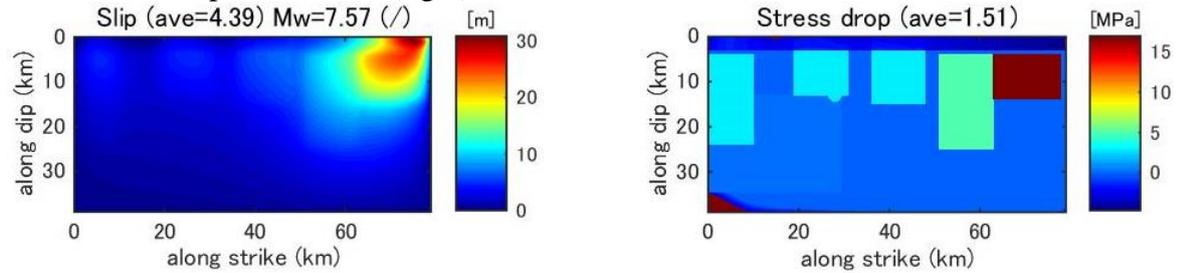
Figure B7. Slip distribution (left) from the dynamic asperity model (Masp7) that correspond to the stress drop distribution (right).

Appendix C. Slip distribution from dynamic rupture models with uniform stress drop.
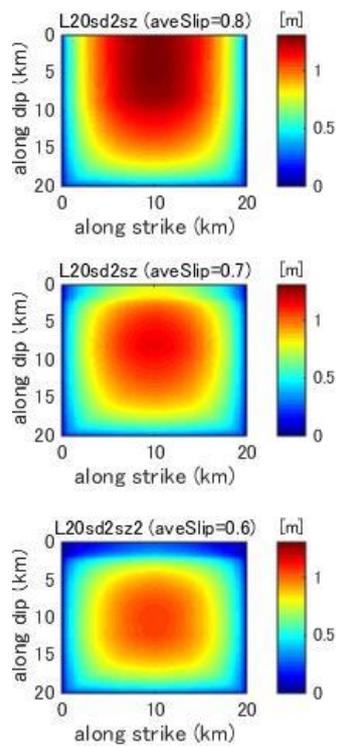
Figure C1. Final slip distribution predicted by dynamic rupture model for a fault with fault length 20km and stress drop 2.0MPa. [Top] no shallow zone model; [middle] weak shallow zone stress drop 0.0MPa; [bottom] weak shallow zone stress drop -2.0MPa.
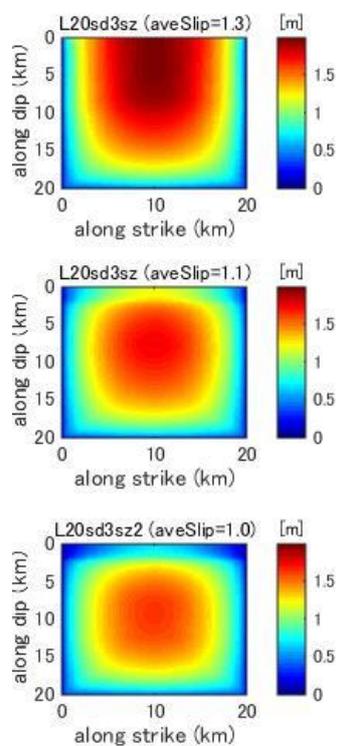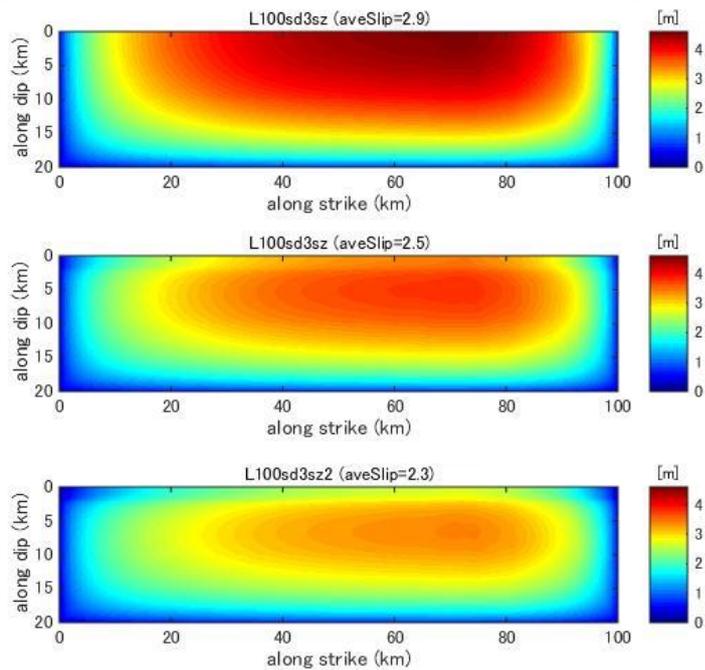

Figure C2. Final slip distribution predicted by dynamic rupture model for a fault with fault length 20km and stress drop 3.0MPa.
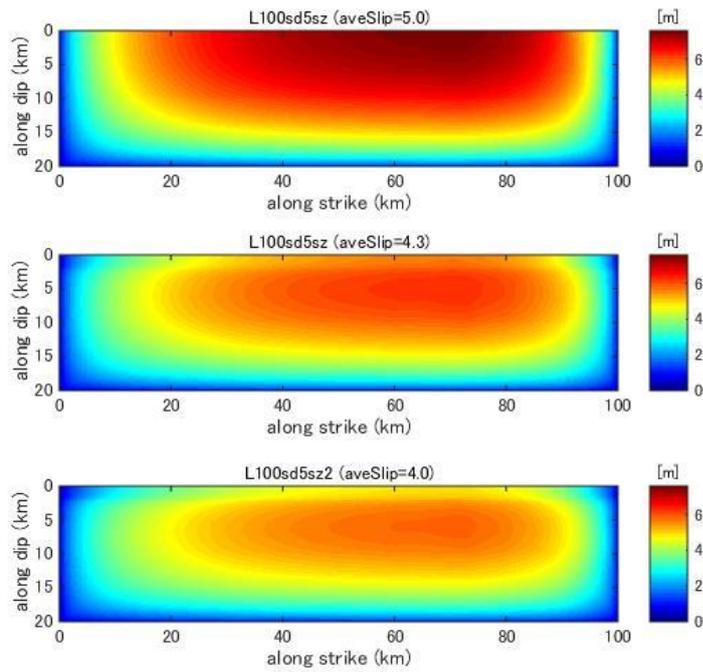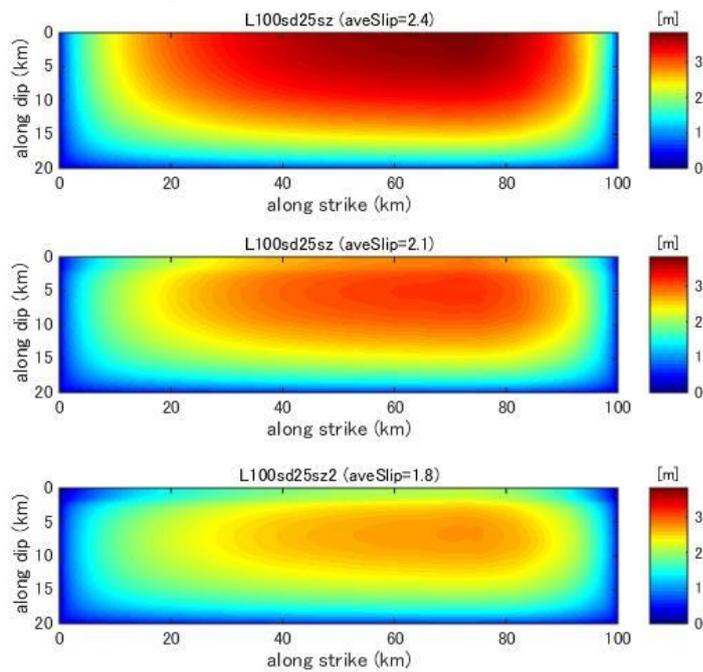
A-32
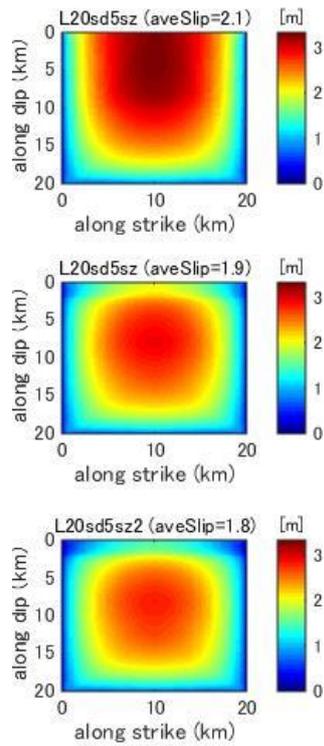
Figure C3. Final slip distribution predicted by dynamic rupture model for a fault with fault length 20km and stress drop 5.0MPa.
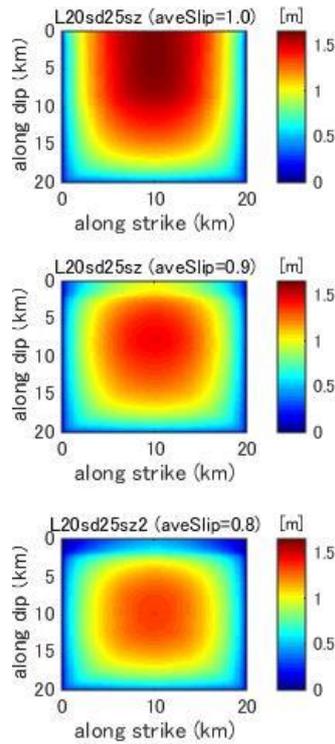
Figure C4. Final slip distribution predicted by dynamic rupture model for a fault with fault length 20km and stress drop 2.5MPa.
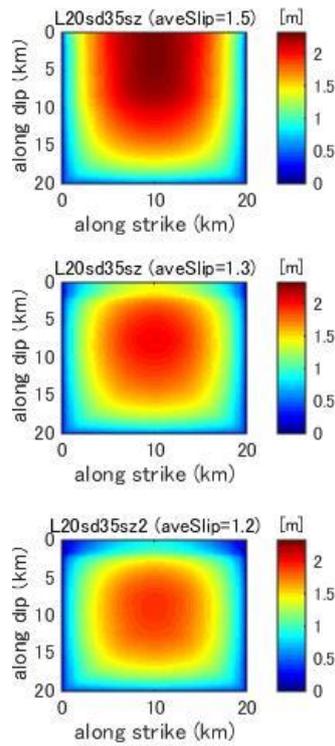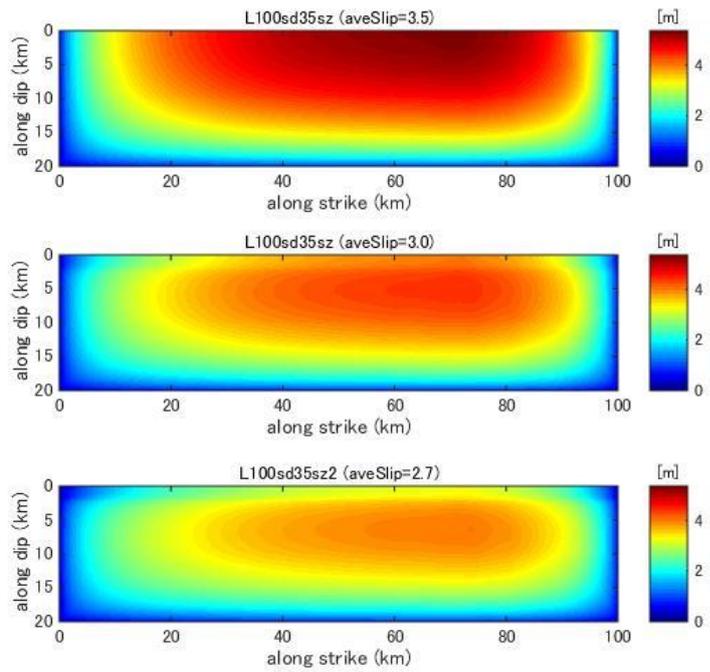
Figure C5. Final slip distribution predicted by dynamic rupture model for a fault with fault length 20km and stress drop 3.5MPa.
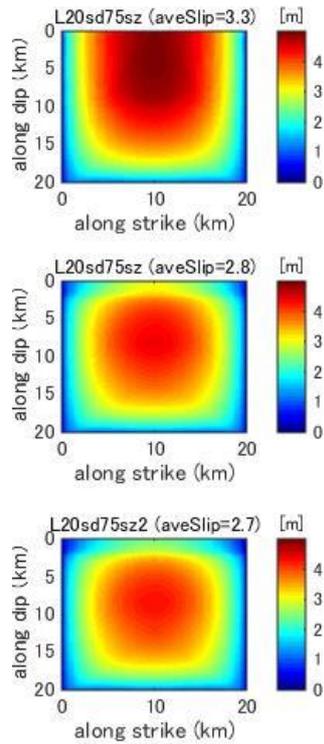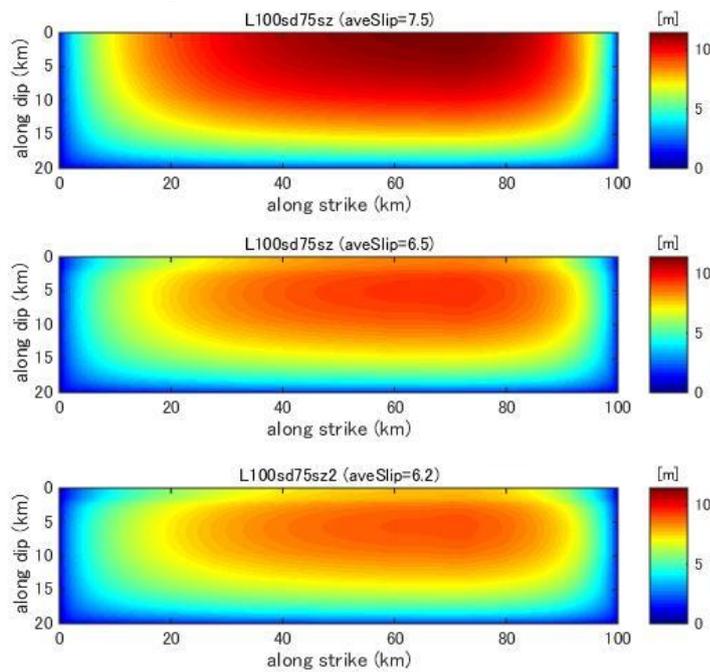

Figure C6. Final slip distribution predicted by dynamic rupture model for a fault with fault length 20km and stress drop 7.5MPa.
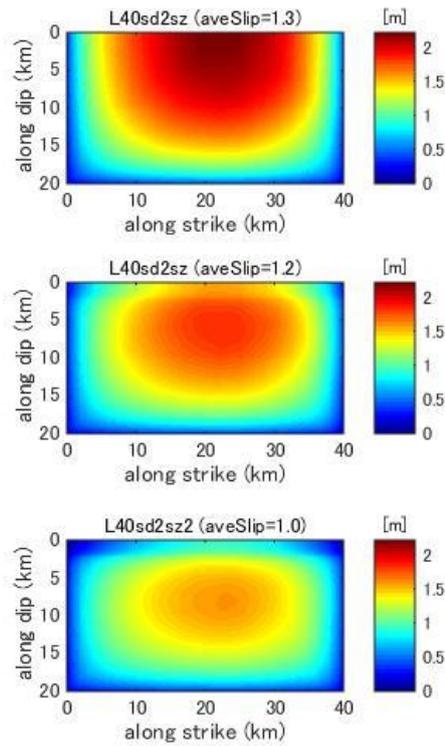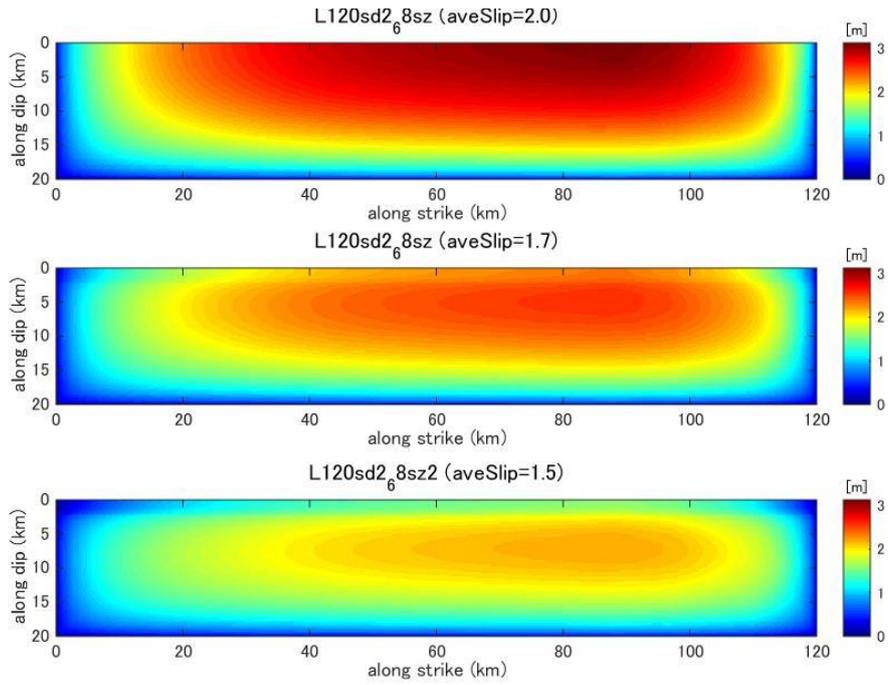
Figure C7. Final slip distribution predicted by dynamic rupture model for a fault with fault length 40km and stress drop 2.0MPa. [Top] no shallow zone model; [middle] weak shallow zone stress drop 0.0MPa; [bottom] weak shallow zone stress drop -2.0MPa.
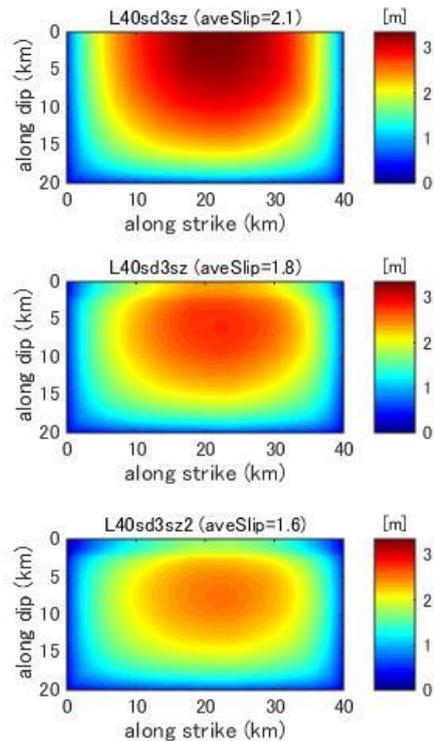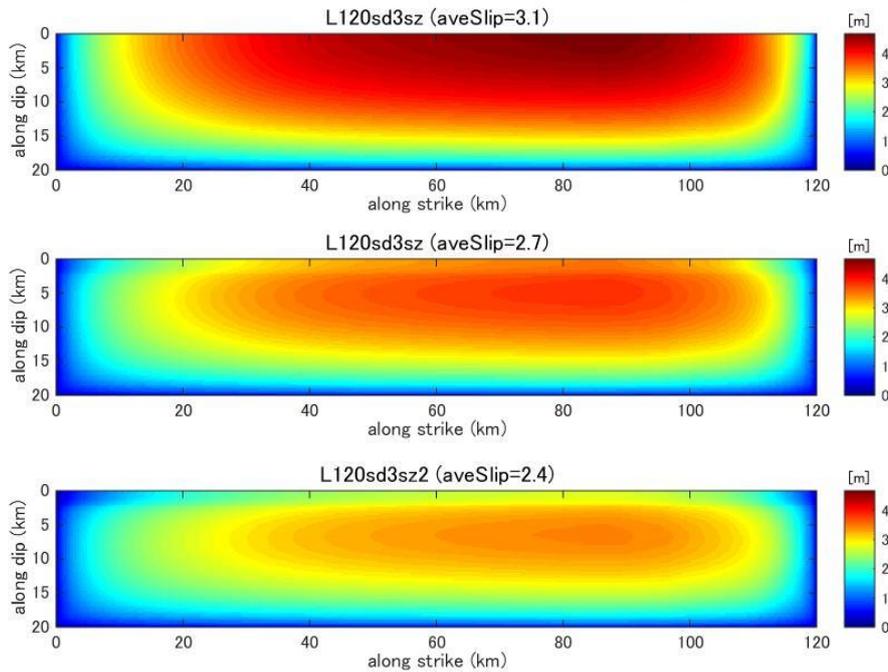

Figure C8. Final slip distribution predicted by dynamic rupture model for a fault with fault length 40km and stress drop 3.0MPa.
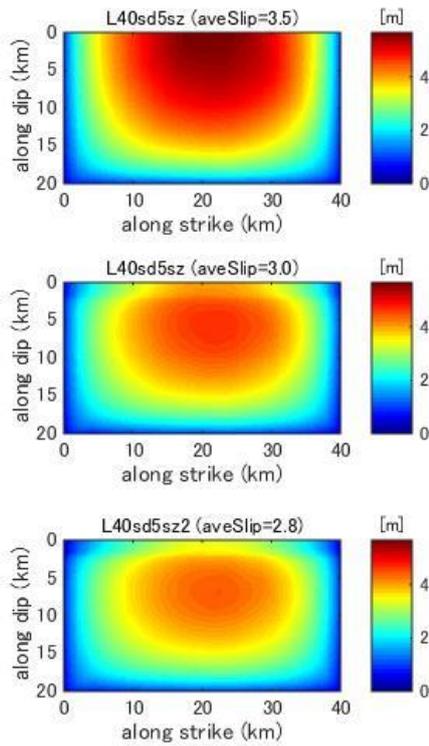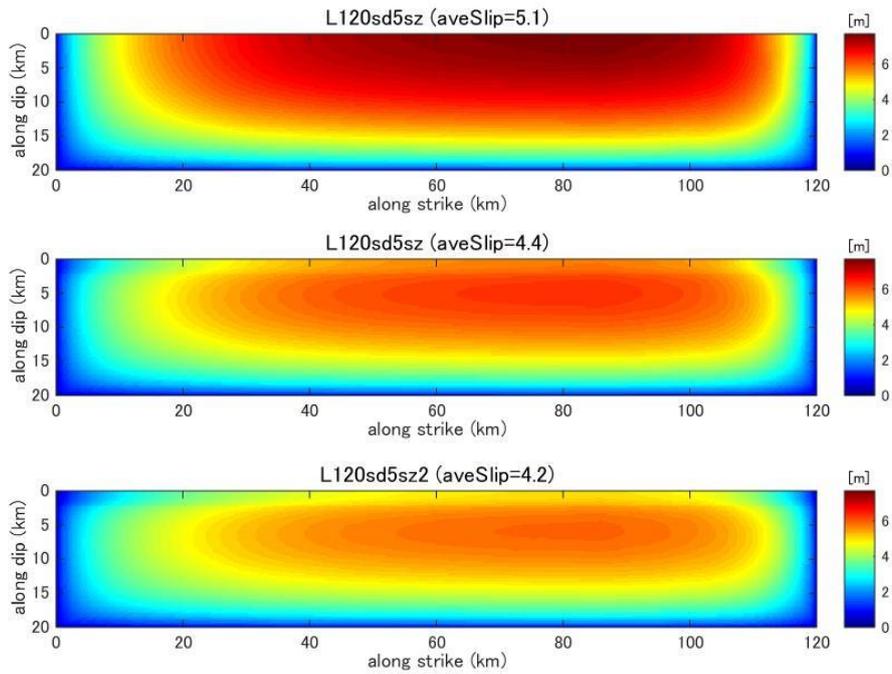
Figure C9. Final slip distribution predicted by dynamic rupture model for a fault with fault length 40km and stress drop 5.0MPa.
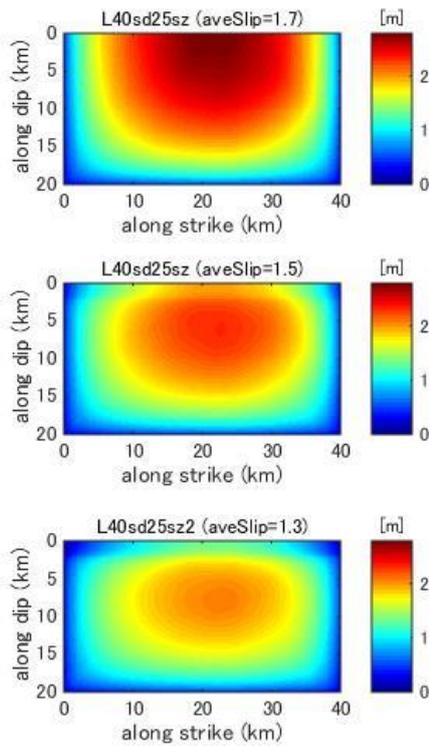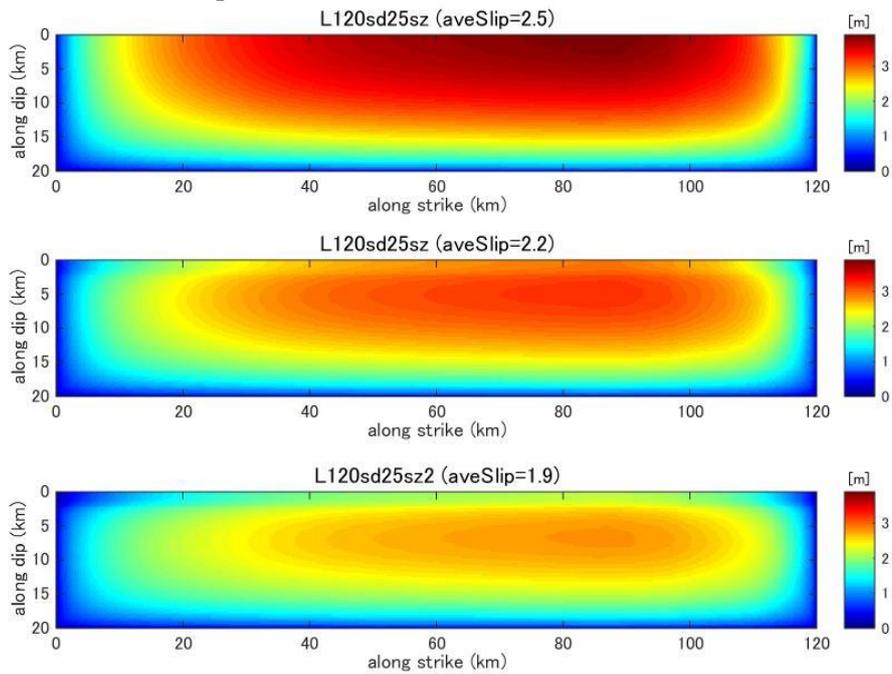

Figure C10. Final slip distribution predicted by dynamic rupture model for a fault with fault length 40km and stress drop 2.5MPa.
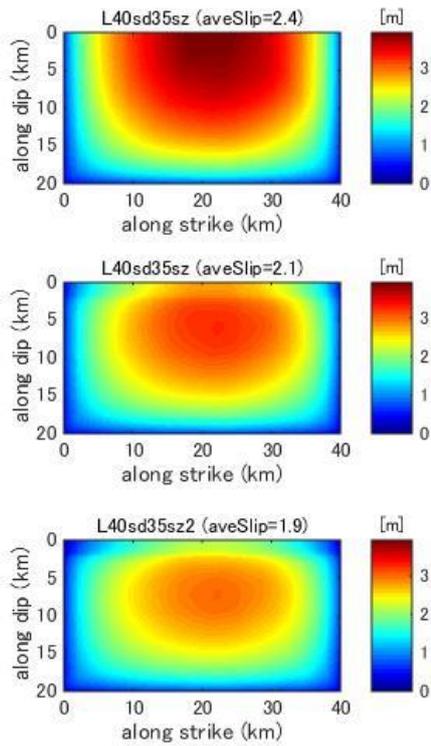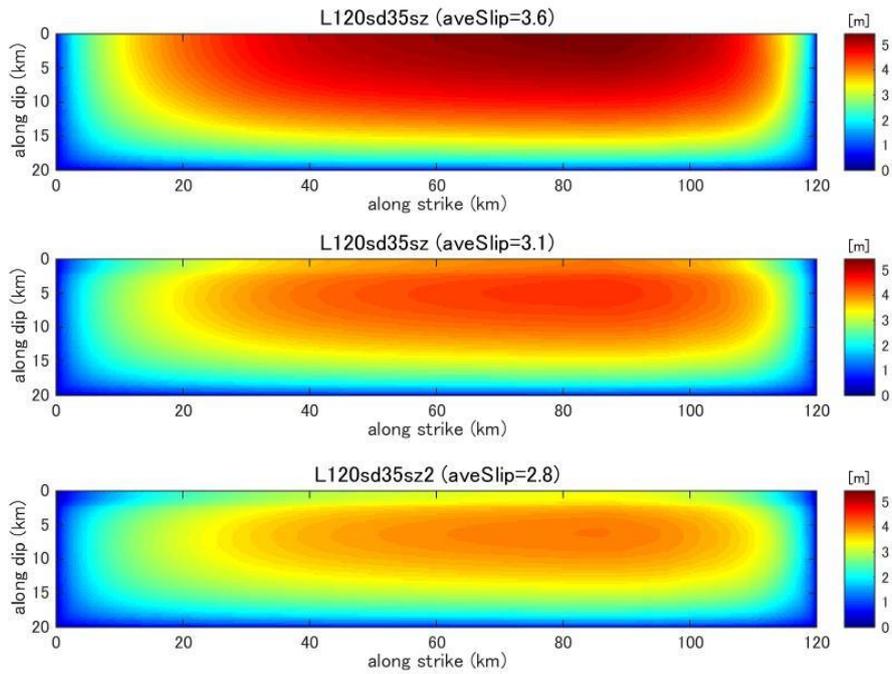
Figure C11. Final slip distribution predicted by dynamic rupture model for a fault with fault length 40km and stress drop 3.5MPa.
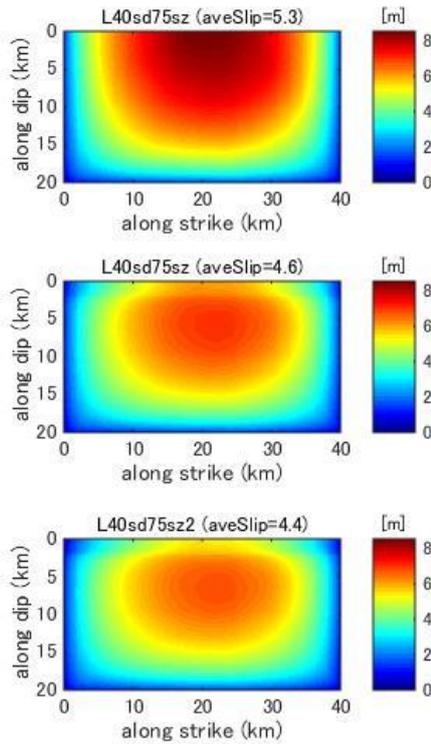
Figure C12. Final slip distribution predicted by dynamic rupture model for a fault with fault length 40km and stress drop 7.5MPa.
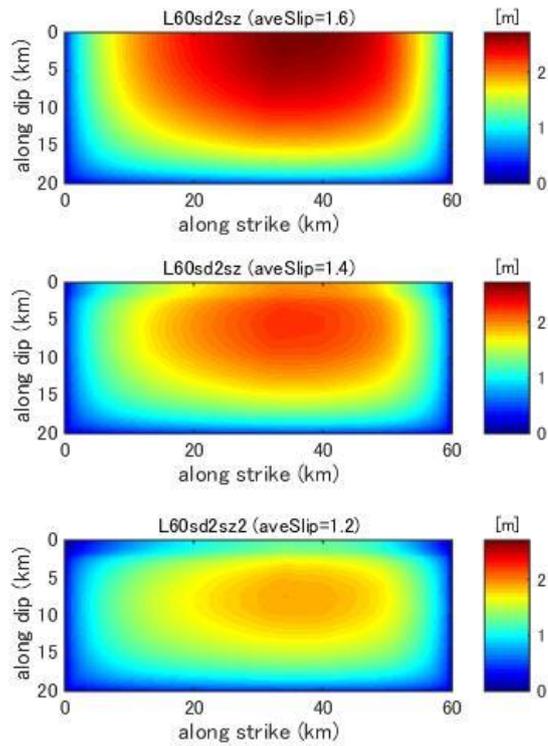
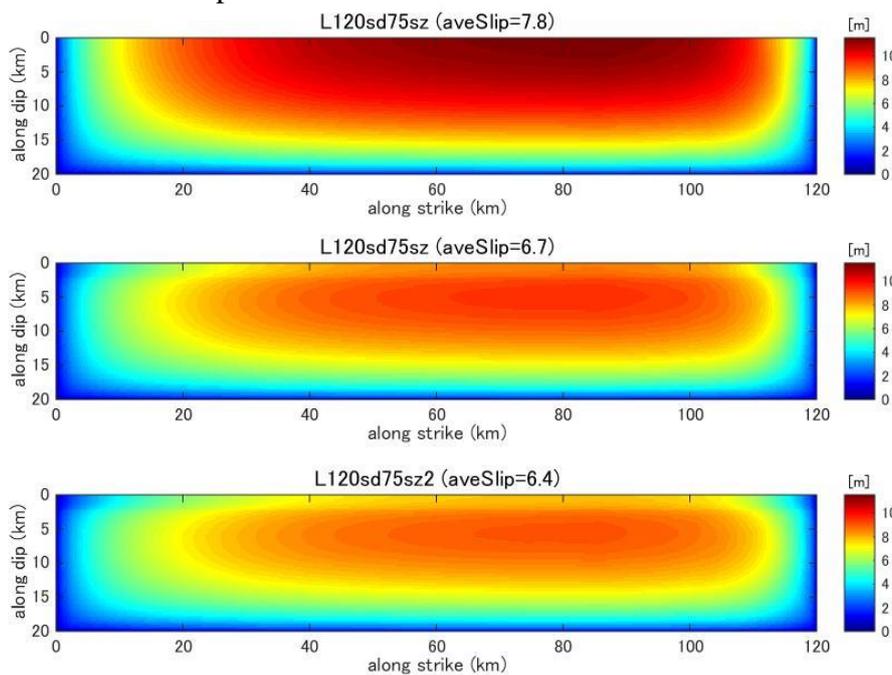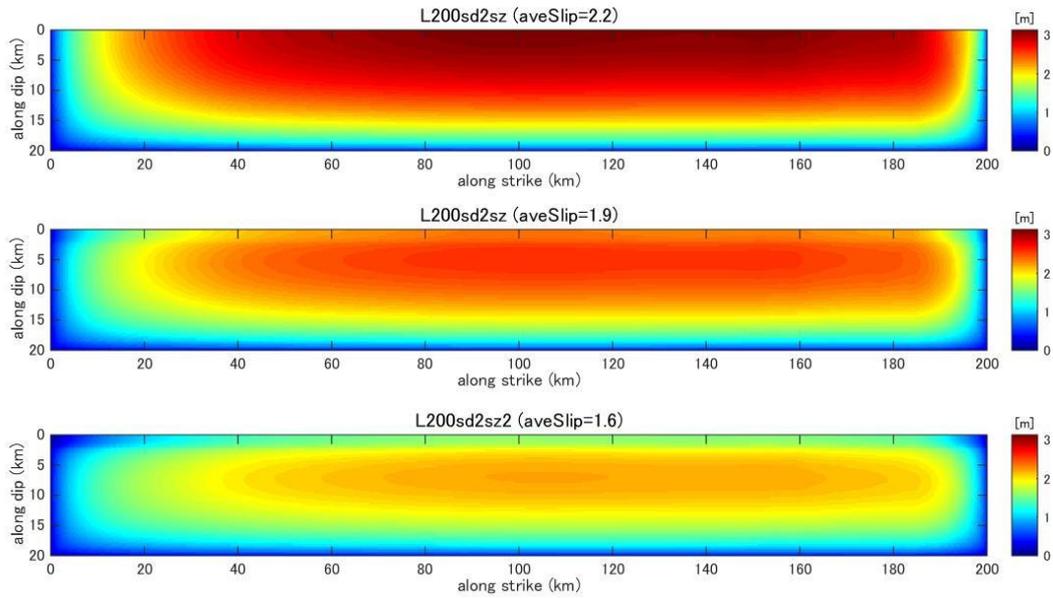**Figure C13.** Final slip distribution predicted by dynamic rupture model for a fault with fault length 60km and stress drop 2.0MPa. [Top] no shallow zone model; [middle] weak shallow zone stress drop 0.0MPa; [bottom] weak shallow zone stress drop -2.0MPa.
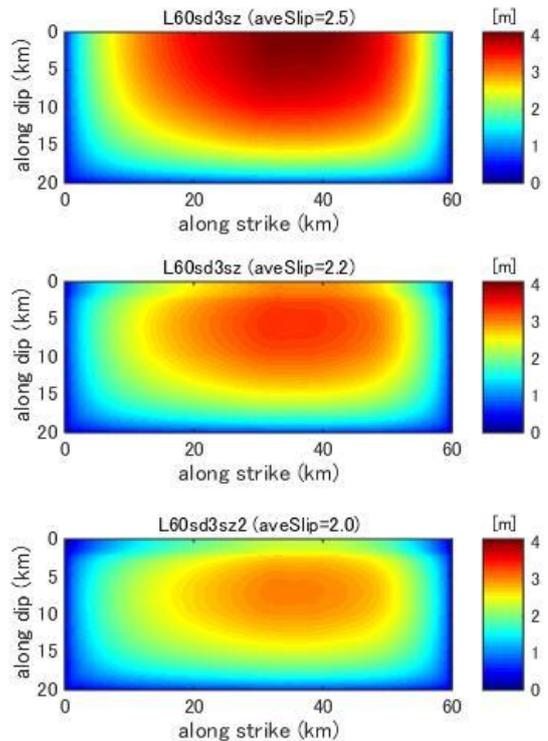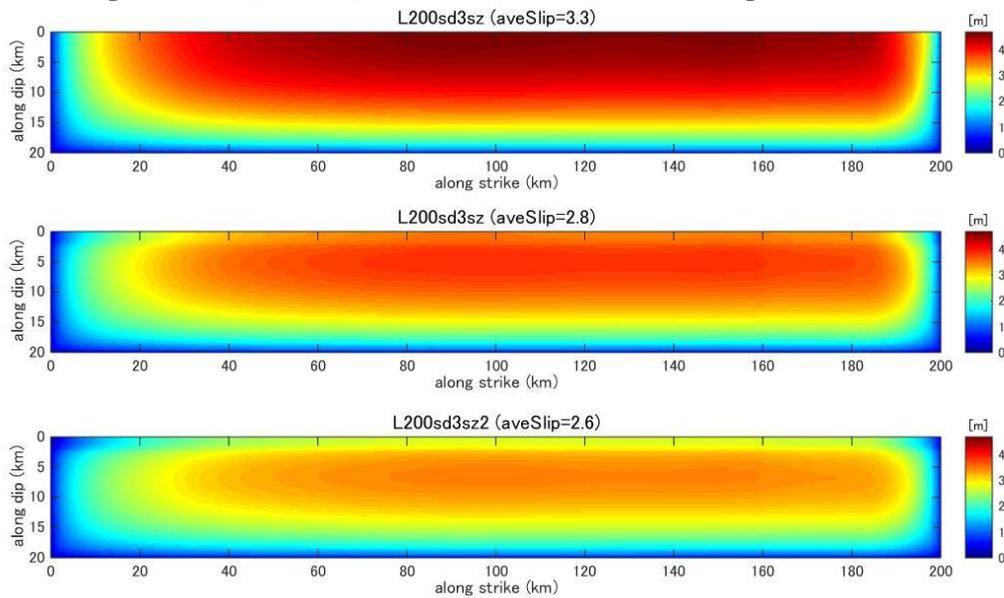

Figure C14. Final slip distribution predicted by dynamic rupture model for a fault with fault length 60km and stress drop 3.0MPa.
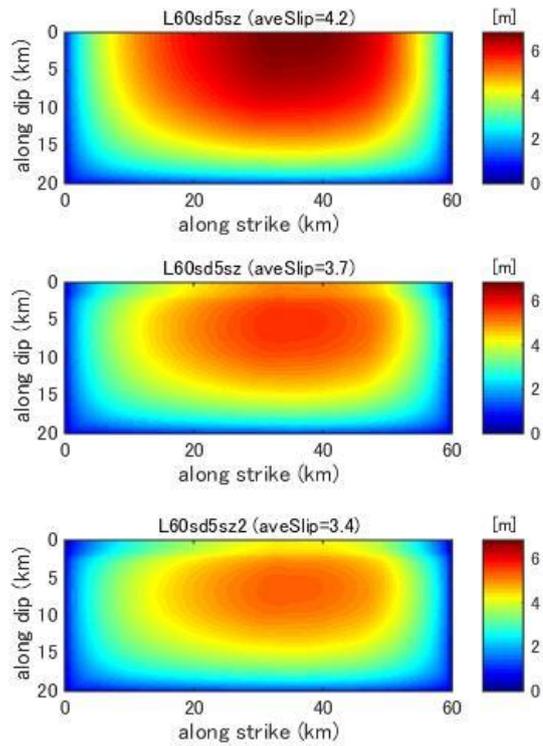
Figure C15. Final slip distribution predicted by dynamic rupture model for a fault with fault length 60km and stress drop 5.0MPa.
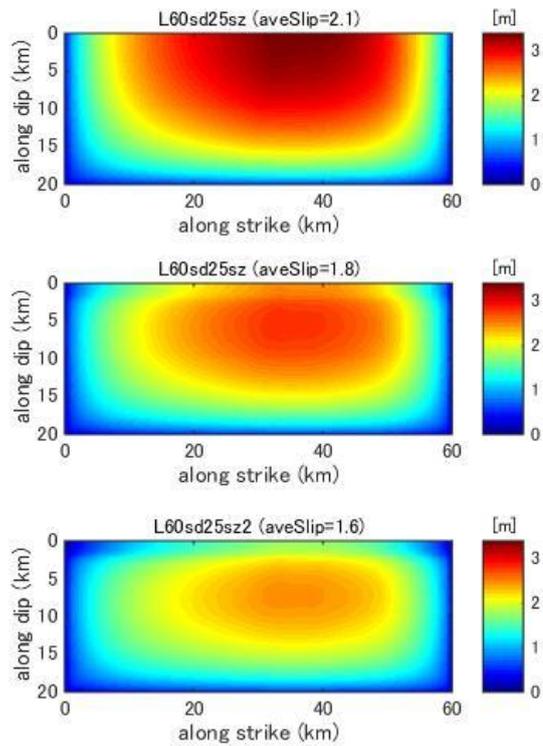
Figure C16. Final slip distribution predicted by dynamic rupture model for a fault with fault length 60km and stress drop 2.5MPa.
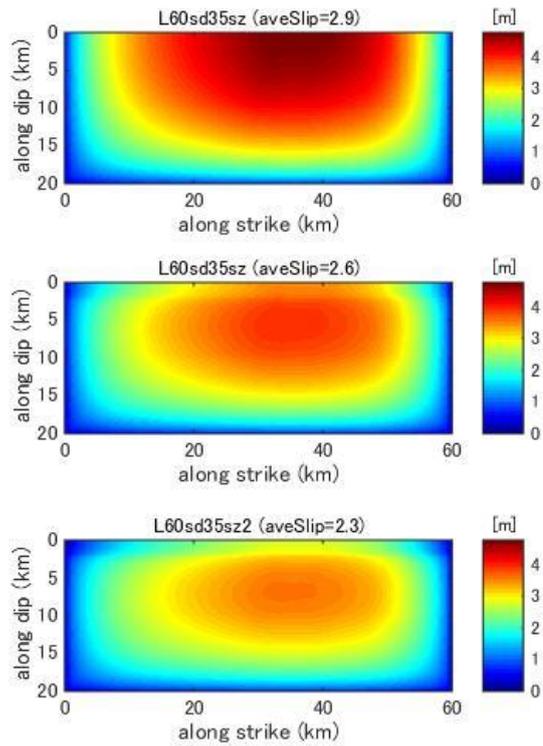
Figure C17. Final slip distribution predicted by dynamic rupture model for a fault with fault length 60km and stress drop 3.5MPa.
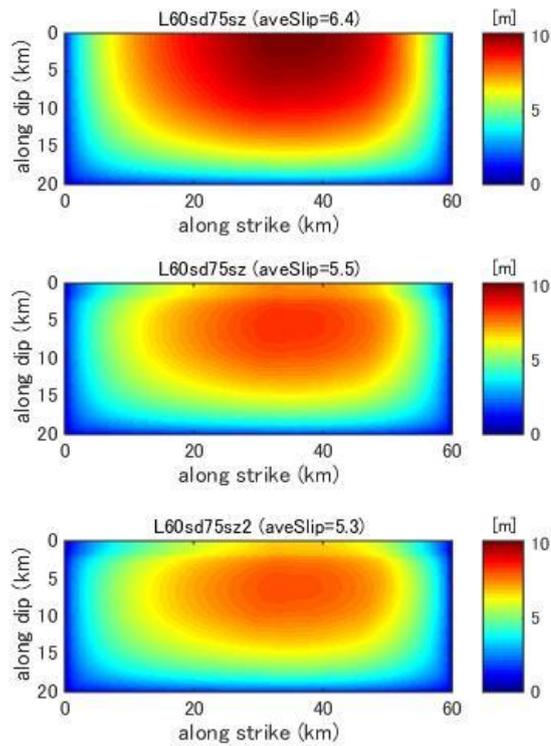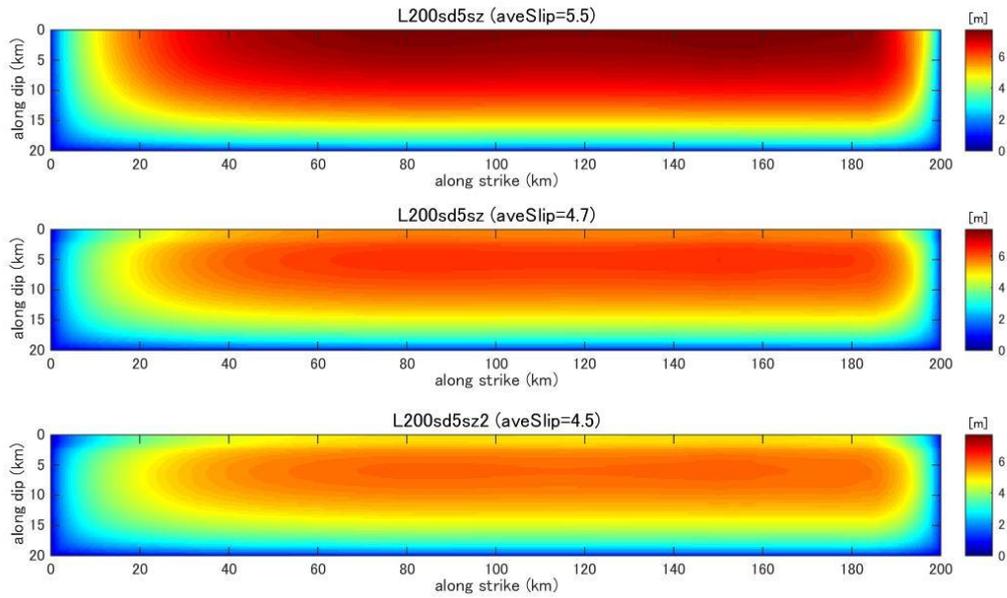

Figure C18. Final slip distribution predicted by dynamic rupture model for a fault with fault length 60km and stress drop 7.5MPa.
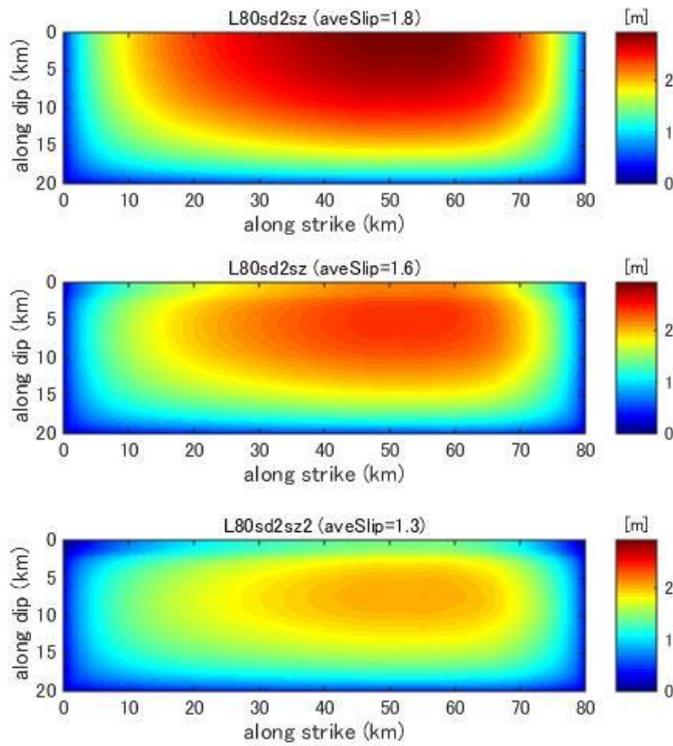
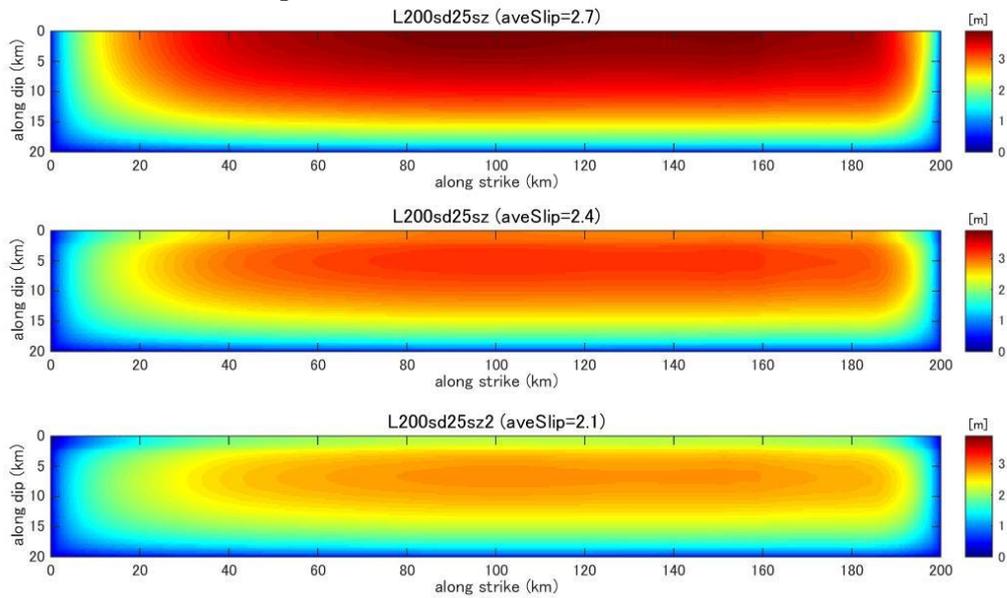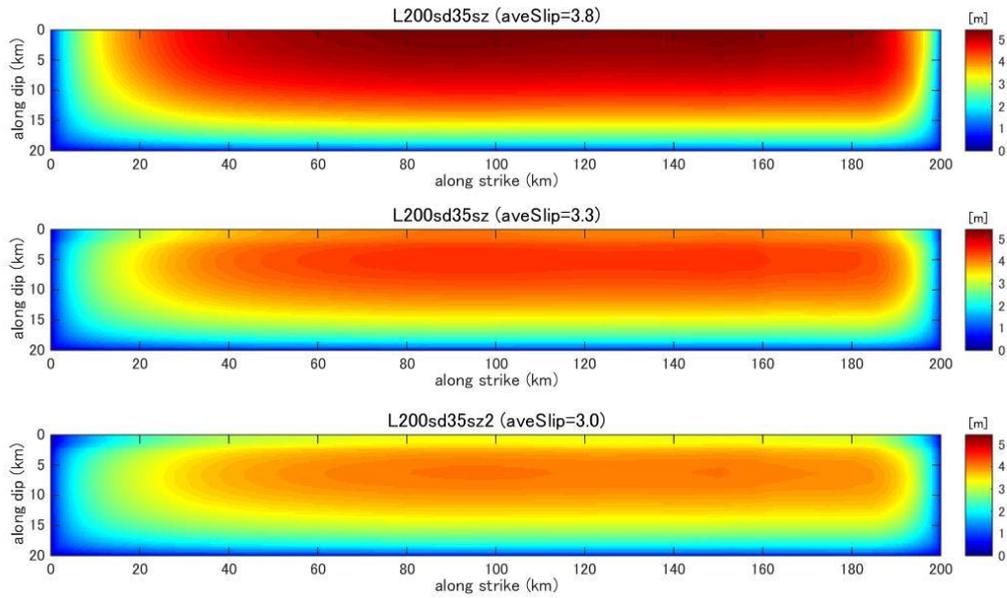**Figure C19.** Final slip distribution predicted by dynamic rupture model for a fault with fault length 80km and stress drop 2.0MPa. [Top] no shallow zone model; [middle] weak shallow zone stress drop 0.0MPa; [bottom] weak shallow zone stress drop -2.0MPa.
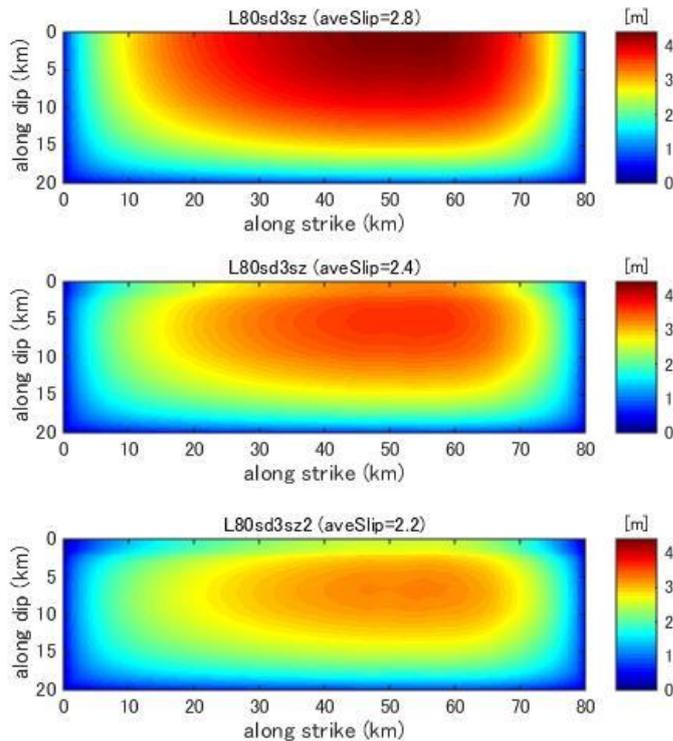
Figure C20. Final slip distribution predicted by dynamic rupture model for a fault with fault length 80km and stress drop 3.0MPa.
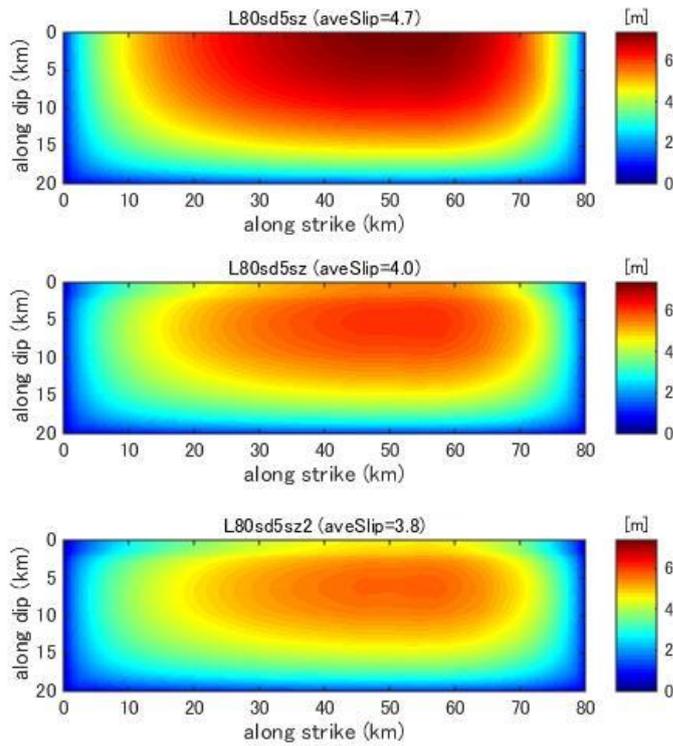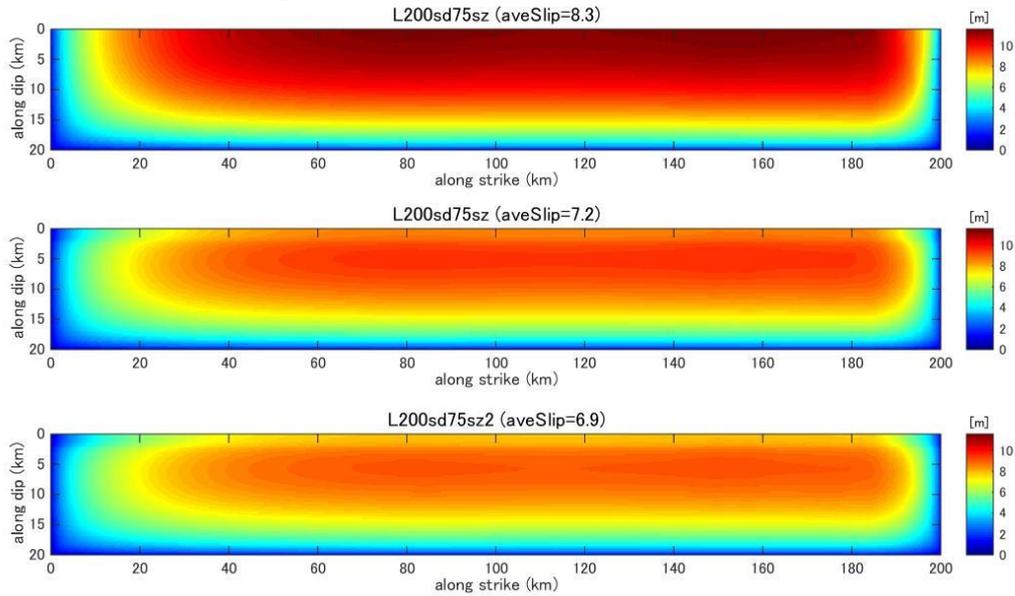
Figure C21. Final slip distribution predicted by dynamic rupture model for a fault with fault length 80km and stress drop 5.0MPa.
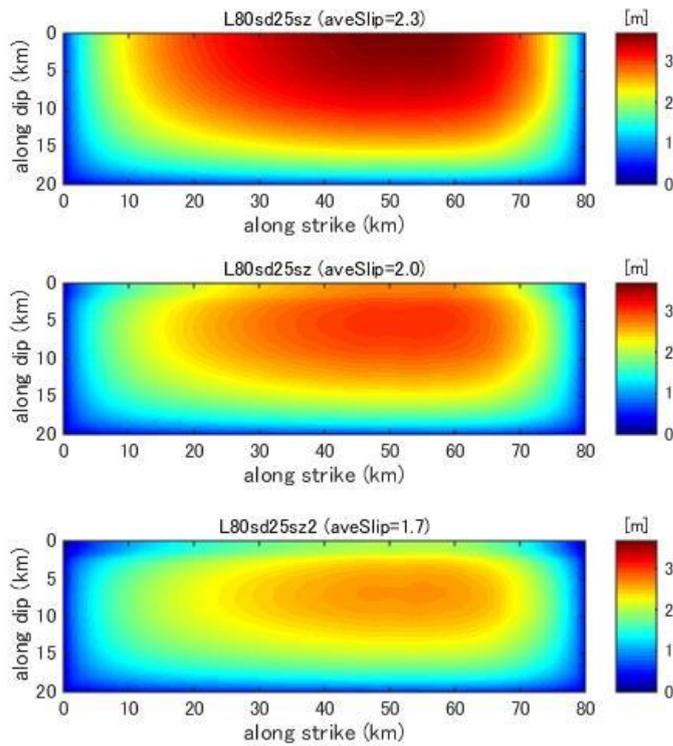
Figure C22. Final slip distribution predicted by dynamic rupture model for a fault with fault length 80km and stress drop 2.5MPa.
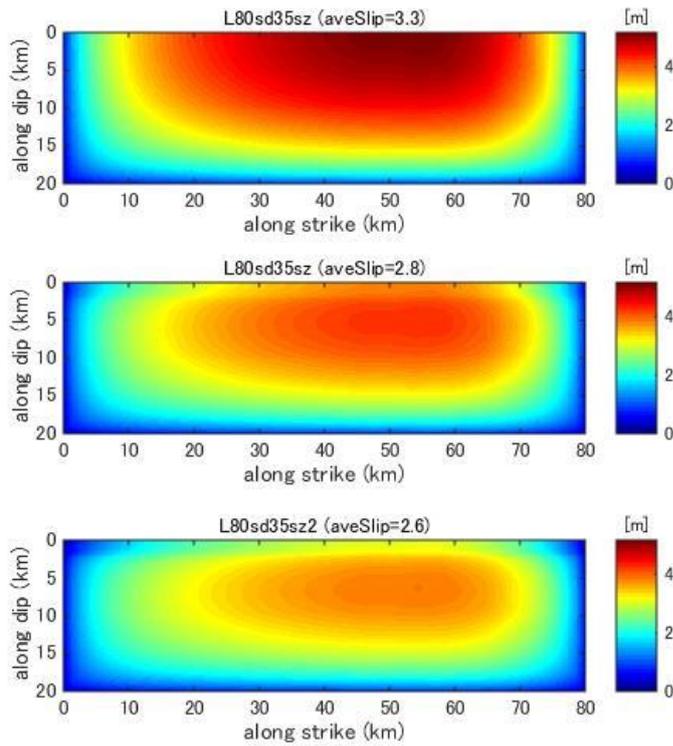
Figure C23. Final slip distribution predicted by dynamic rupture model for a fault with fault length 80km and stress drop 3.5MPa.
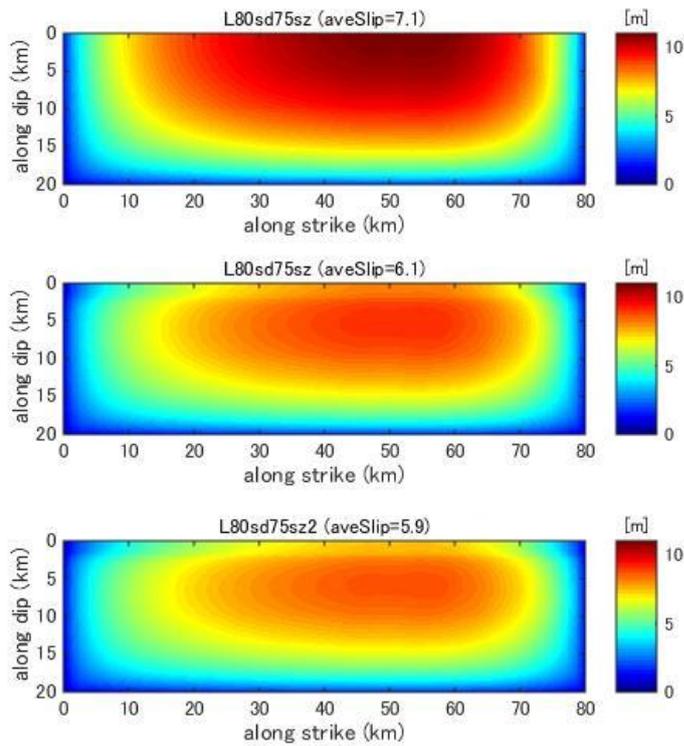
Figure C24. Final slip distribution predicted by dynamic rupture model for a fault with fault length 80km and stress drop 7.5MPa.
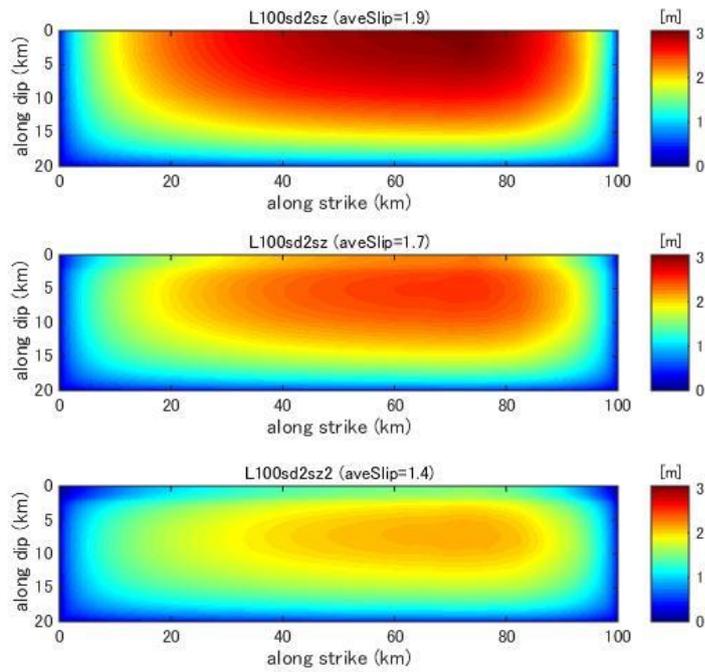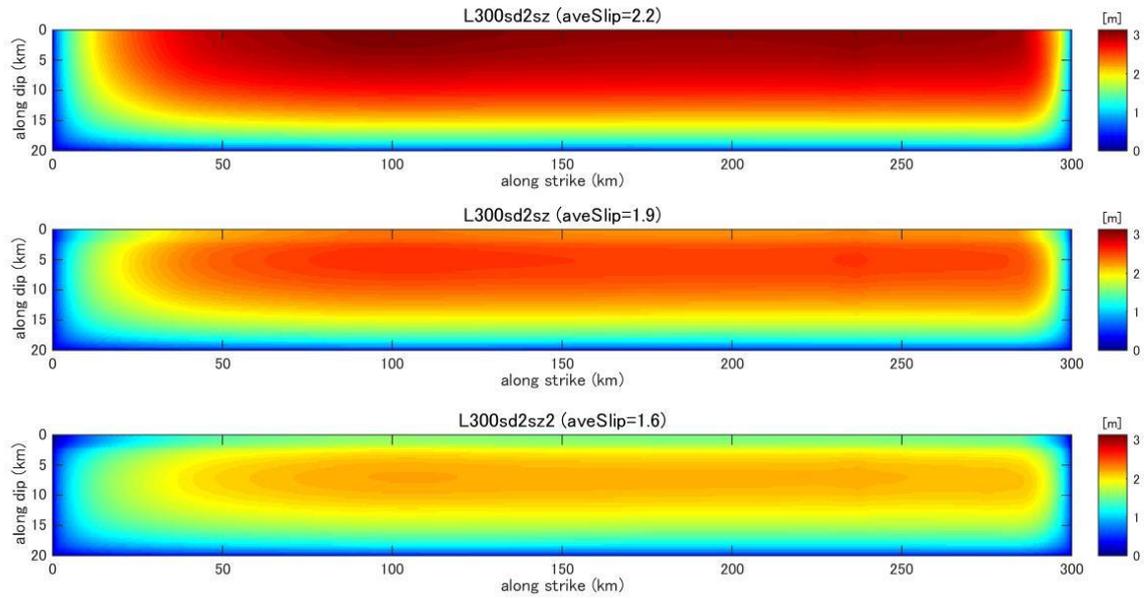
Figure C25. Final slip distribution predicted by dynamic rupture model for a fault with fault length 100km and stress drop 2.0MPa. [Top] no shallow zone model; [middle] weak shallow zone stress drop 0.0MPa; [bottom] weak shallow zone stress drop -2.0MPa.
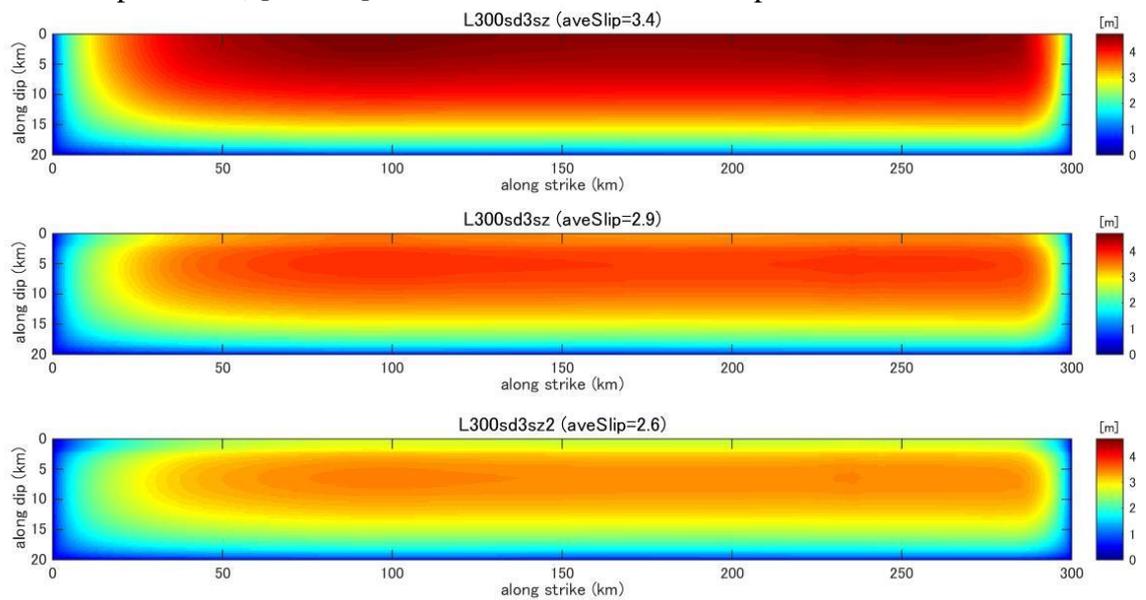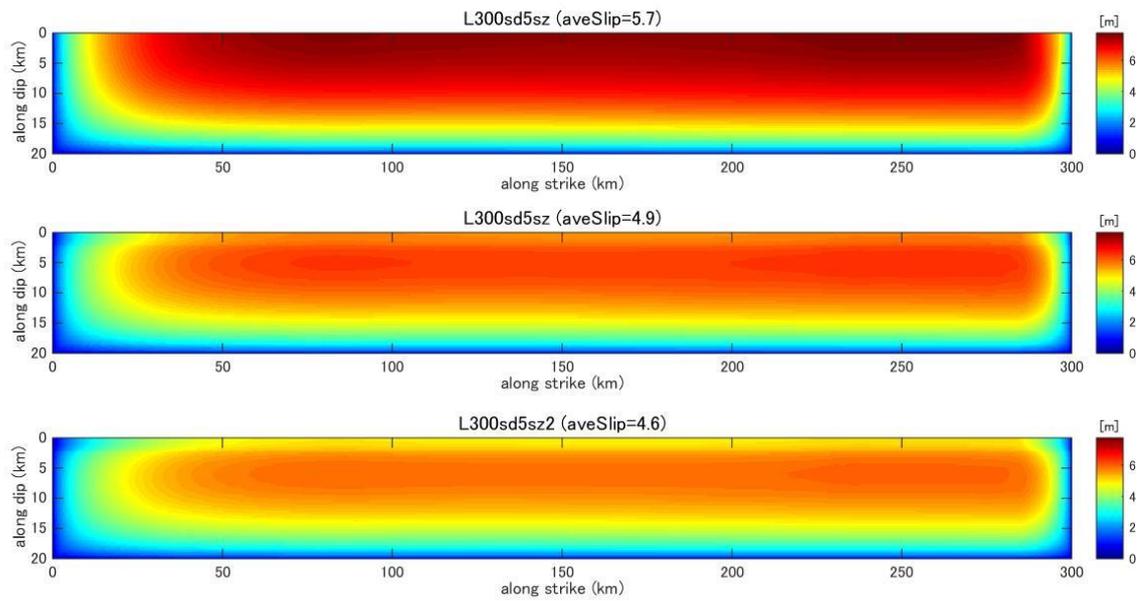

Figure C26. Final slip distribution predicted by dynamic rupture model for a fault with fault length 100km and stress drop 3.0MPa.

Figure C27. Final slip distribution predicted by dynamic rupture model for a fault with fault length 100km and stress drop 5.0MPa.
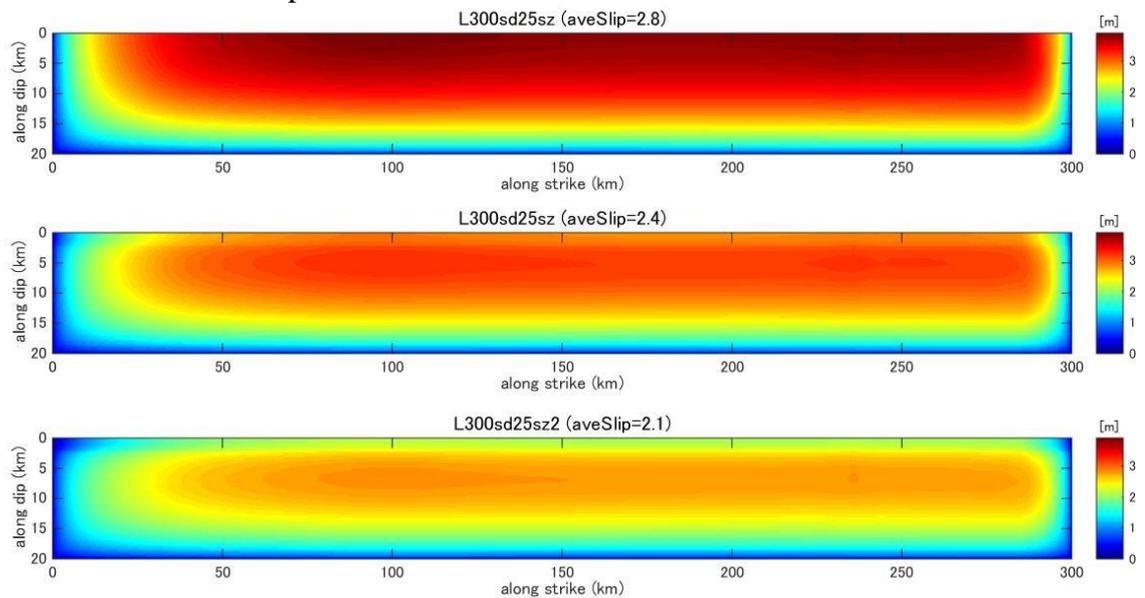

Figure C28. Final slip distribution predicted by dynamic rupture model for a fault with fault length 100km and stress drop 2.5MPa.
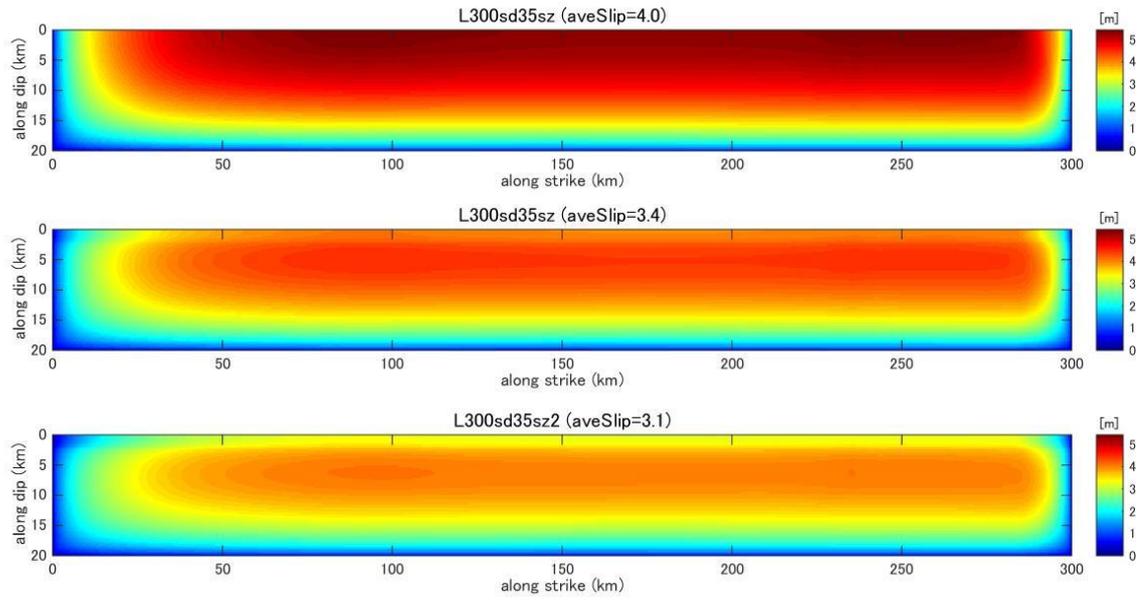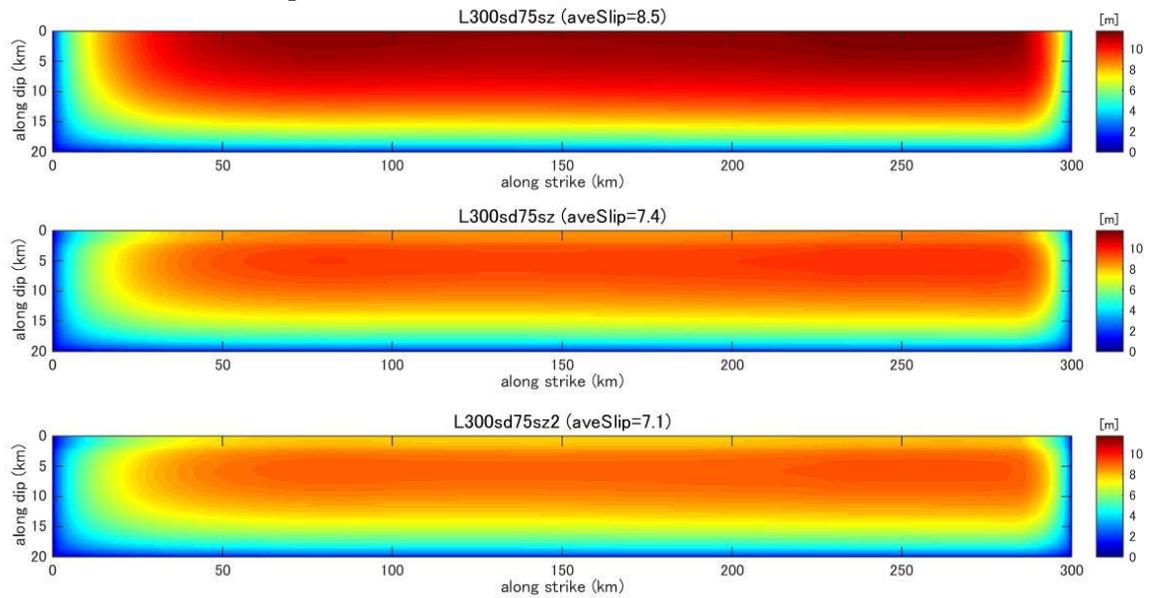
A-45

Figure C29. Final slip distribution predicted by dynamic rupture model for a fault with fault length 100km and stress drop 3.5MPa.

Figure C30. Final slip distribution predicted by dynamic rupture model for a fault with fault length 100km and stress drop 7.5MPa.
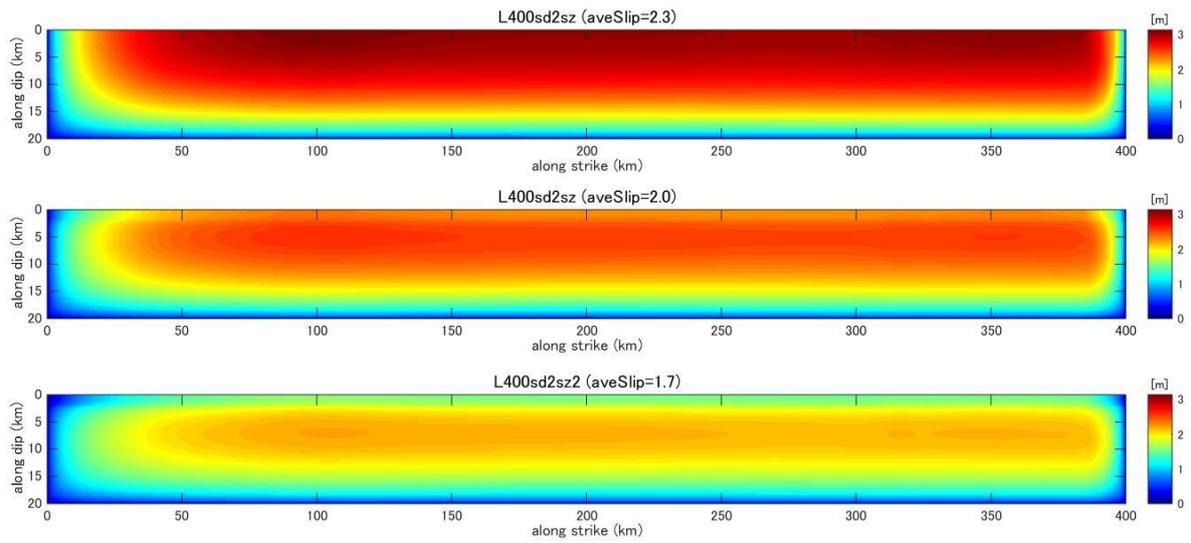
Figure C31. Final slip distribution predicted by dynamic rupture model for a fault with fault length 120km and stress drop 2.0MPa. [Top] no shallow zone model; [middle] weak shallow zone stress drop 0.0MPa; [bottom] weak shallow zone stress drop -2.0MPa.
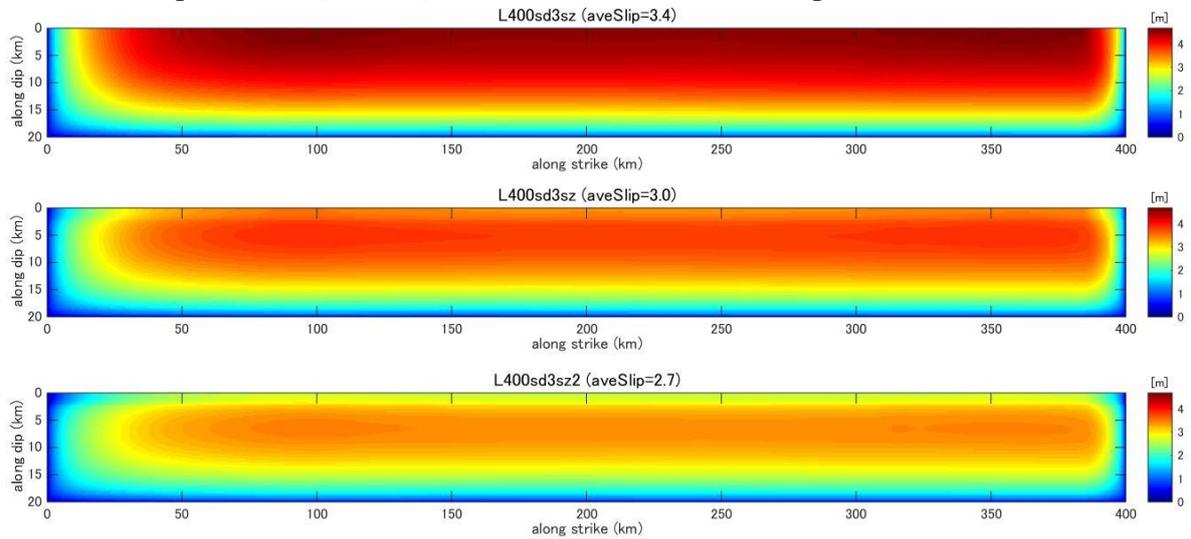

Figure C32. Final slip distribution predicted by dynamic rupture model for a fault with fault length 120km and stress drop 3.0MPa.
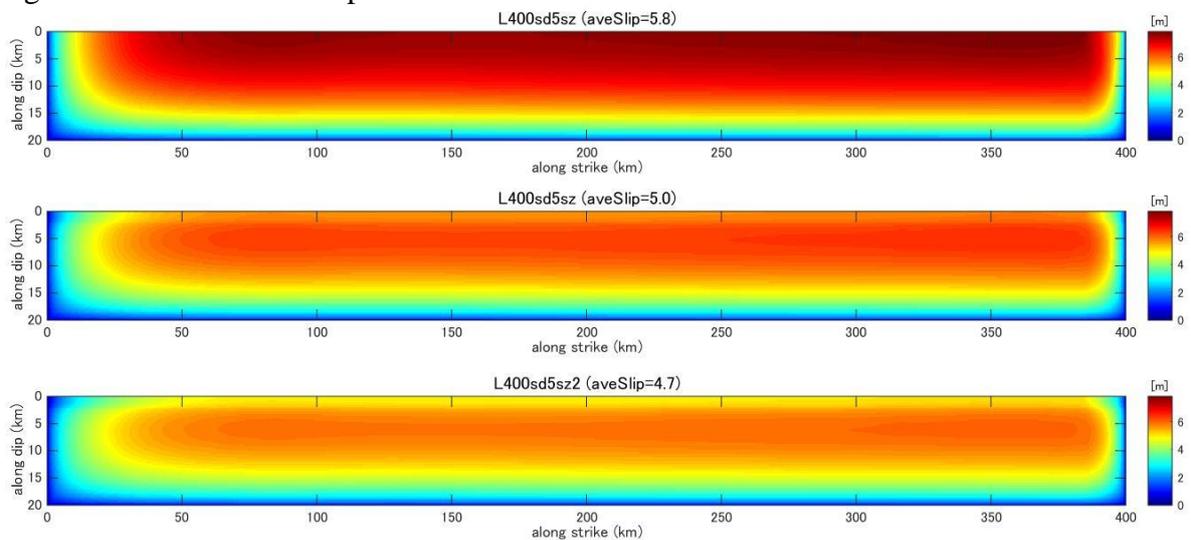
Figure C33. Final slip distribution predicted by dynamic rupture model for a fault with fault length 120km and stress drop 5.0MPa.

Figure C34 Final slip distribution predicted by dynamic rupture model for a fault with fault length 120km and stress drop 2.5MPa.

Figure C35. Final slip distribution predicted by dynamic rupture model for a fault with fault length 120km and stress drop 3.5MPa.
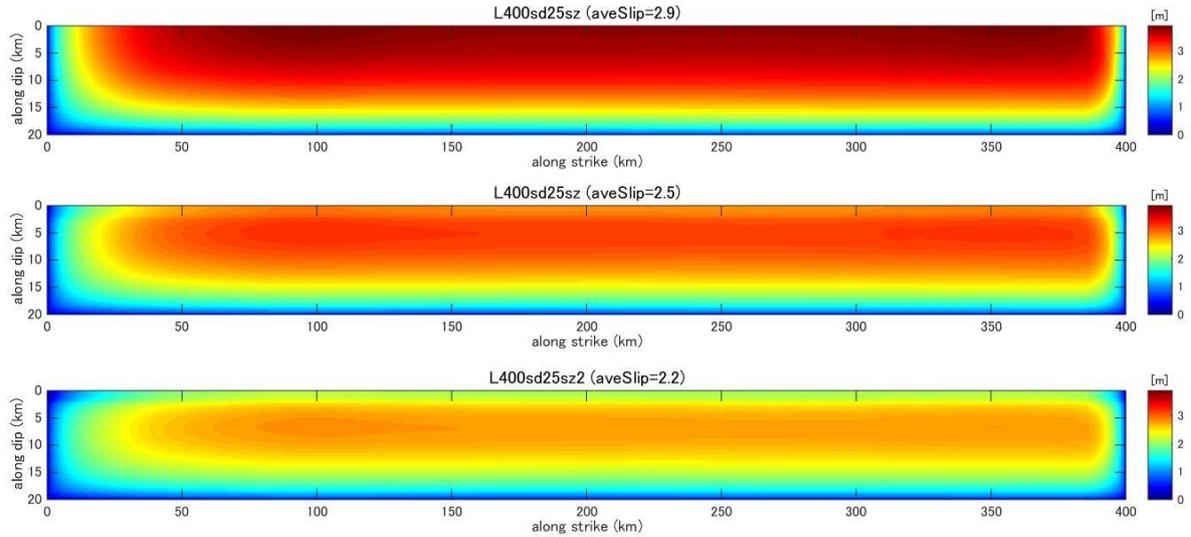

Figure C36. Final slip distribution predicted by dynamic rupture model for a fault with fault length 120km and stress drop 7.5MPa.

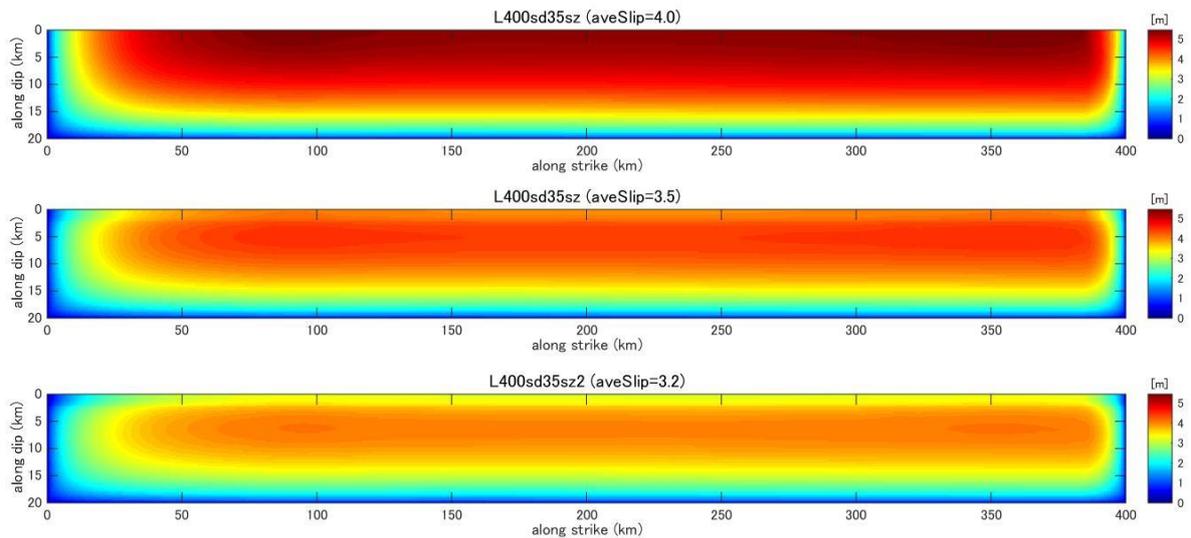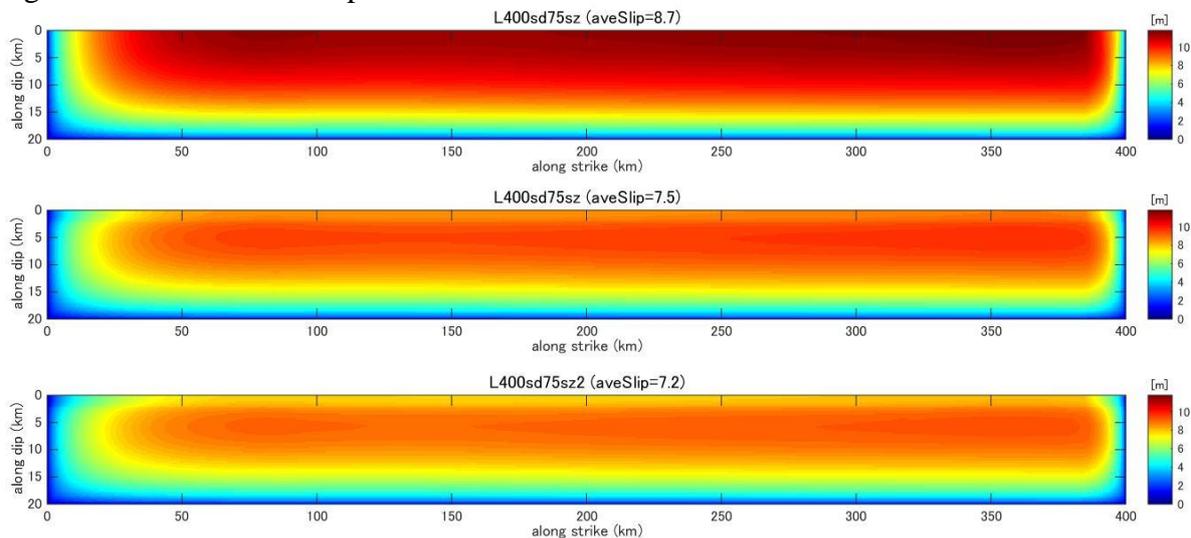**Figure C37.** Final slip distribution predicted by dynamic rupture model for a fault with fault length 200km and stress drop 2.0MPa. [Top] no shallow zone model; [middle] weak shallow zone stress drop 0.0MPa; [bottom] weak shallow zone stress drop -2.0MPa.

Figure C38. Final slip distribution predicted by dynamic rupture model for a fault with fault length 200km and stress drop 3.0MPa.

A-50

Figure C39. Final slip distribution predicted by dynamic rupture model for a fault with fault length 200km and stress drop 5.0MPa.

Figure C40. Final slip distribution predicted by dynamic rupture model for a fault with fault length 200km and stress drop 2.5MPa.

Figure C41. Final slip distribution predicted by dynamic rupture model for a fault with fault length 200km and stress drop 3.5MPa.
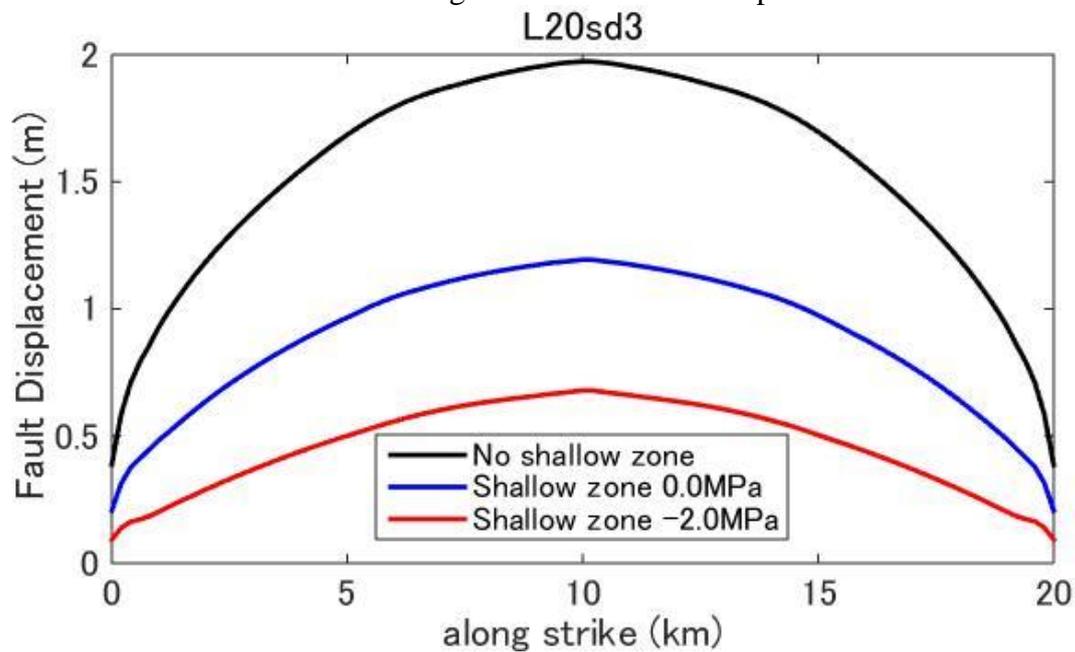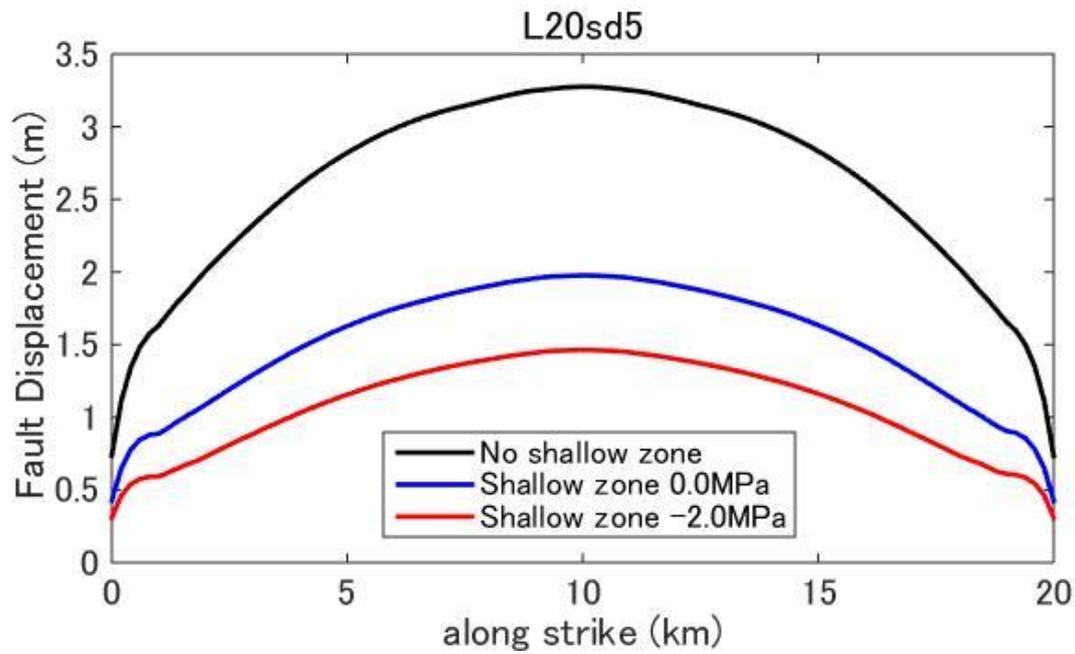

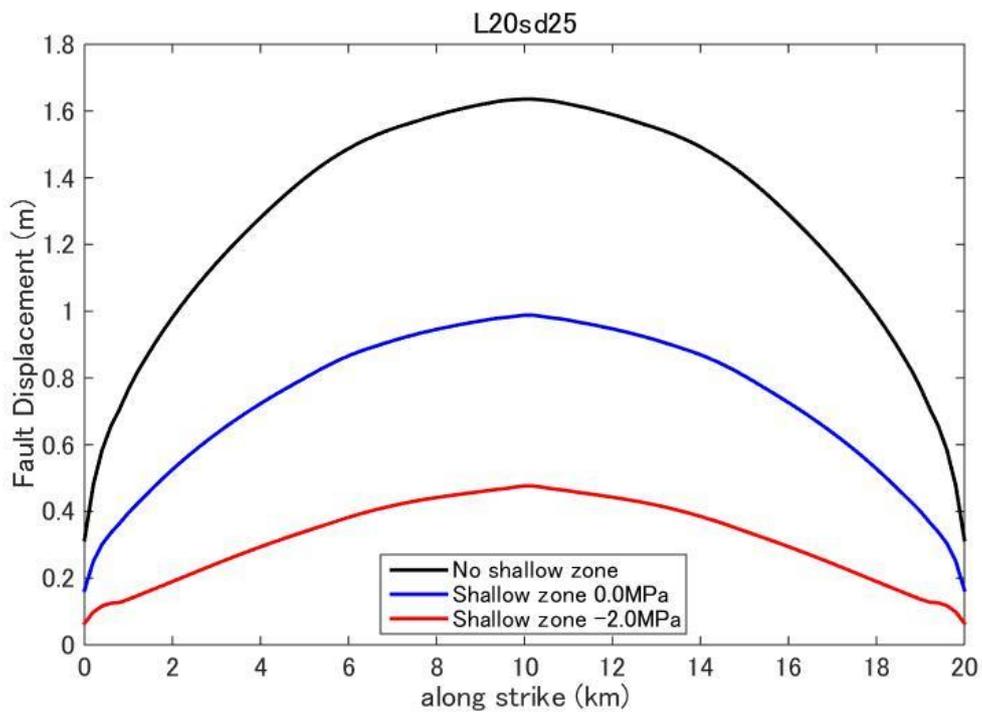**Figure C42.** Final slip distribution predicted by dynamic rupture model for a fault with fault length 200km and stress drop 7.5MPa.

Figure C43. Final slip distribution predicted by dynamic rupture model for a fault with fault length 300km and stress drop 2.0MPa. [Top] no shallow zone model; [middle] weak shallow zone stress drop 0.0MPa; [bottom] weak shallow zone stress drop -2.0MPa.

Figure C44. Final slip distribution predicted by dynamic rupture model for a fault with fault length 300km and stress drop 3.0MPa.

Figure C45. Final slip distribution predicted by dynamic rupture model for a fault with fault length 300km and stress drop 5.0MPa.

Figure C46. Final slip distribution predicted by dynamic rupture model for a fault with fault length 300km and stress drop 2.5MPa.

Figure C47. Final slip distribution predicted by dynamic rupture model for a fault with fault length 300km and stress drop 3.5MPa.
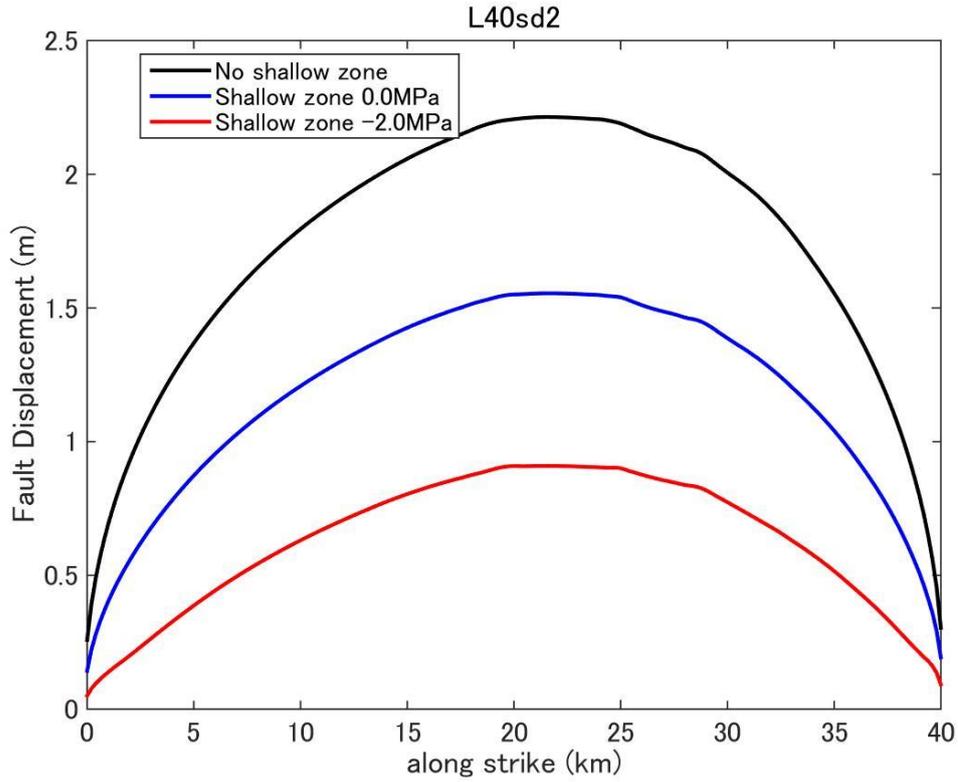

Figure C48. Final slip distribution predicted by dynamic rupture model for a fault with fault length 300km and stress drop 7.5MPa.

Figure C49. Final slip distribution predicted by dynamic rupture model for a fault with fault length 400km and stress drop 2.0MPa. [Top] no shallow zone model; [middle] weak shallow zone stress drop 0.0MPa; [bottom] weak shallow zone stress drop -2.0MPa.
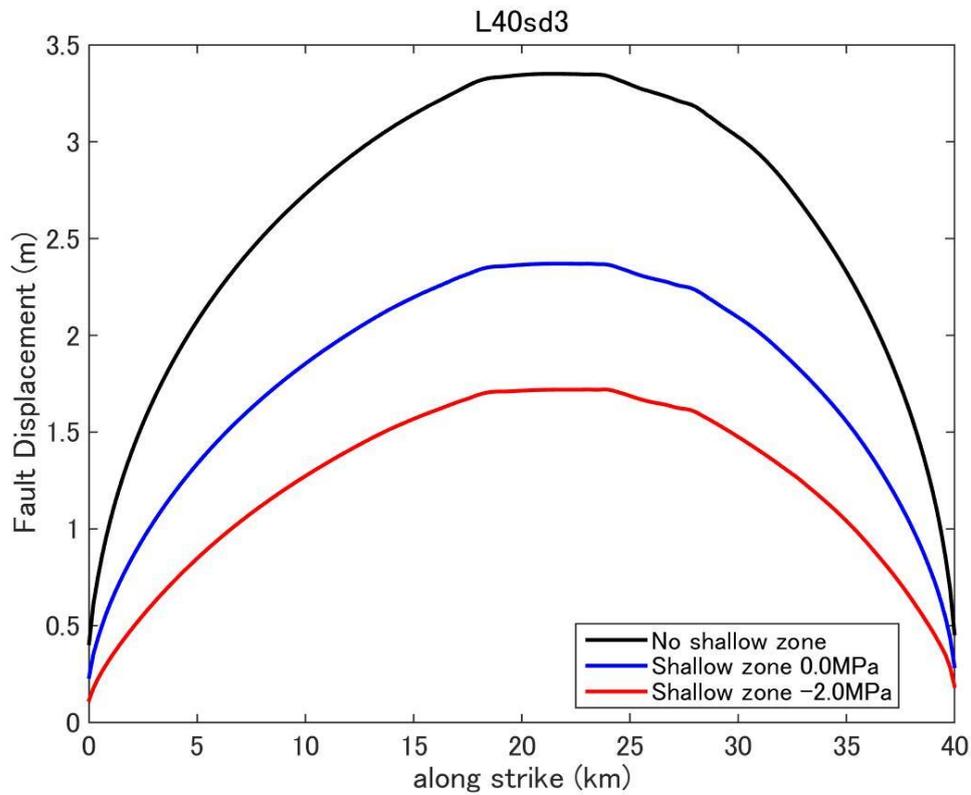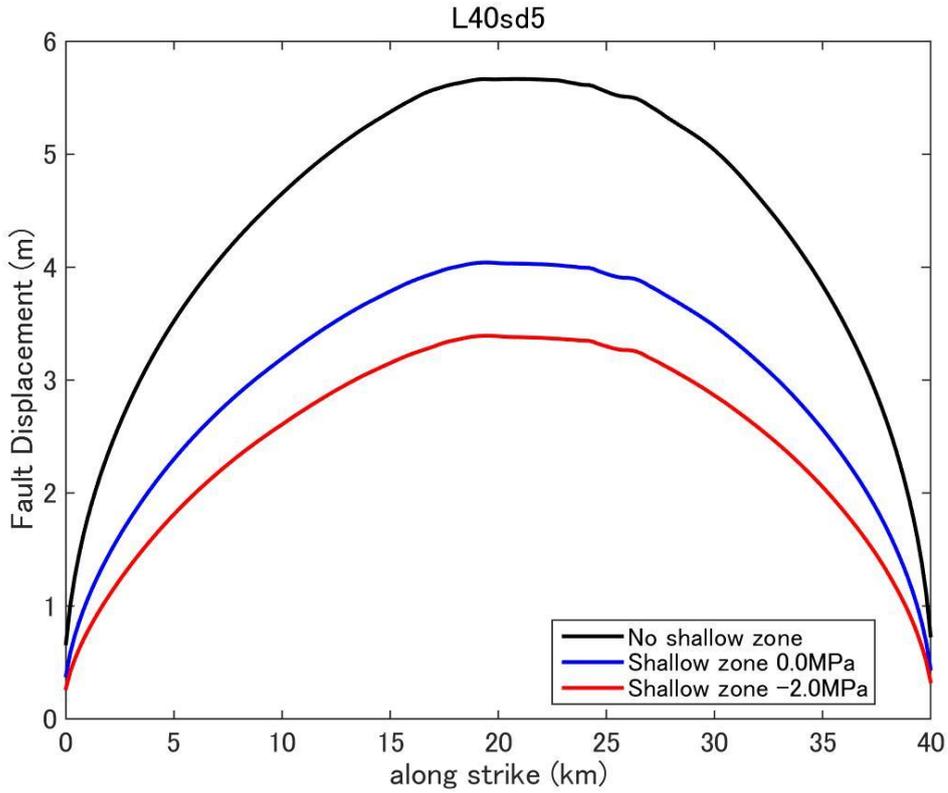

Figure C50. Final slip distribution predicted by dynamic rupture model for a fault with fault length 400km and stress drop 3.0MPa.

Figure C51. Final slip distribution predicted by dynamic rupture model for a fault with fault

length 400km and stress drop 5.0MPa.

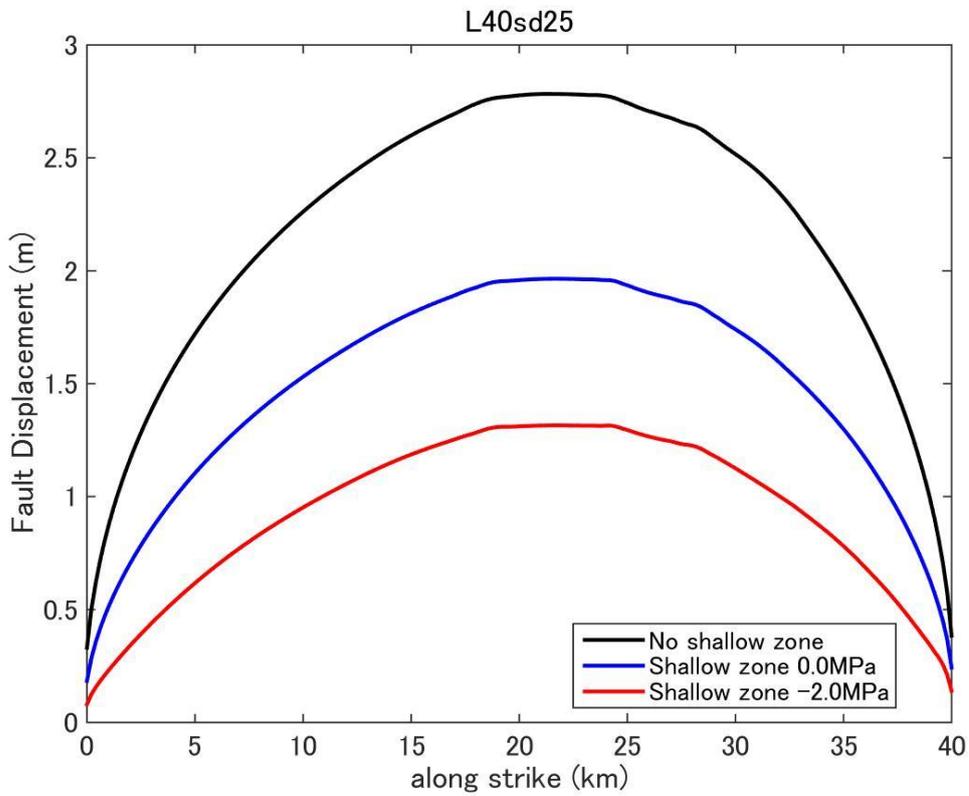**Figure C52.** Final slip distribution predicted by dynamic rupture model for a fault with fault length 400km and stress drop 2.5MPa.

Figure C53. Final slip distribution predicted by dynamic rupture model for a fault with fault length 400km and stress drop 3.5MPa.

Figure C54. Final slip distribution predicted by dynamic rupture model for a fault with fault length 400km and stress drop 7.5MPa.

Appendix D. Final fault displacement distribution from dynamic rupture models with uniform stress drop.
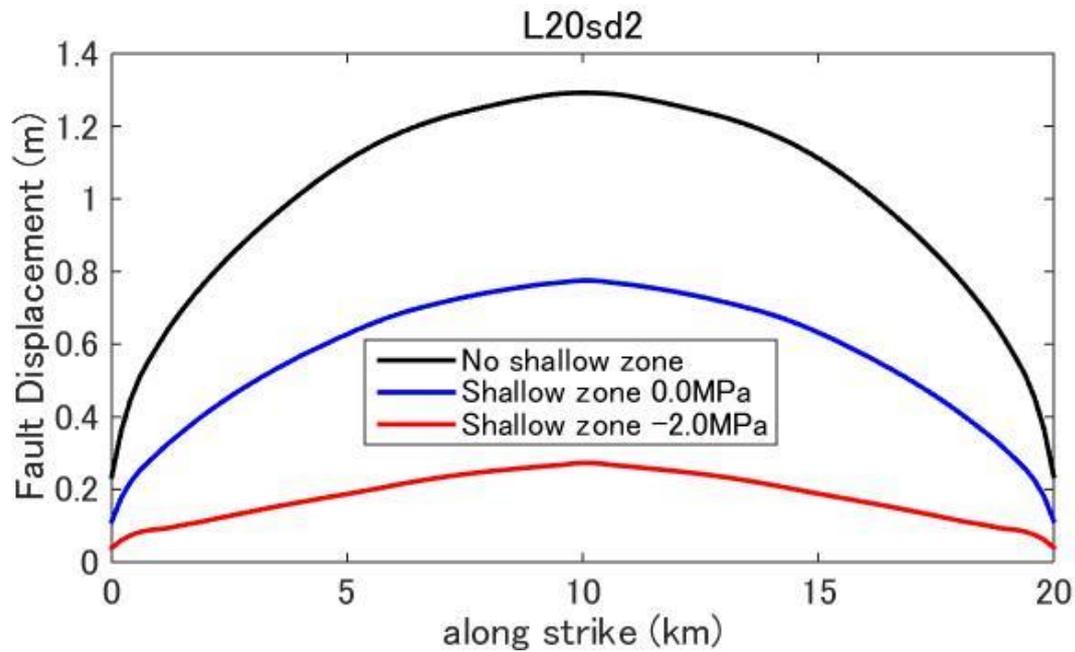
Figure D1. Fault displacement (surface rupture slip) distribution predicted by dynamic rupture model for a fault with fault length 20km and stress drop 2.0MPa.
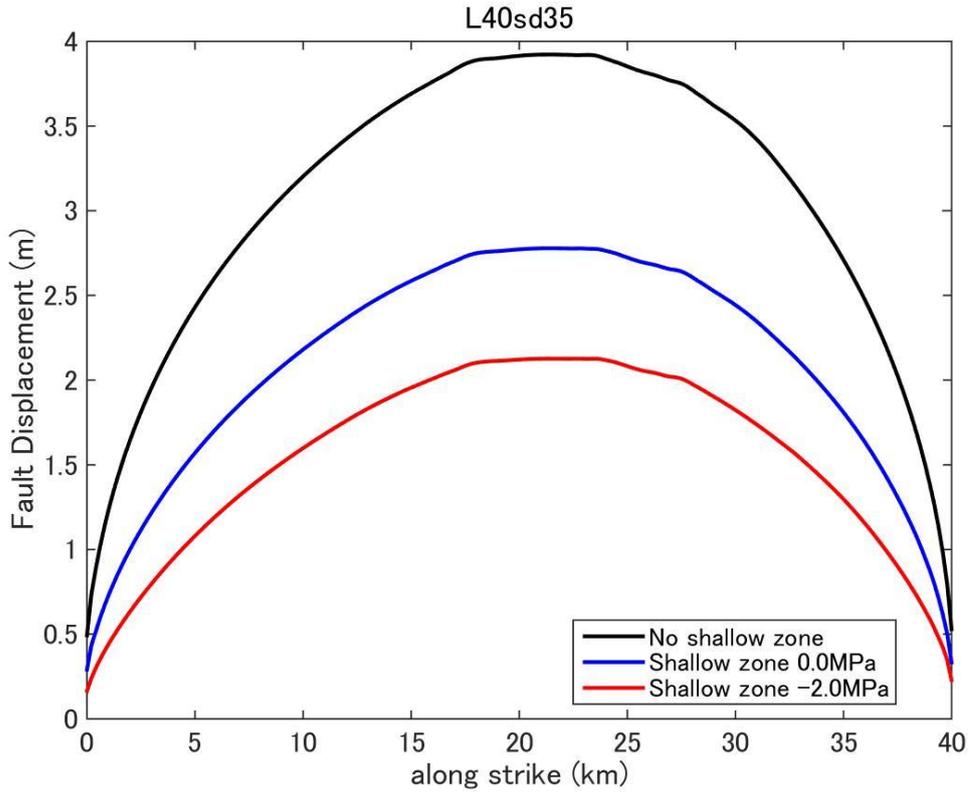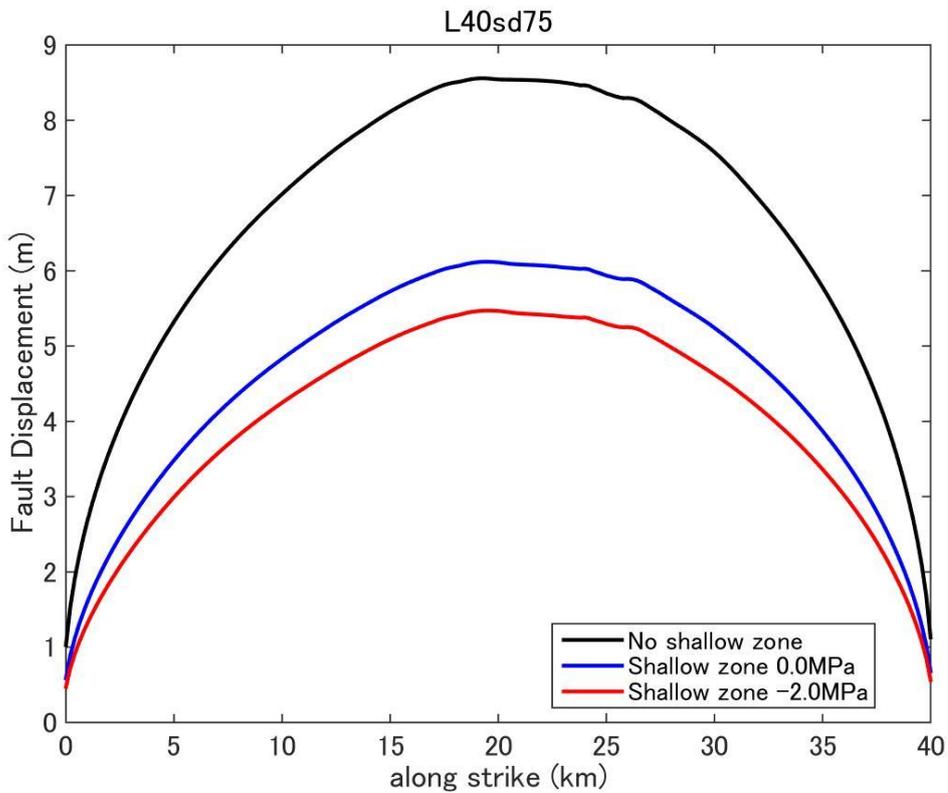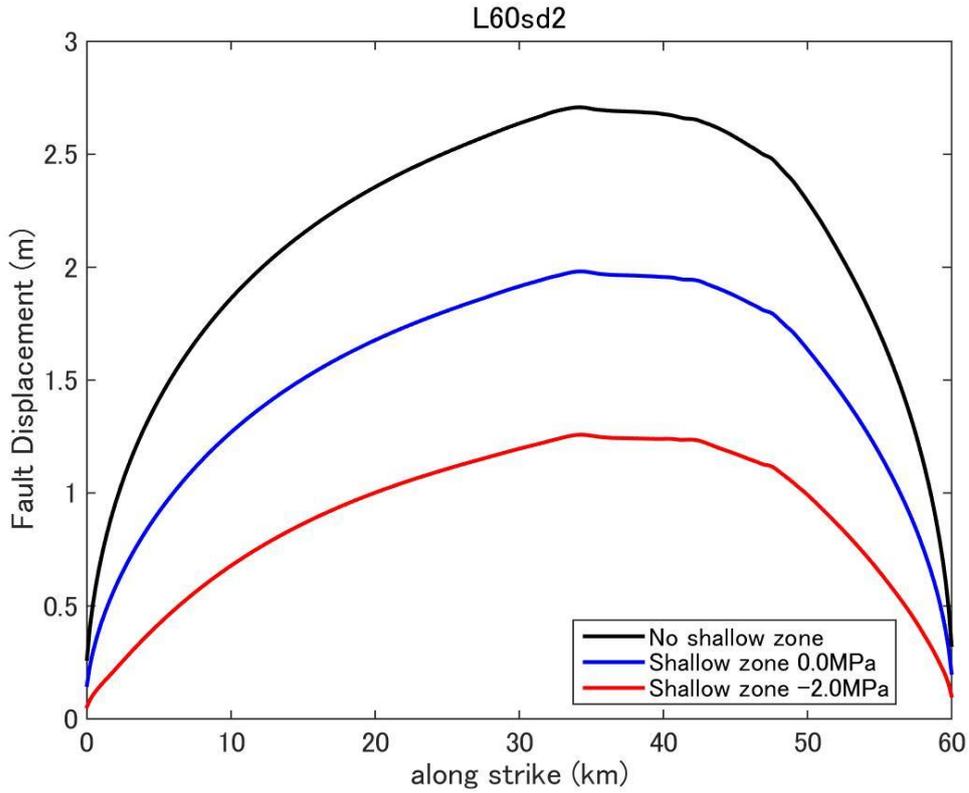

Figure D2. Fault displacement (surface rupture slip) distribution predicted by dynamic rupture model for a fault with fault length 20km and stress drop 3.0MPa.
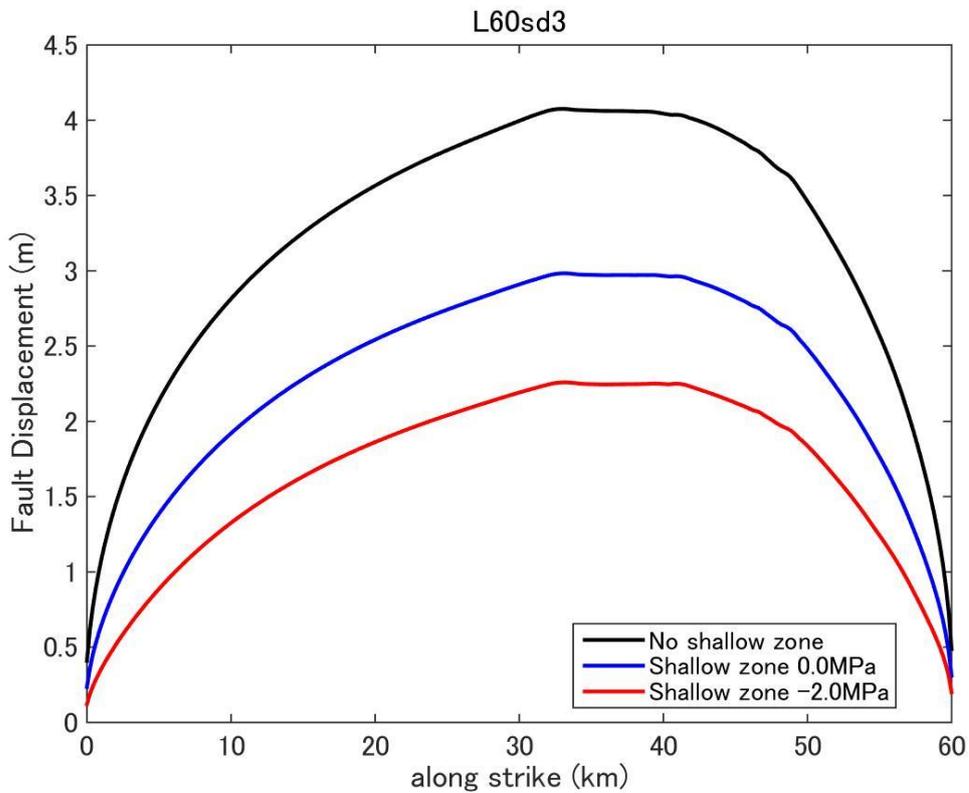
Figure D3. Fault displacement (surface rupture slip) distribution predicted by dynamic rupture model for a fault with fault length 20km and stress drop 5.0MPa.
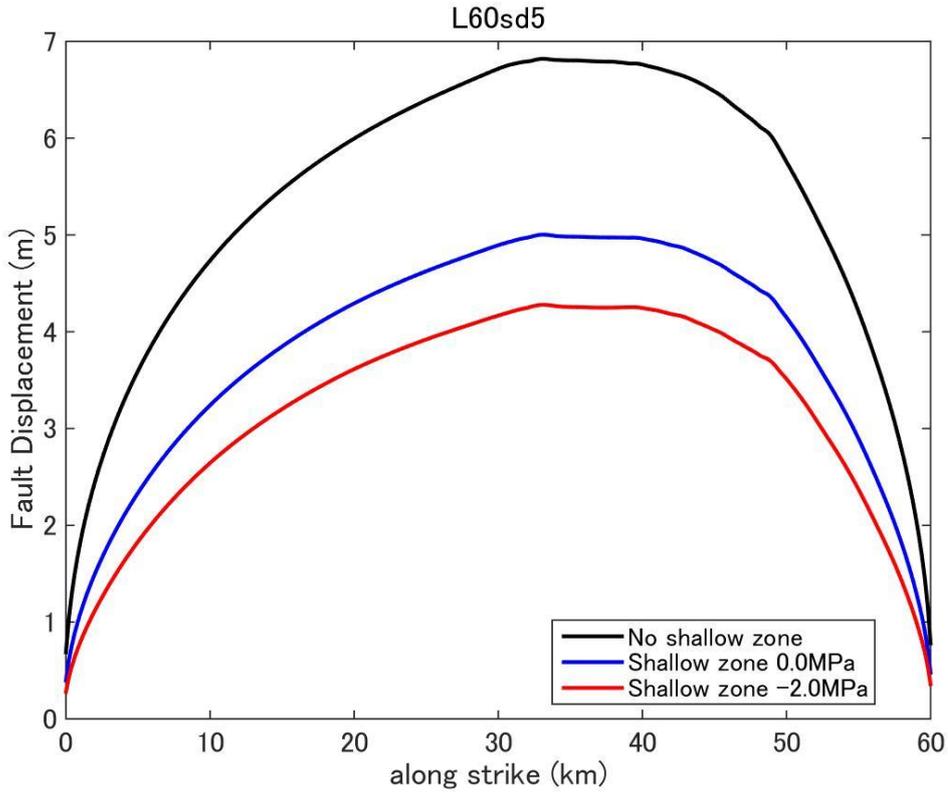

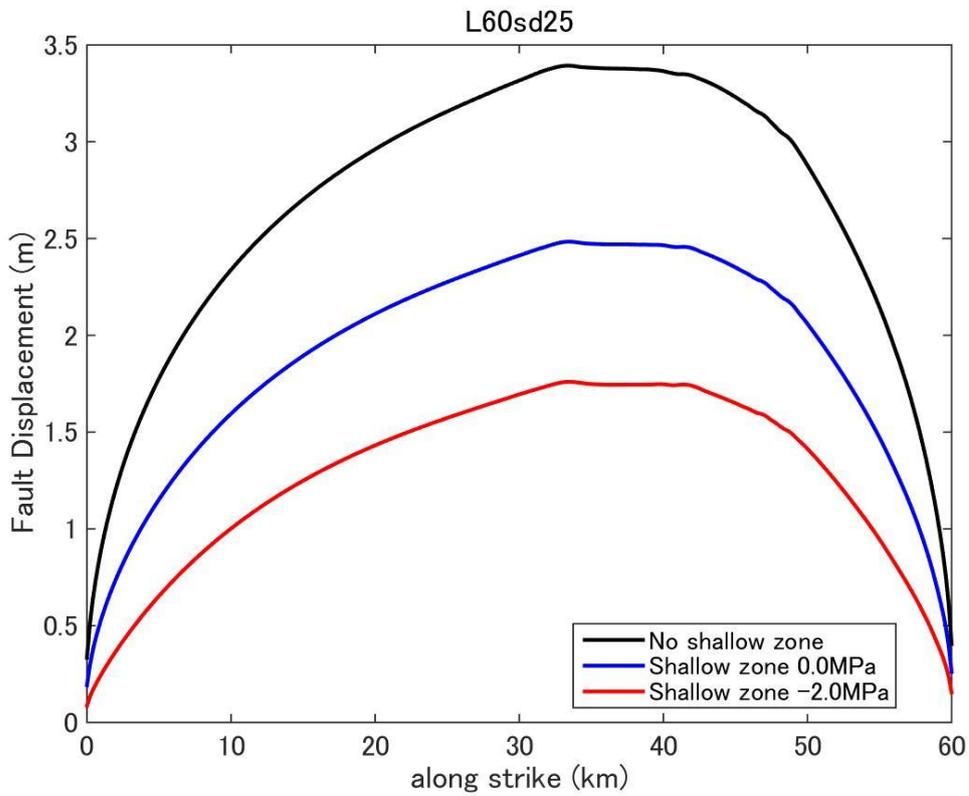**Figure D4.** Fault displacement (surface rupture slip) distribution predicted by dynamic rupture model for a fault with fault length 20km and stress drop 2.5MPa.
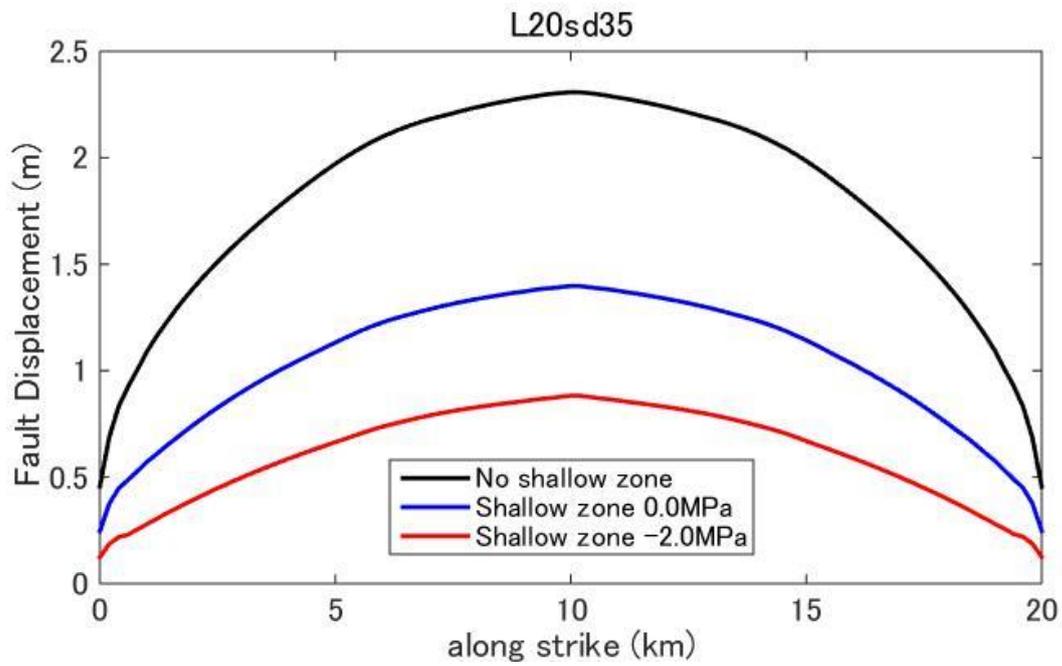
Figure D5. Fault displacement (surface rupture slip) distribution predicted by dynamic rupture model for a fault with fault length 20km and stress drop 3.5MPa.
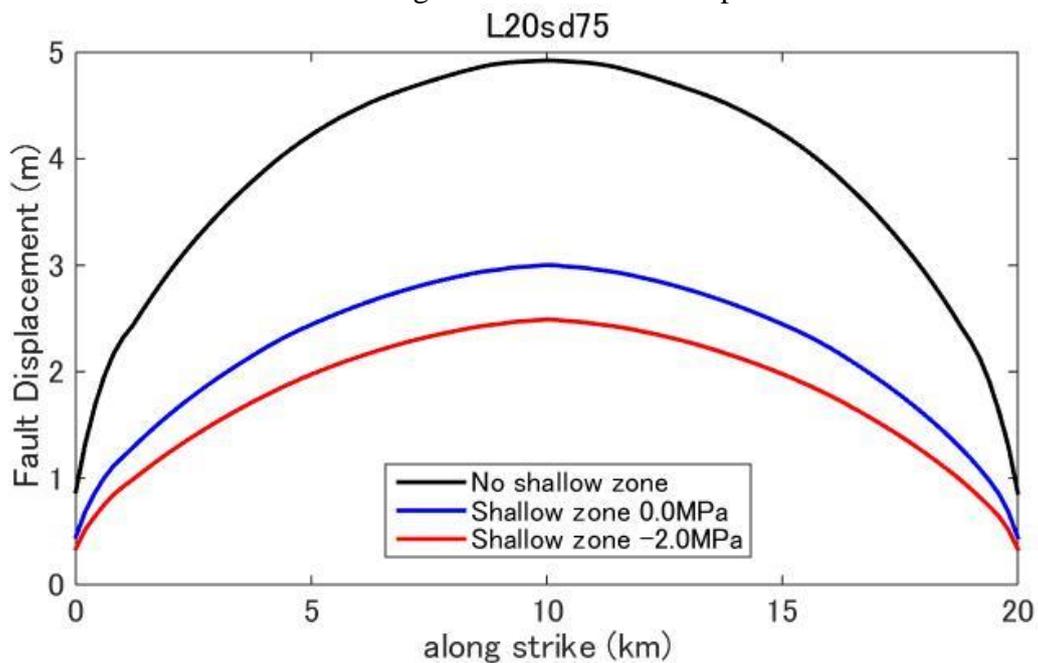
Figure D6. Fault displacement (surface rupture slip) distribution predicted by dynamic rupture model for a fault with fault length 20km and stress drop 7.5MPa.
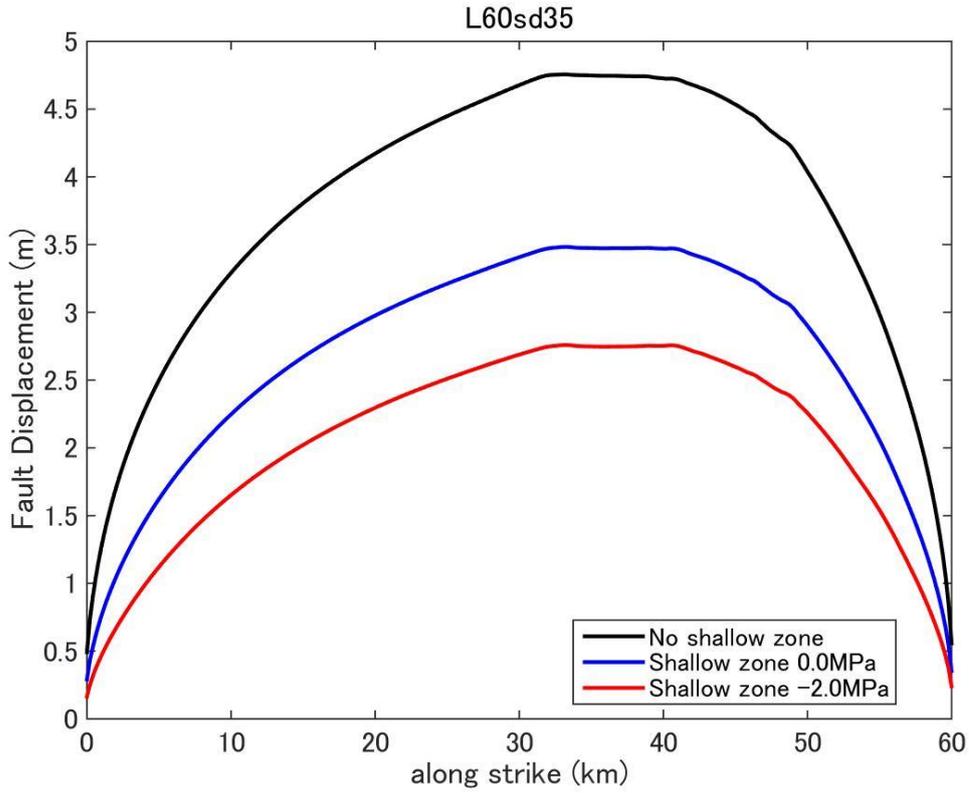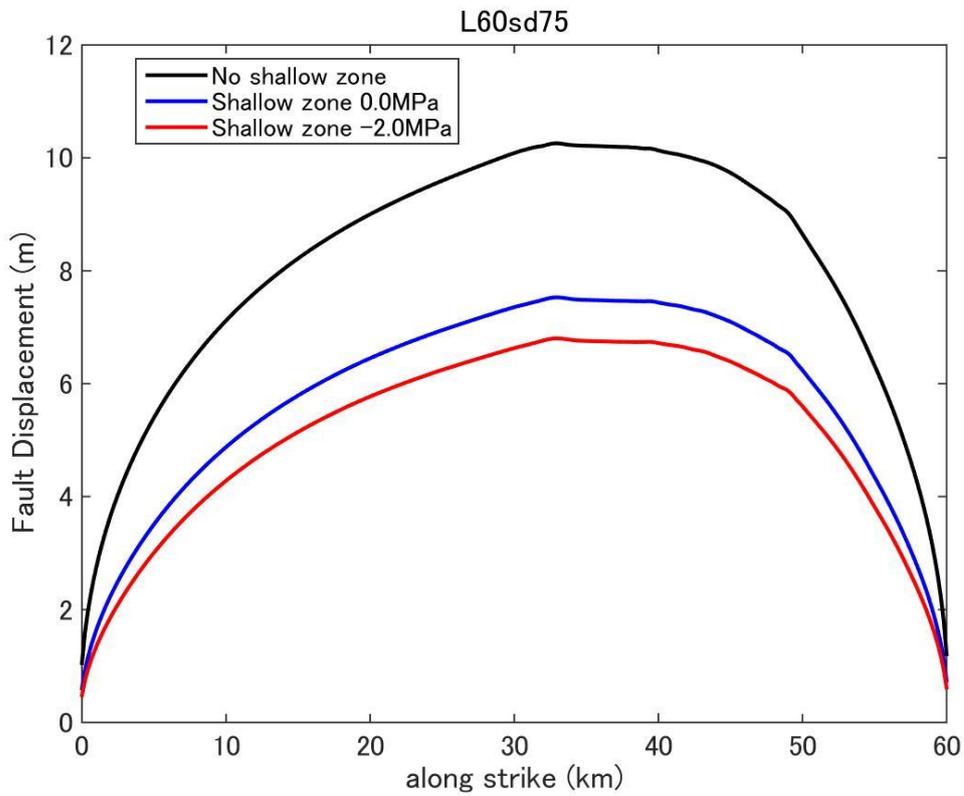
Figure D7. Fault displacement (surface rupture slip) distribution predicted by dynamic rupture model for a fault with fault length 40km and stress drop 2.0MPa.

Figure D8. Fault displacement (surface rupture slip) distribution predicted by dynamic rupture model for a fault with fault length 40km and stress drop 3.0MPa.
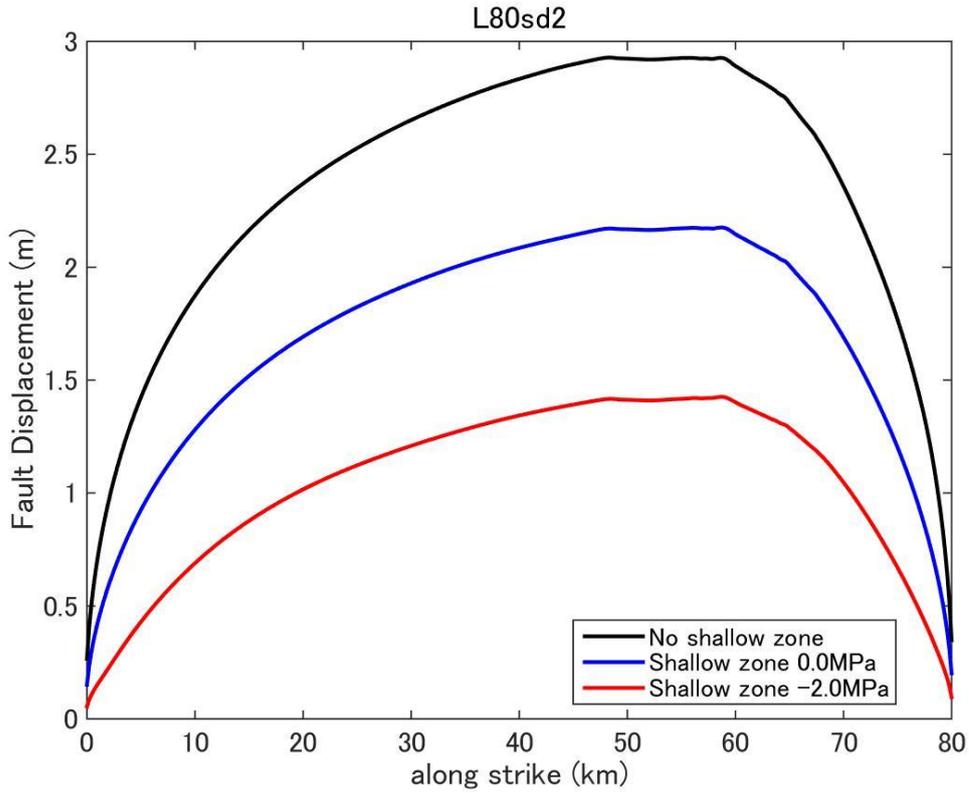
Figure D9. Fault displacement (surface rupture slip) distribution predicted by dynamic rupture model for a fault with fault length 40km and stress drop 5.0MPa.

Figure D10. Fault displacement (surface rupture slip) distribution predicted by dynamic rupture model for a fault with fault length 40km and stress drop 2.5MPa.
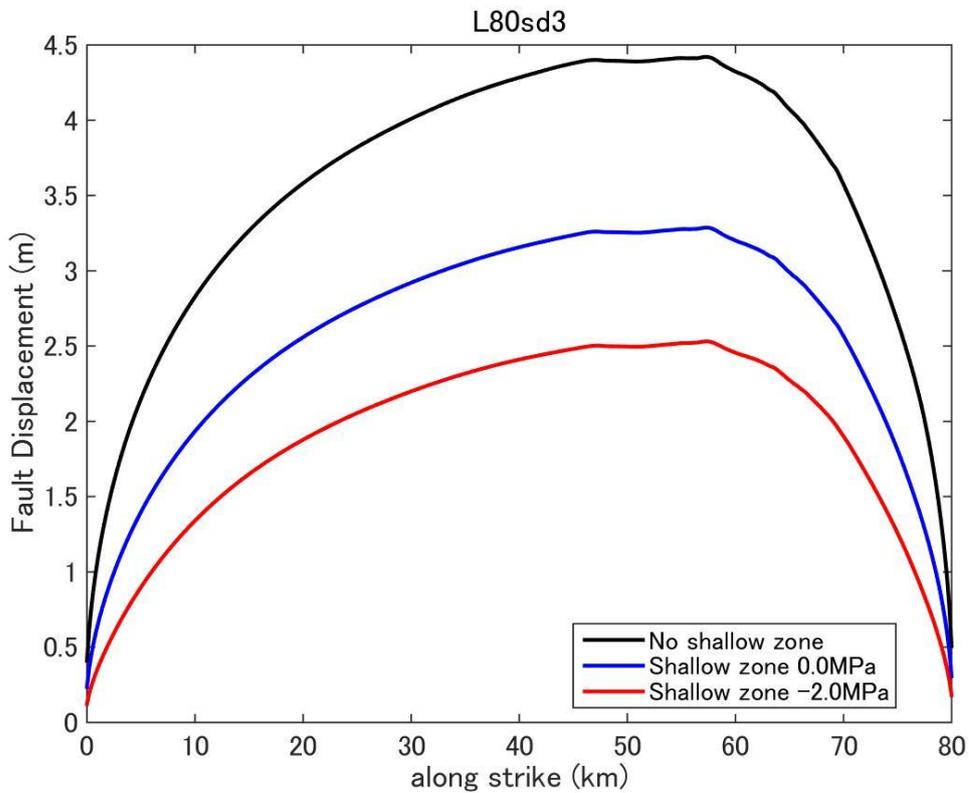
Figure D11. Fault displacement (surface rupture slip) distribution predicted by dynamic rupture model for a fault with fault length 40km and stress drop 3.5MPa.
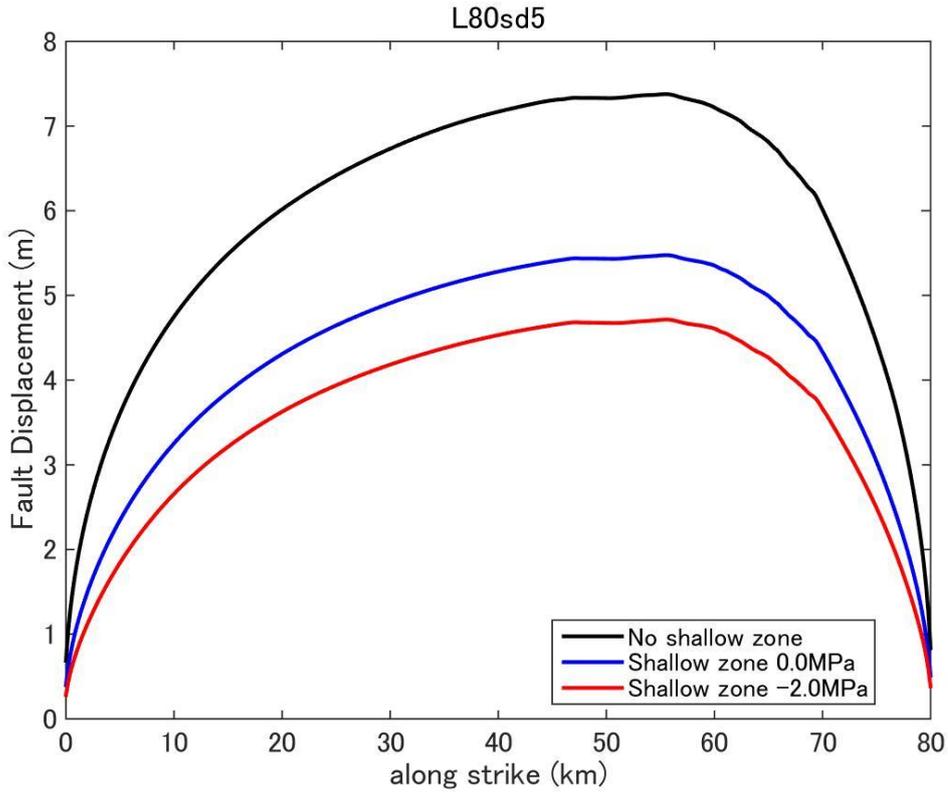

Figure D12. Fault displacement (surface rupture slip) distribution predicted by dynamic rupture model for a fault with fault length 40km and stress drop 7.5MPa.

Figure D13. Fault displacement (surface rupture slip) distribution predicted by dynamic rupture model for a fault with fault length 60km and stress drop 2.0MPa.
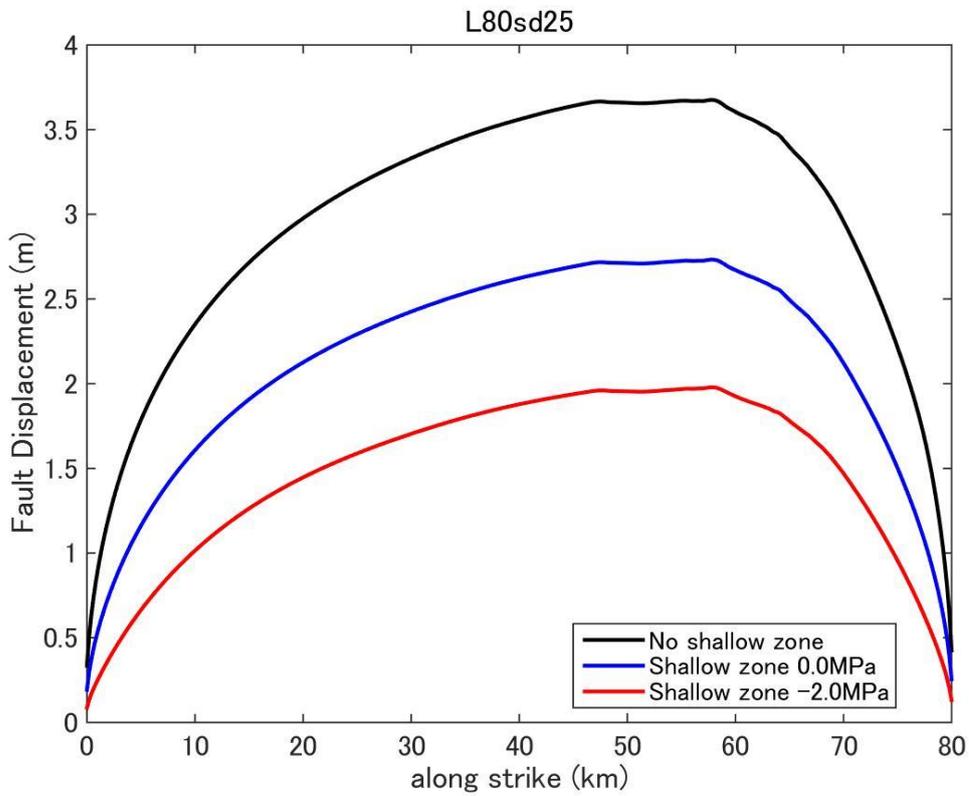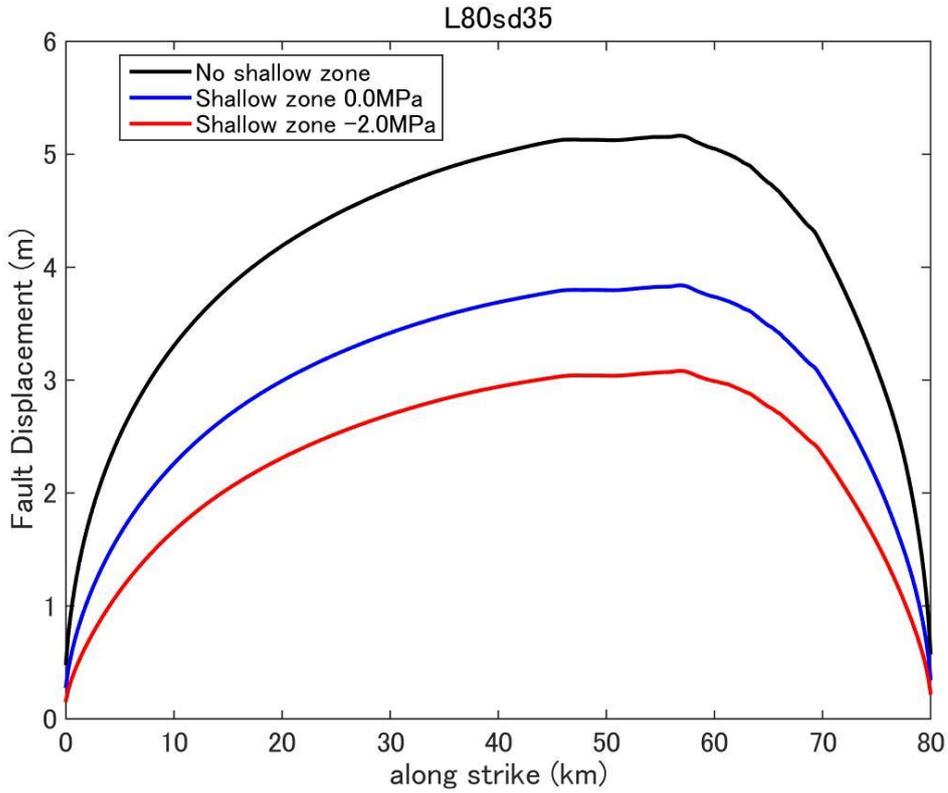

Figure D14. Fault displacement (surface rupture slip) distribution predicted by dynamic rupture model for a fault with fault length 60km and stress drop 3.0MPa.
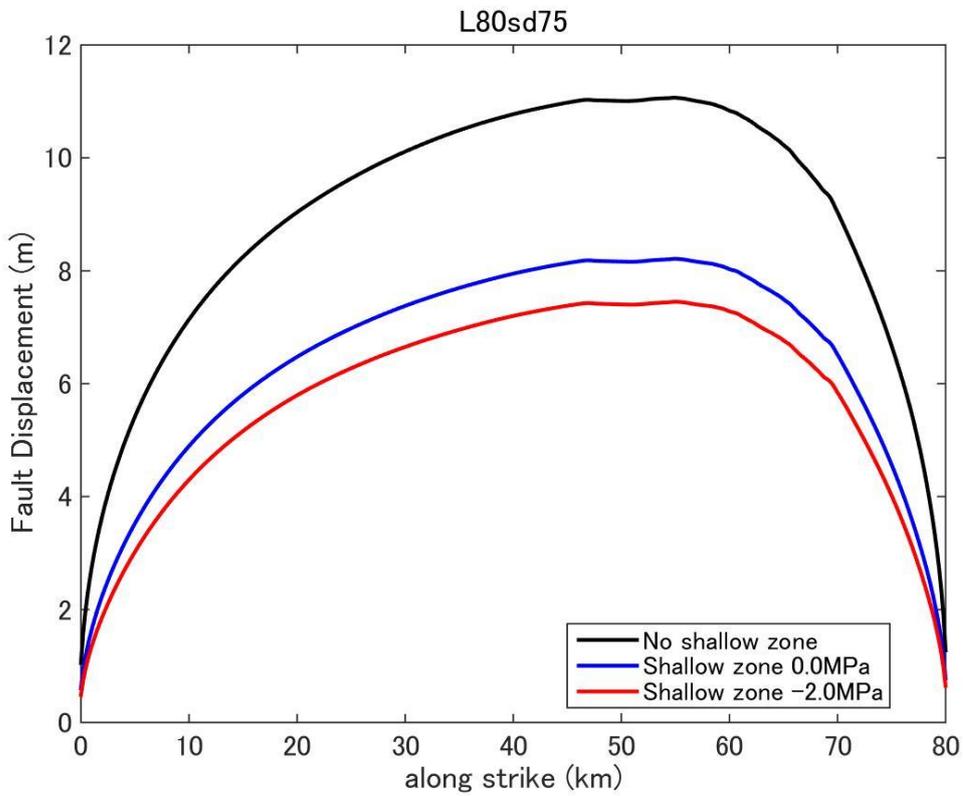
Figure D15. Fault displacement (surface rupture slip) distribution predicted by dynamic rupture model for a fault with fault length 60km and stress drop 5.0MPa.

Figure D16. Fault displacement (surface rupture slip) distribution predicted by dynamic rupture model for a fault with fault length 60km and stress drop 2.5MPa.

Figure D17. Fault displacement (surface rupture slip) distribution predicted by dynamic rupture model for a fault with fault length 60km and stress drop 3.5MPa.

Figure D18. Fault displacement (surface rupture slip) distribution predicted by dynamic rupture model for a fault with fault length 60km and stress drop 7.5MPa.
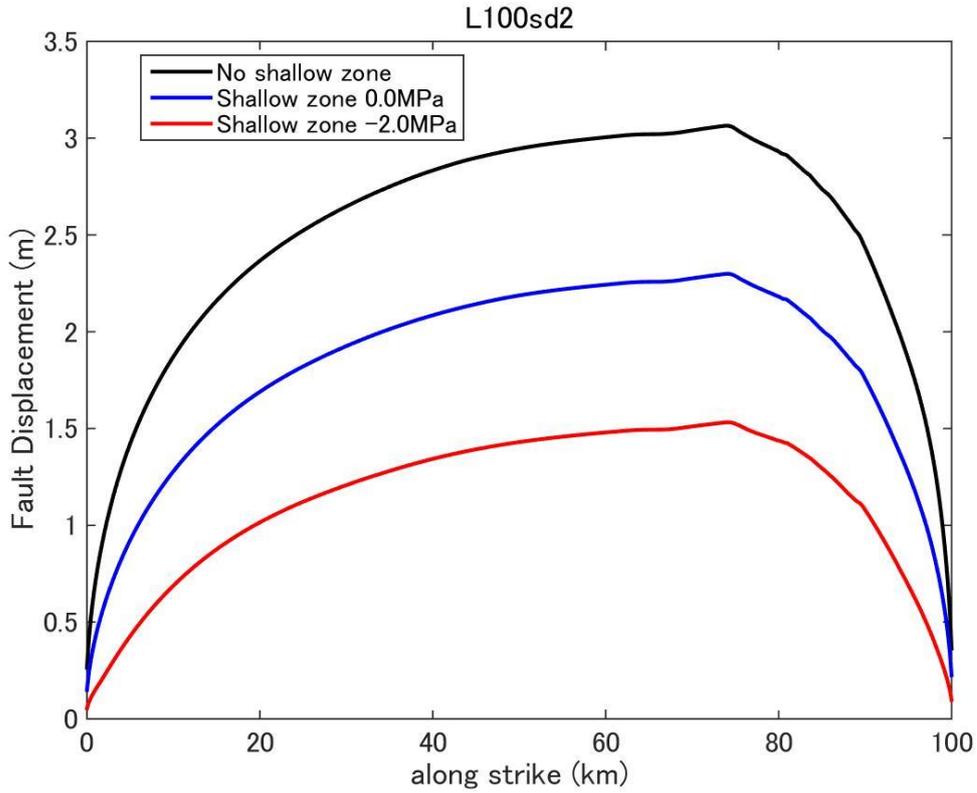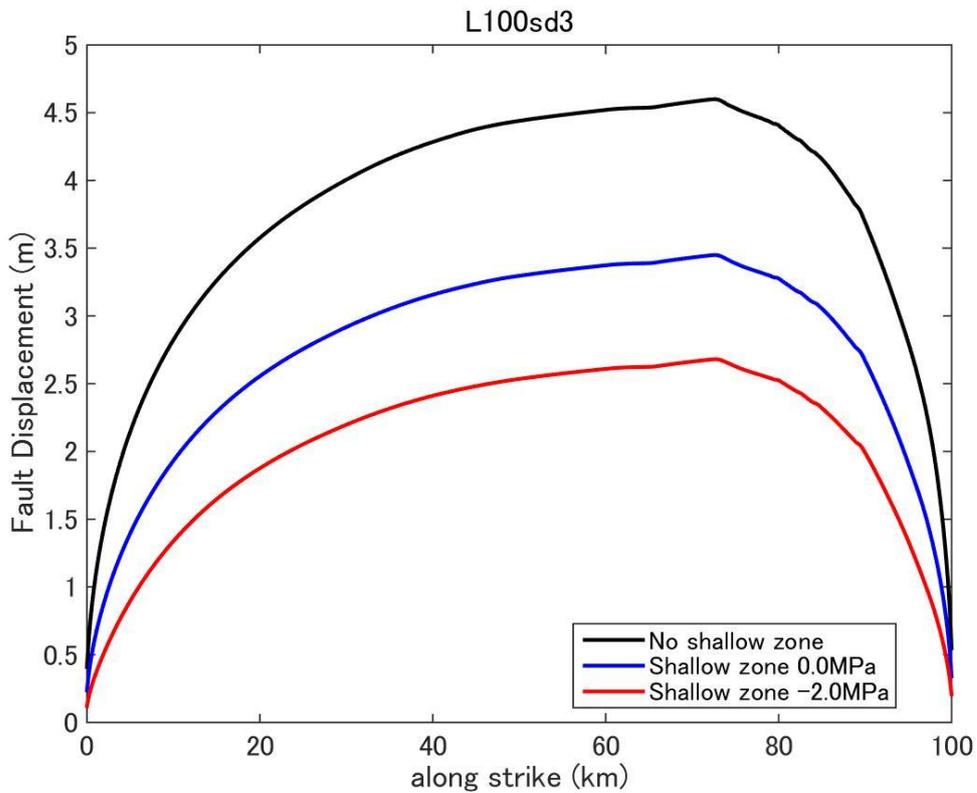
Figure D19. Fault displacement (surface rupture slip) distribution predicted by dynamic rupture model for a fault with fault length 80km and stress drop 2.0MPa.

Figure D20. Fault displacement (surface rupture slip) distribution predicted by dynamic rupture model for a fault with fault length 80km and stress drop 3.0MPa.
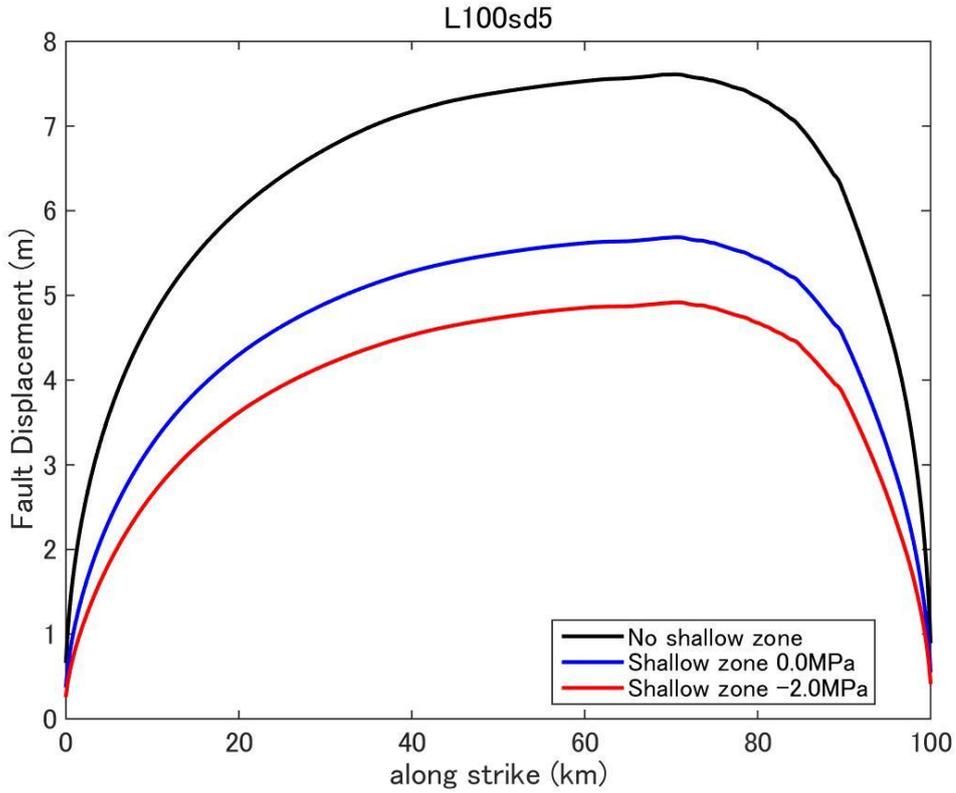
Figure D21. Fault displacement (surface rupture slip) distribution predicted by dynamic rupture model for a fault with fault length 80km and stress drop 5.0MPa.
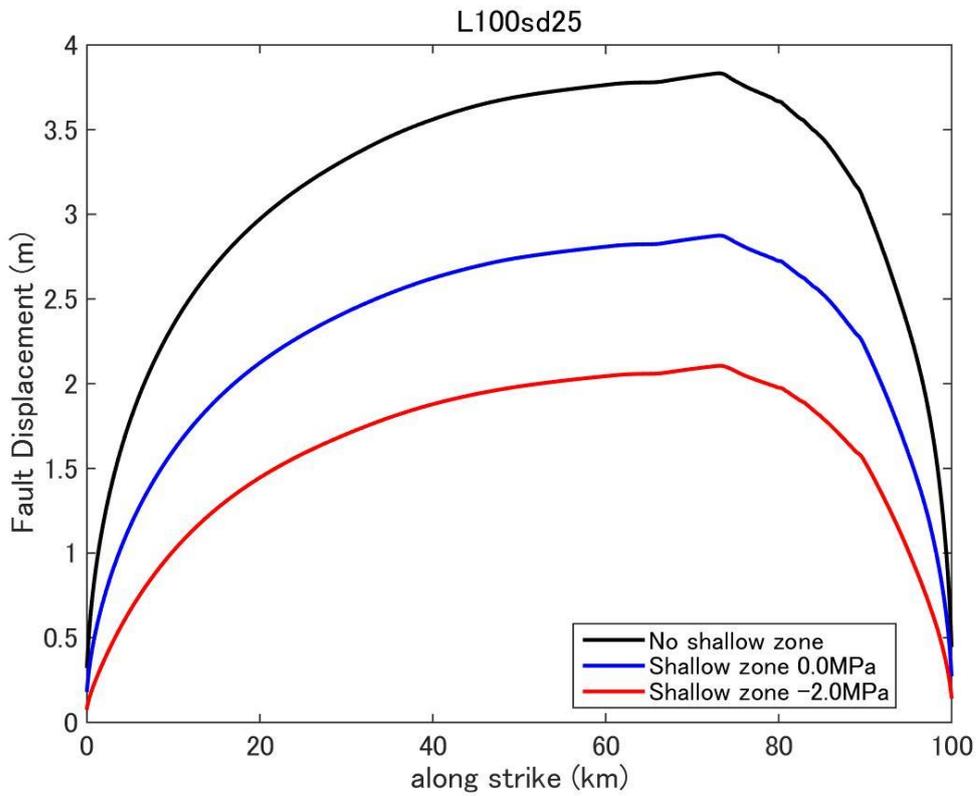

Figure D22. Fault displacement (surface rupture slip) distribution predicted by dynamic rupture model for a fault with fault length 80km and stress drop 2.5MPa.
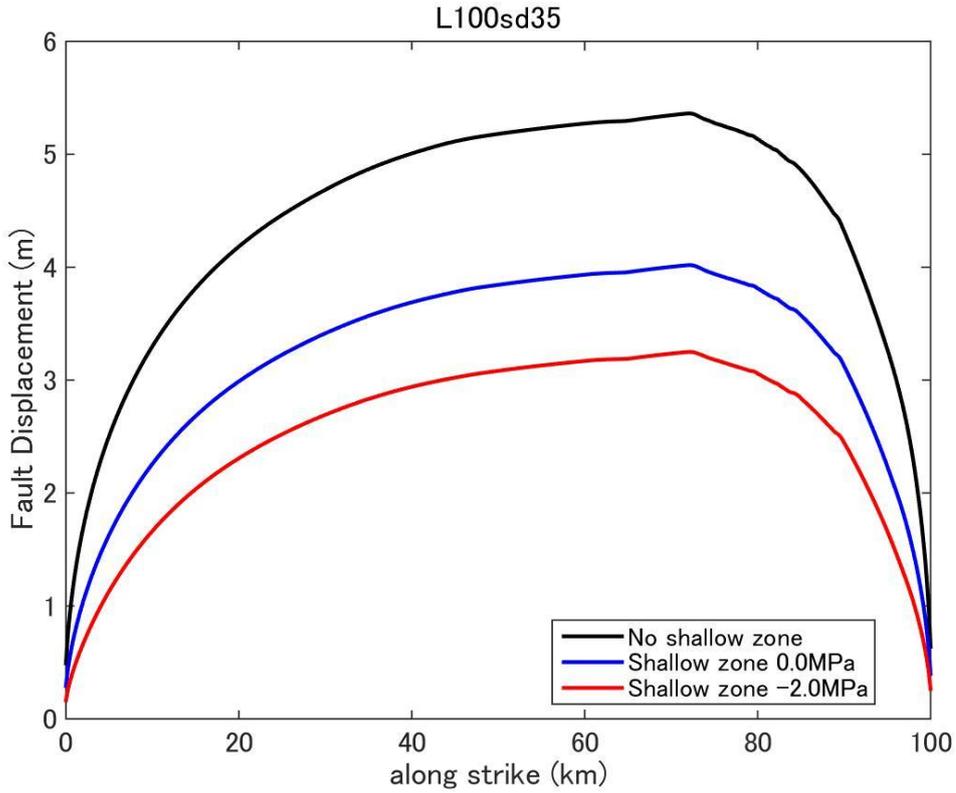
Figure D23. Fault displacement (surface rupture slip) distribution predicted by dynamic rupture model for a fault with fault length 80km and stress drop 3.5MPa.
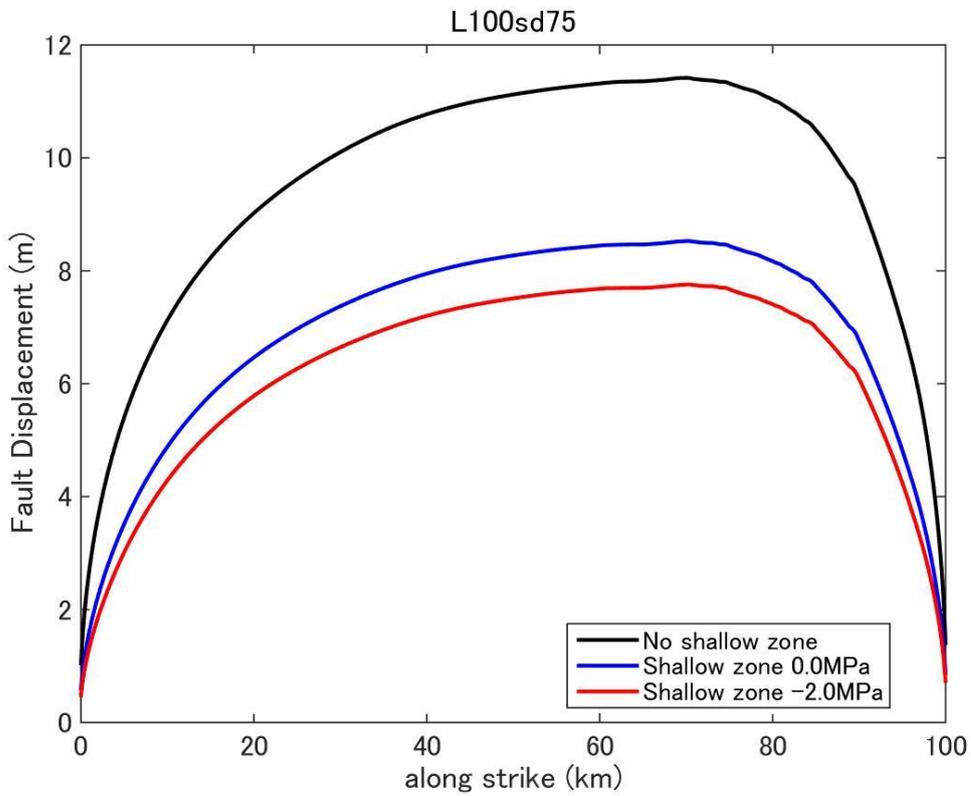

Figure D24. Fault displacement (surface rupture slip) distribution predicted by dynamic rupture model for a fault with fault length 80km and stress drop 7.5MPa.
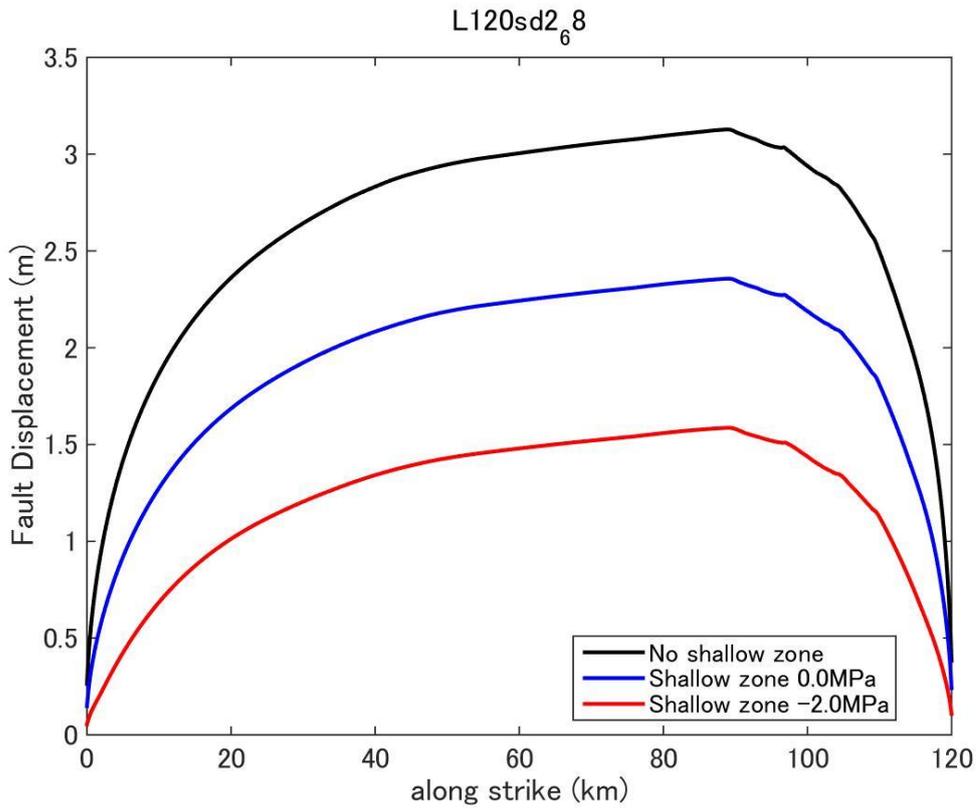
Figure D25. Fault displacement (surface rupture slip) distribution predicted by dynamic rupture model for a fault with fault length 100km and stress drop 2.0MPa.
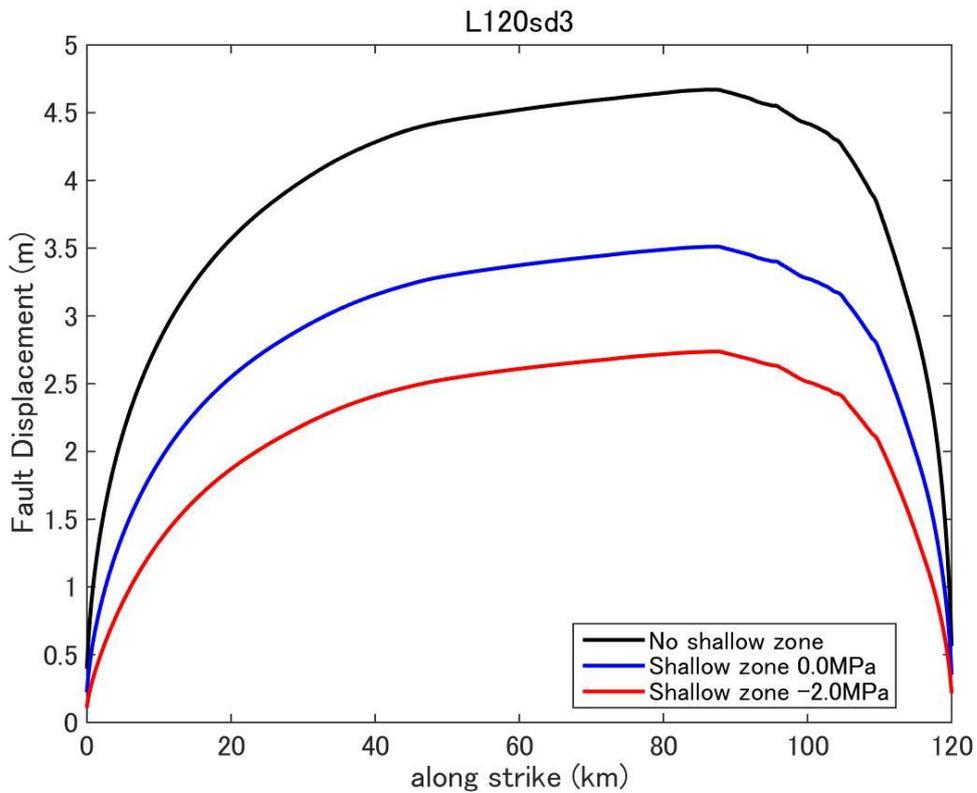

Figure D26. Fault displacement (surface rupture slip) distribution predicted by dynamic rupture model for a fault with fault length 100km and stress drop 3.0MPa.
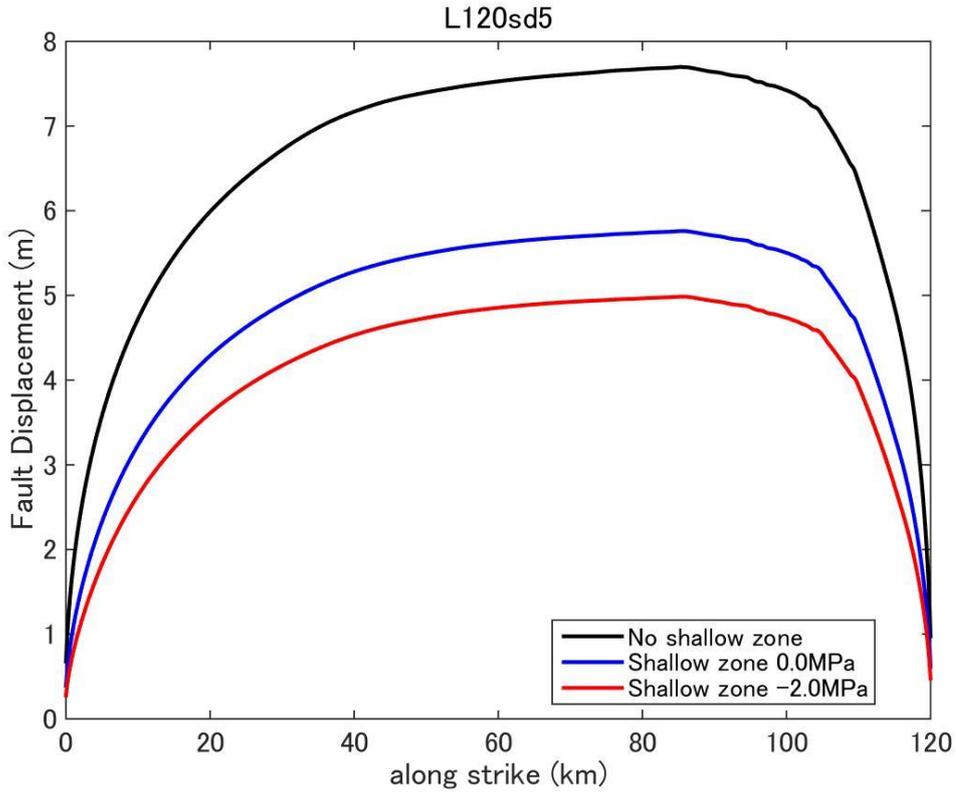
Figure D27. Fault displacement (surface rupture slip) distribution predicted by dynamic rupture model for a fault with fault length 100km and stress drop 5.0MPa.

Figure D28. Fault displacement (surface rupture slip) distribution predicted by dynamic rupture model for a fault with fault length 100km and stress drop 2.5MPa.
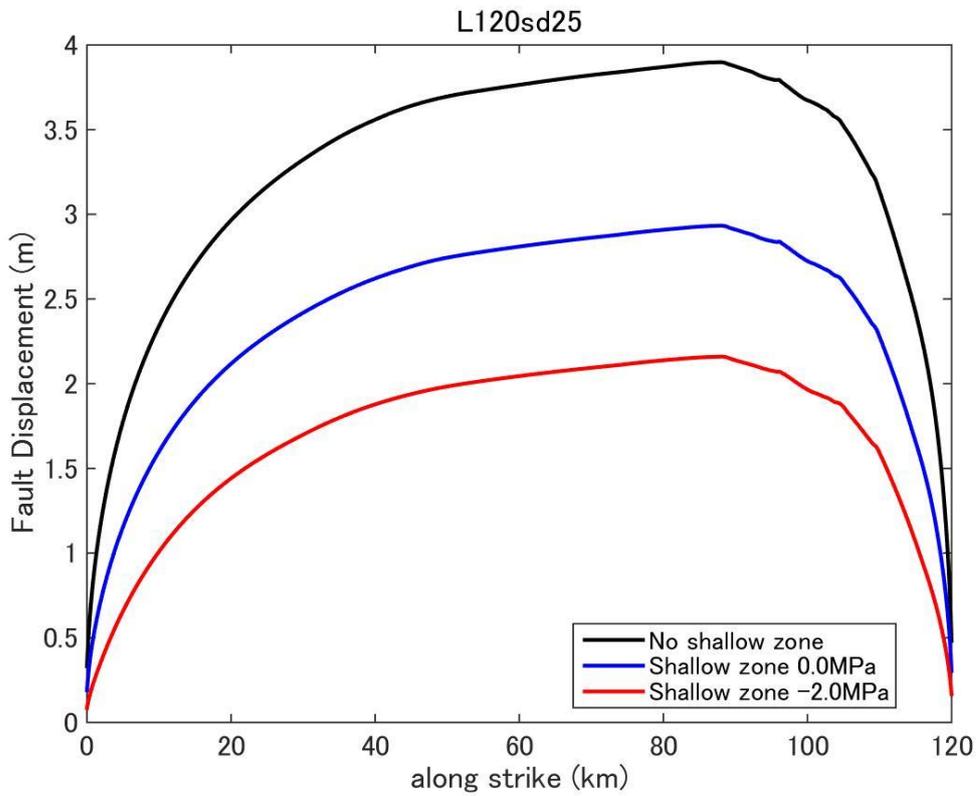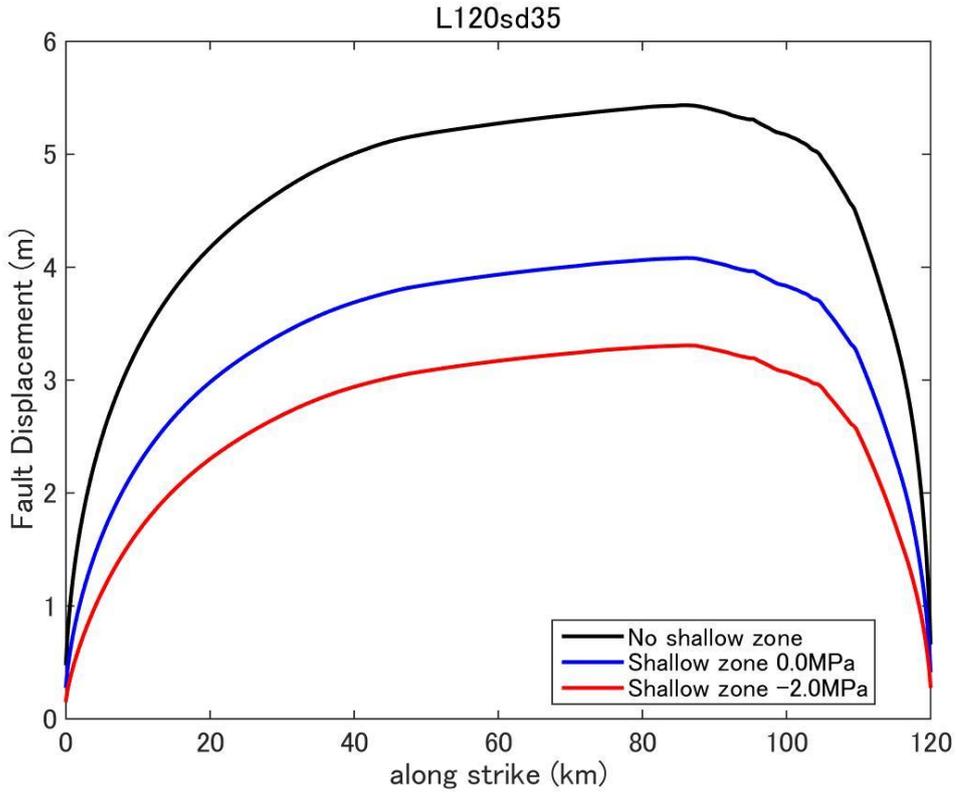
Figure D29. Fault displacement (surface rupture slip) distribution predicted by dynamic rupture model for a fault with fault length 100km and stress drop 3.5MPa.

Figure D30. Fault displacement (surface rupture slip) distribution predicted by dynamic rupture model for a fault with fault length 100km and stress drop 7.5MPa.
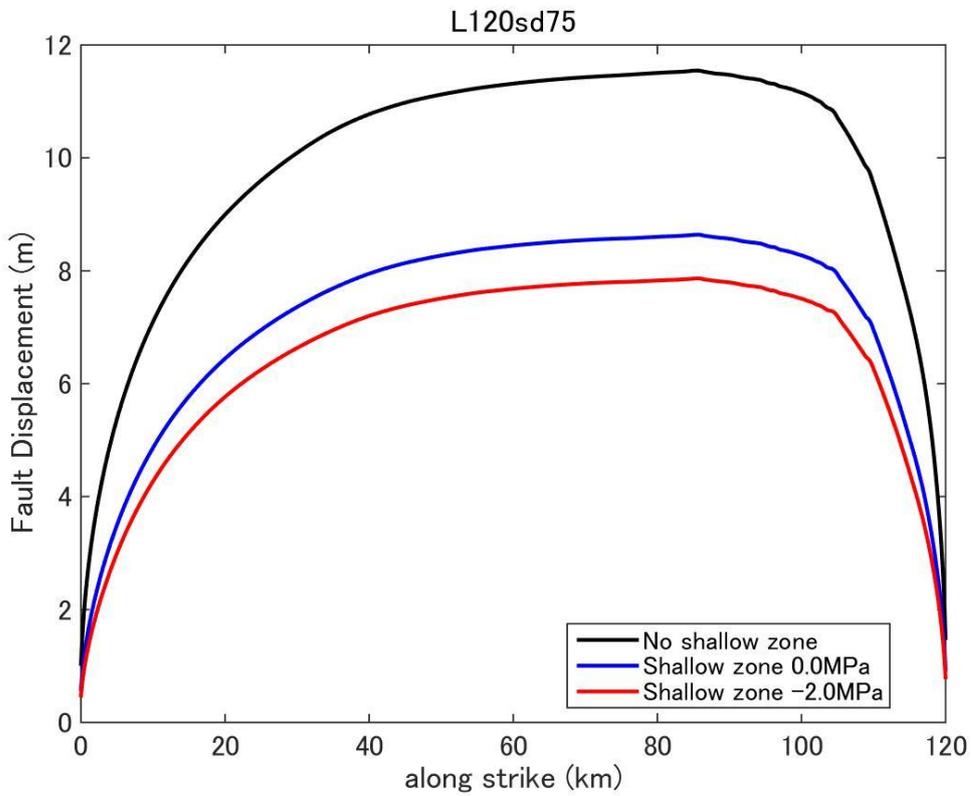
Figure D31. Fault displacement (surface rupture slip) distribution predicted by dynamic rupture model for a fault with fault length 120km and stress drop 2.0MPa.

Figure D32. Fault displacement (surface rupture slip) distribution predicted by dynamic rupture model for a fault with fault length 120km and stress drop 3.0MPa.
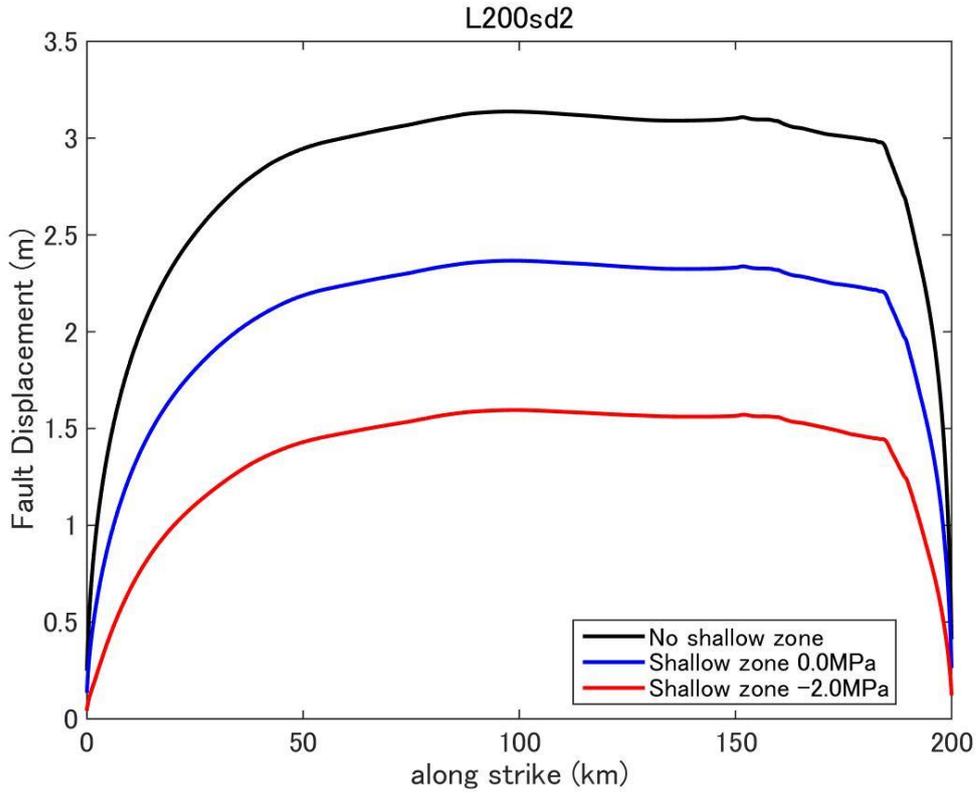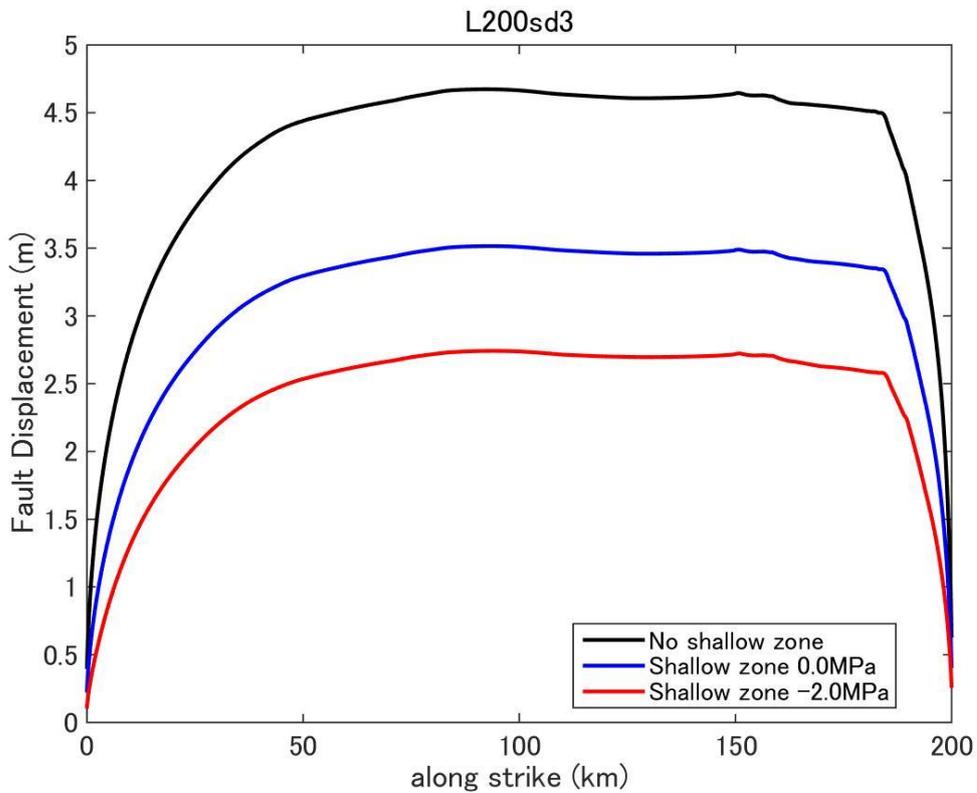
Figure D33. Fault displacement (surface rupture slip) distribution predicted by dynamic rupture model for a fault with fault length 120km and stress drop 5.0MPa.

Figure D34. Fault displacement (surface rupture slip) distribution predicted by dynamic rupture model for a fault with fault length 120km and stress drop 2.5MPa.

Figure D35. Fault displacement (surface rupture slip) distribution predicted by dynamic rupture model for a fault with fault length 120km and stress drop 3.5MPa.
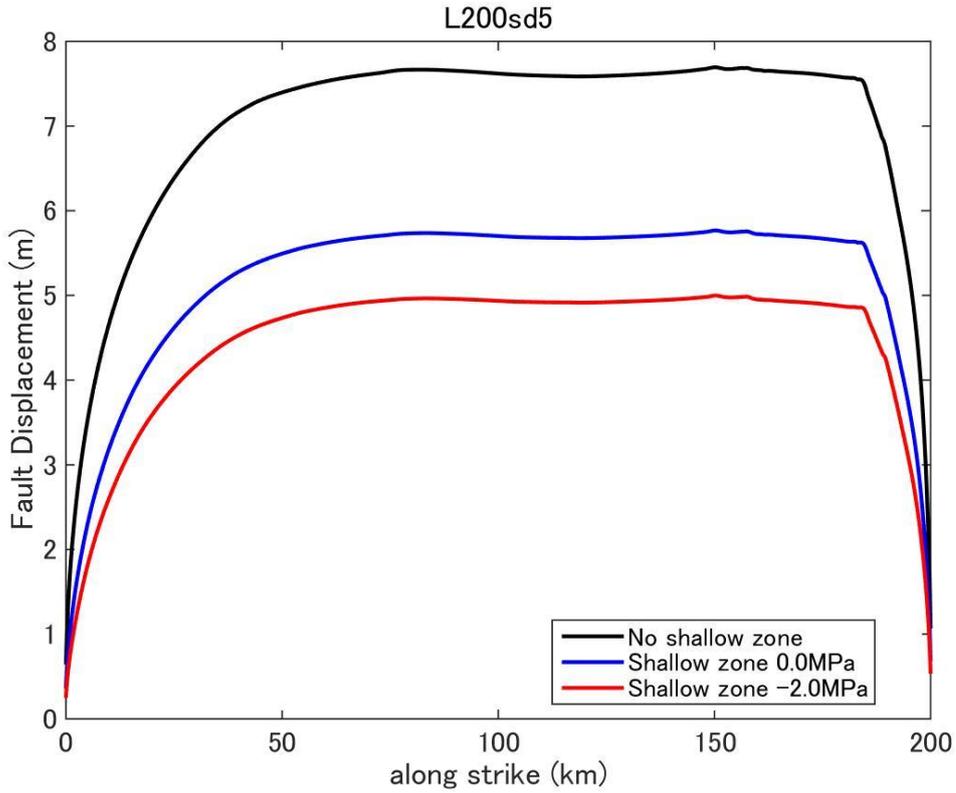

Figure D36. Fault displacement (surface rupture slip) distribution predicted by dynamic rupture model for a fault with fault length 120km and stress drop 7.5MPa.

Figure D37. Fault displacement (surface rupture slip) distribution predicted by dynamic rupture model for a fault with fault length 200km and stress drop 2.0MPa.
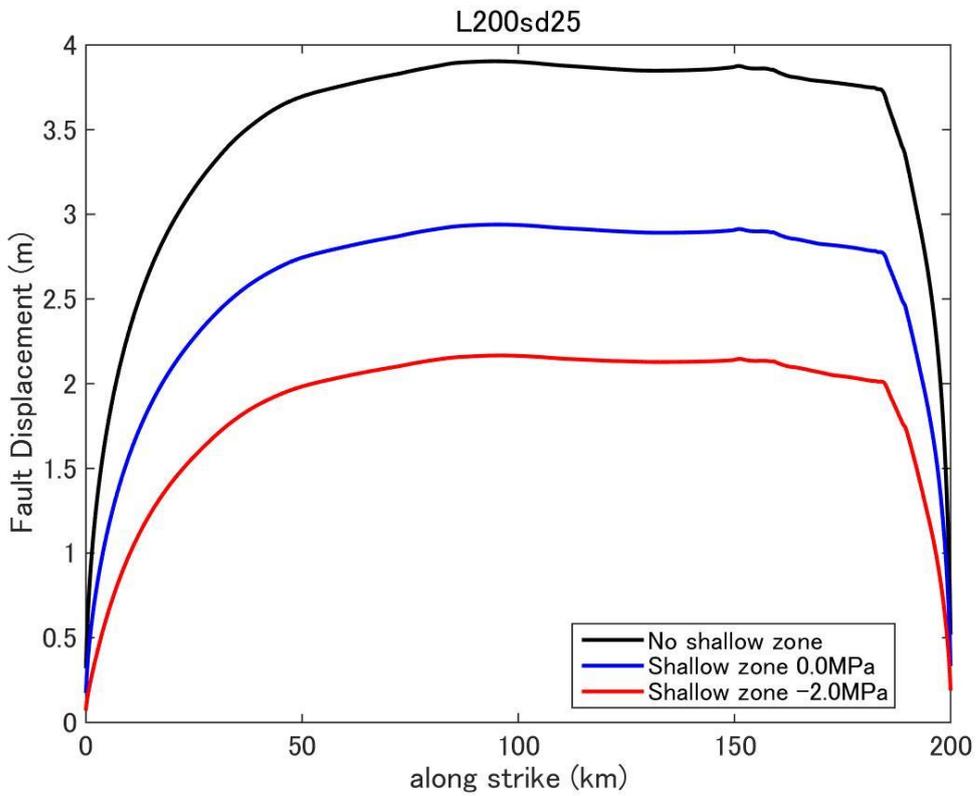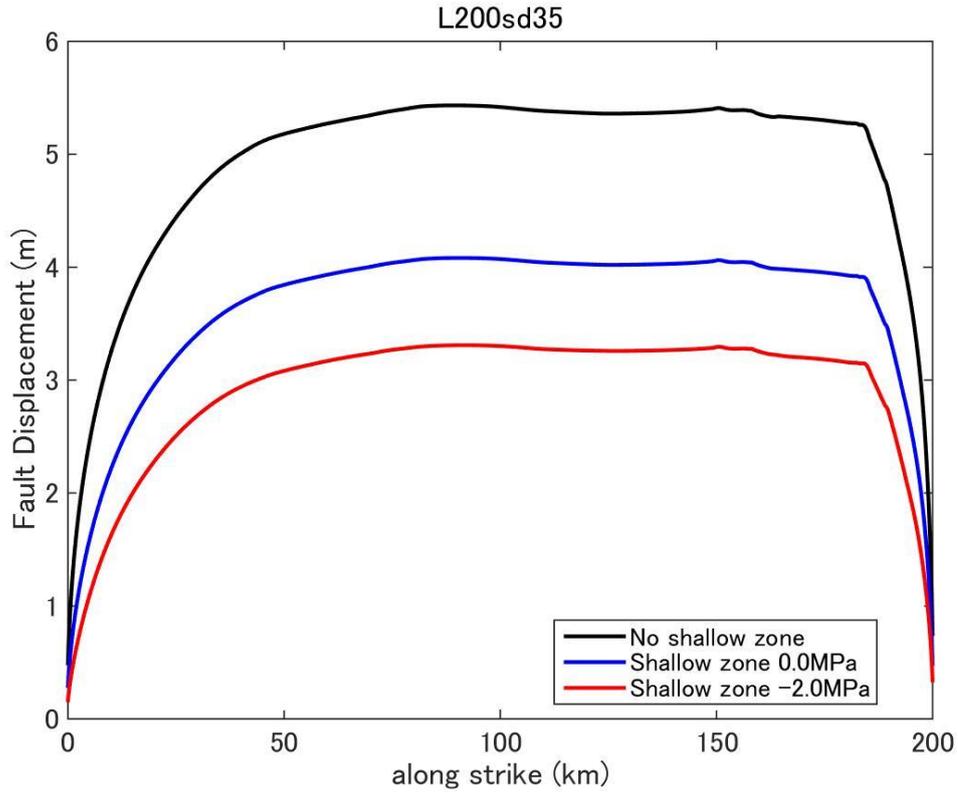

Figure D38. Fault displacement (surface rupture slip) distribution predicted by dynamic rupture model for a fault with fault length 200km and stress drop 3.0MPa.
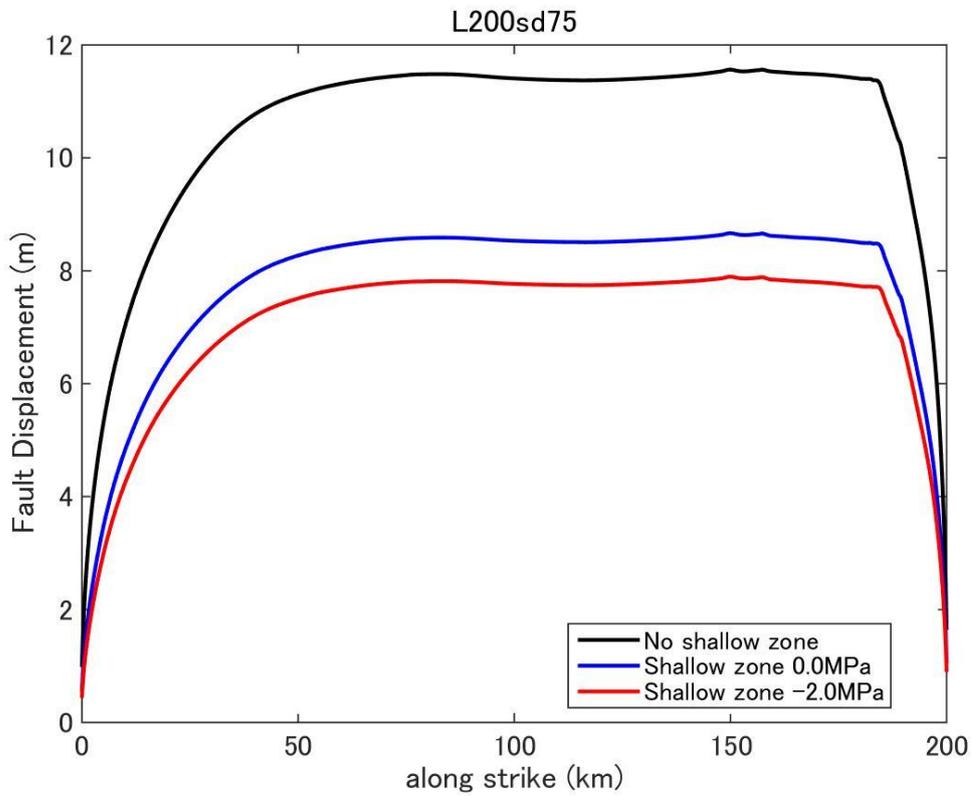
Figure D39. Fault displacement (surface rupture slip) distribution predicted by dynamic rupture model for a fault with fault length 200km and stress drop 5.0MPa.

Figure D40. Fault displacement (surface rupture slip) distribution predicted by dynamic rupture model for a fault with fault length 200km and stress drop 2.5MPa.
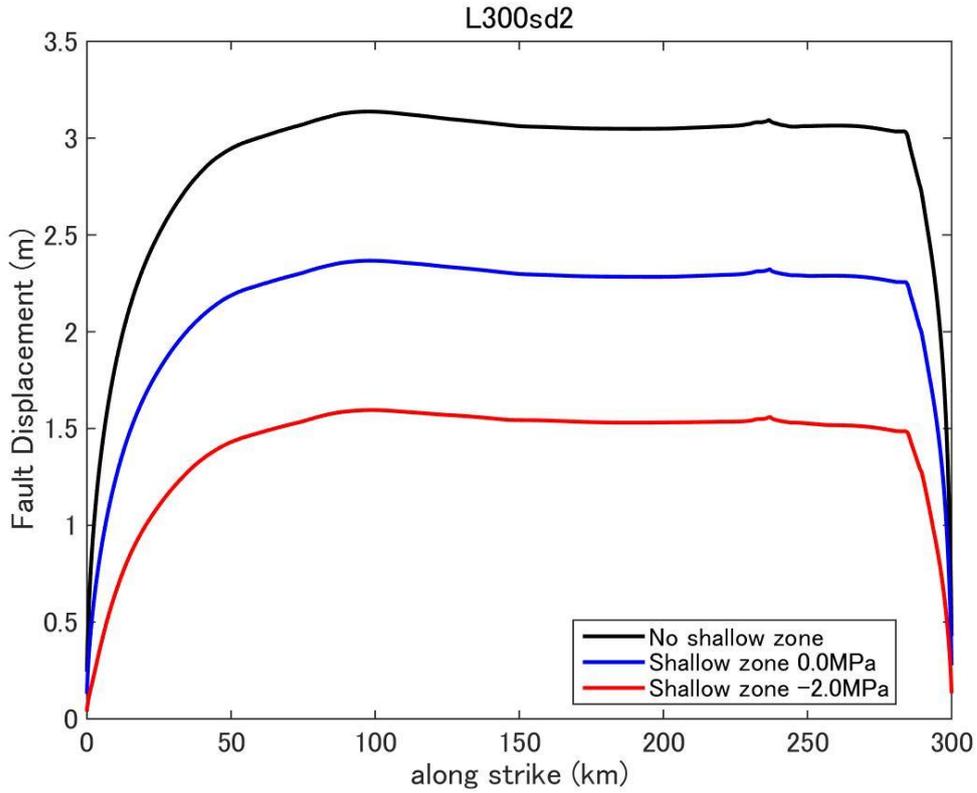
Figure D41. Fault displacement (surface rupture slip) distribution predicted by dynamic rupture model for a fault with fault length 200km and stress drop 3.5MPa.
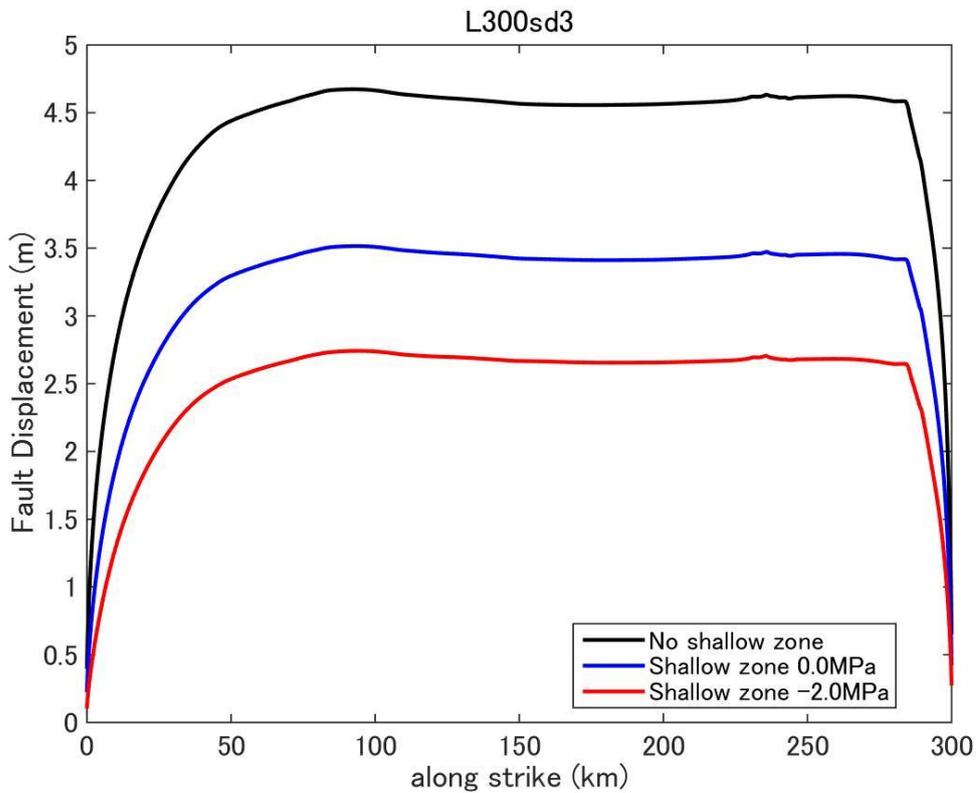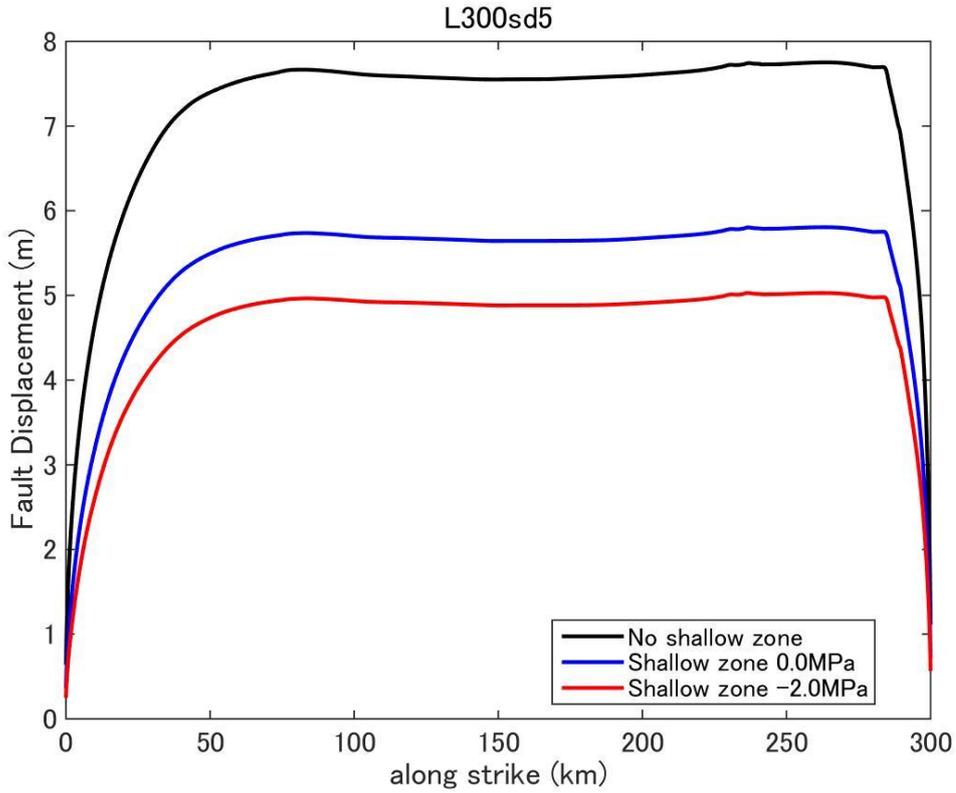

Figure D42. Fault displacement (surface rupture slip) distribution predicted by dynamic rupture model for a fault with fault length 200km and stress drop 7.5MPa.

Figure D43. Fault displacement (surface rupture slip) distribution predicted by dynamic rupture model for a fault with fault length 300km and stress drop 2.0MPa.
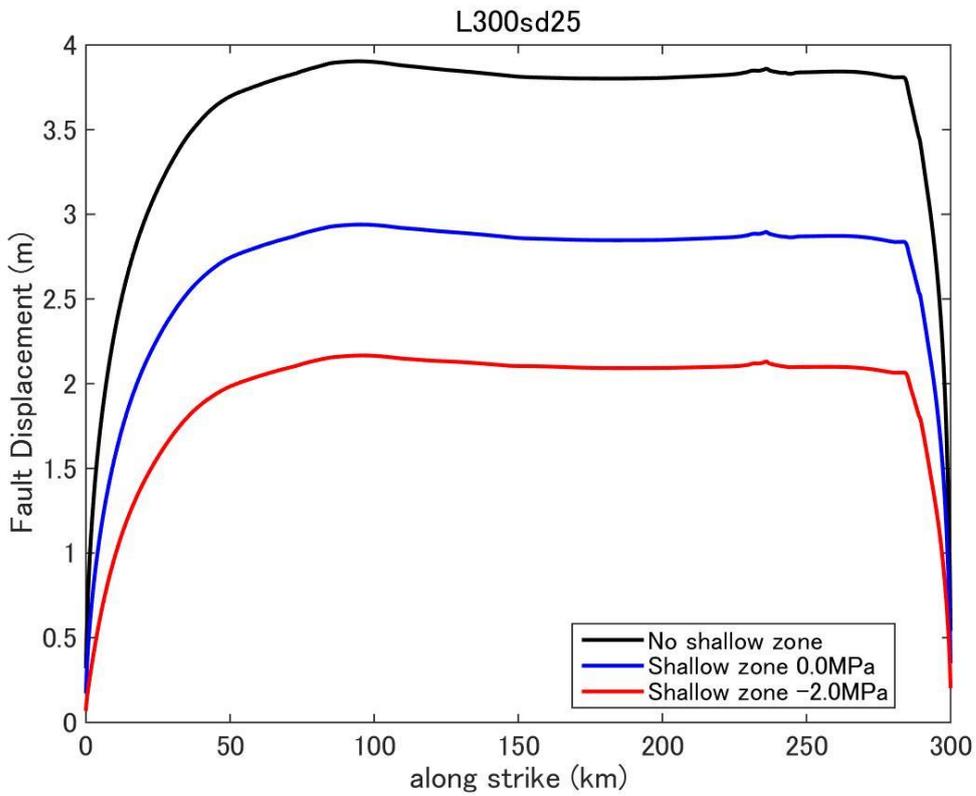

Figure D44. Fault displacement (surface rupture slip) distribution predicted by dynamic rupture model for a fault with fault length 300km and stress drop 3.0MPa.
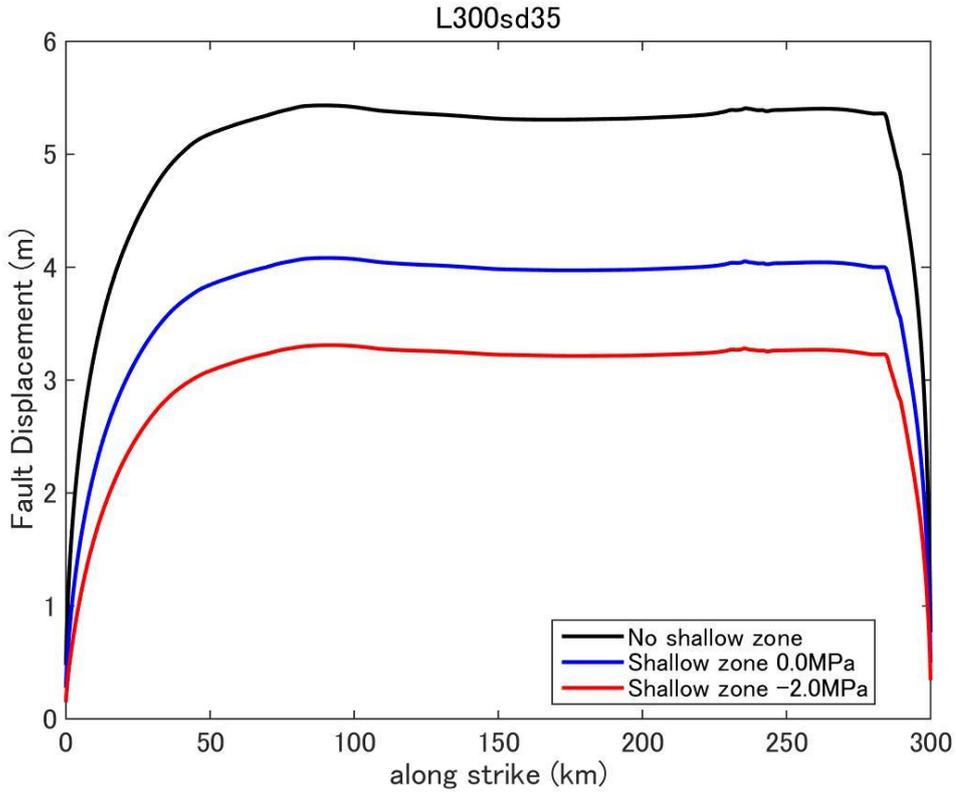
Figure D45. Fault displacement (surface rupture slip) distribution predicted by dynamic rupture model for a fault with fault length 300km and stress drop 5.0MPa.

Figure D46. Fault displacement (surface rupture slip) distribution predicted by dynamic rupture model for a fault with fault length 300km and stress drop 2.5MPa.

Figure D47. Fault displacement (surface rupture slip) distribution predicted by dynamic rupture model for a fault with fault length 300km and stress drop 3.5MPa.
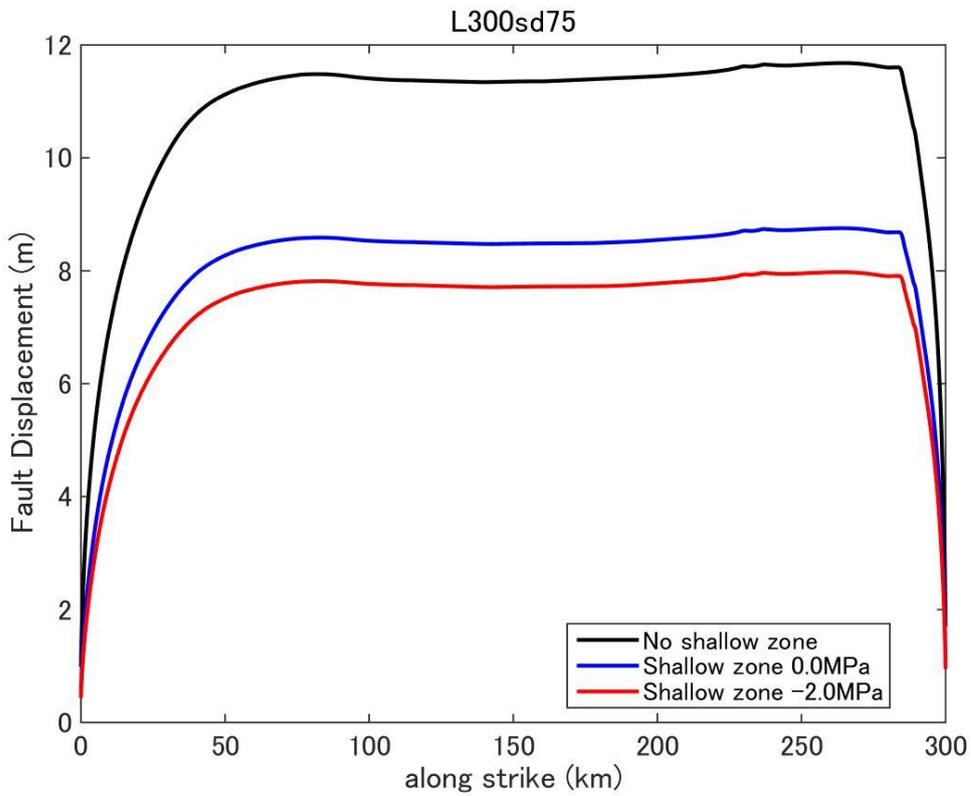

Figure D48. Fault displacement (surface rupture slip) distribution predicted by dynamic rupture model for a fault with fault length 300km and stress drop 7.5MPa.
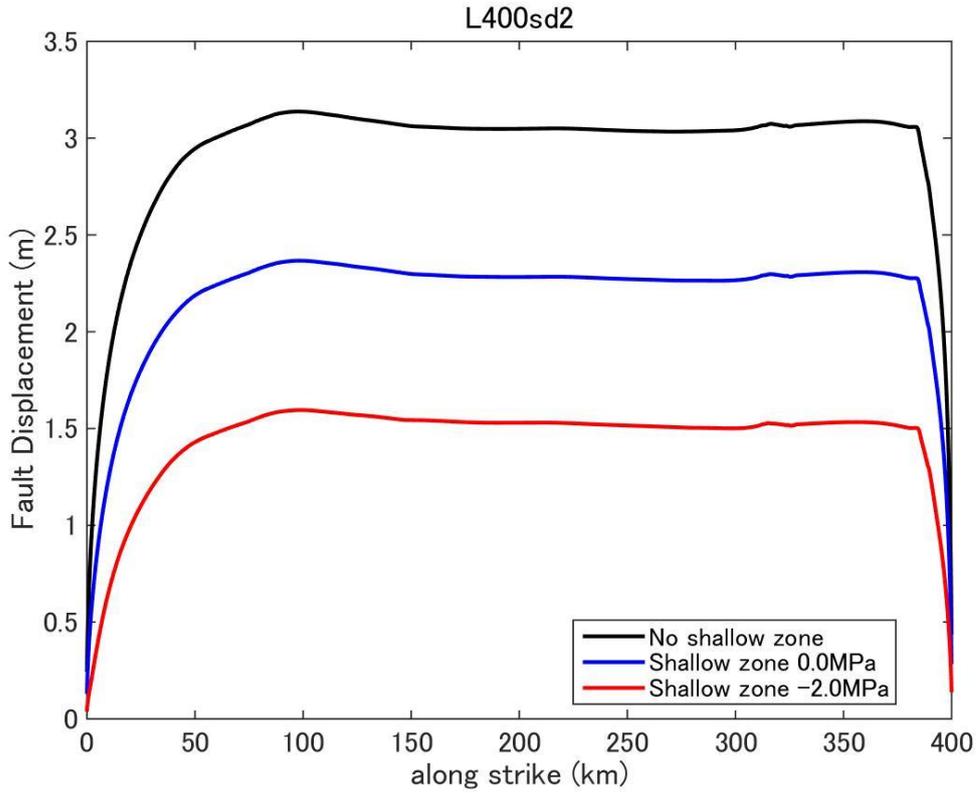
Figure D49. Fault displacement (surface rupture slip) distribution predicted by dynamic rupture model for a fault with fault length 400km and stress drop 2.0MPa.
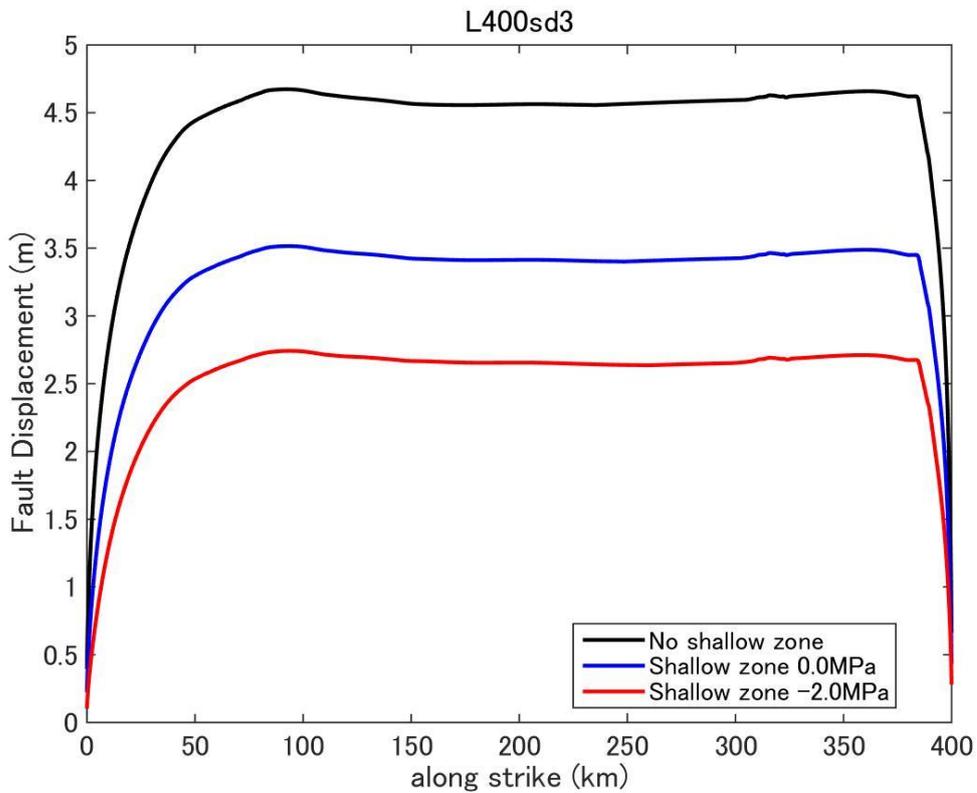

Figure D50. Fault displacement (surface rupture slip) distribution predicted by dynamic rupture model for a fault with fault length 400km and stress drop 3.0MPa.
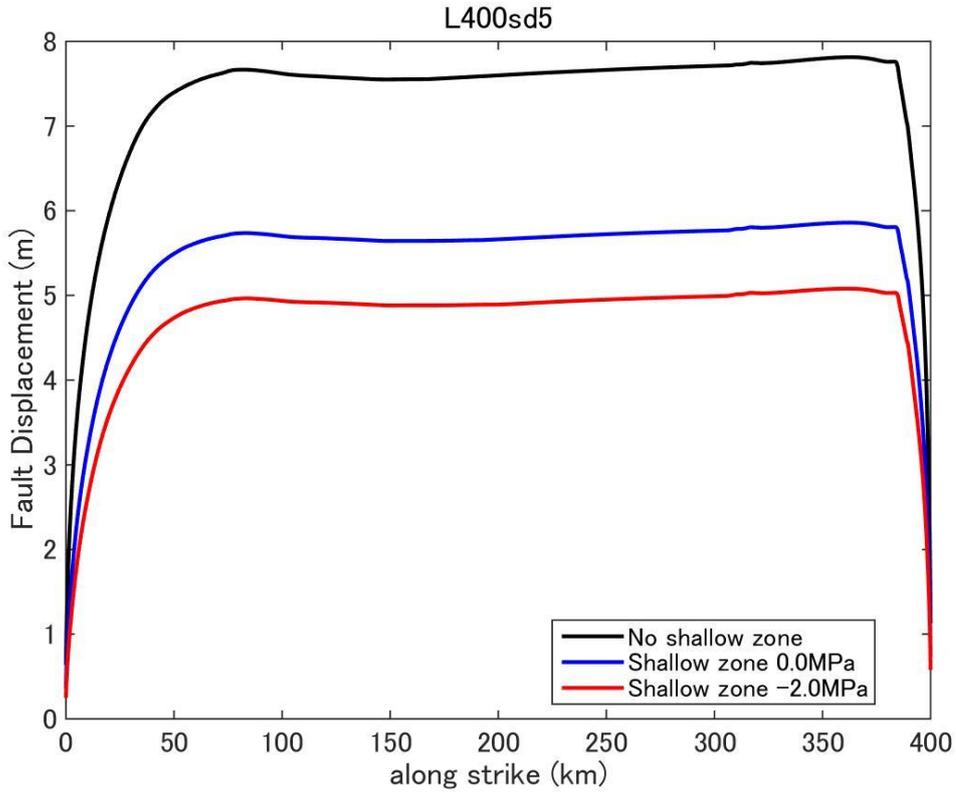
Figure D51. Fault displacement (surface rupture slip) distribution predicted by dynamic rupture model for a fault with fault length 400km and stress drop 5.0MPa.
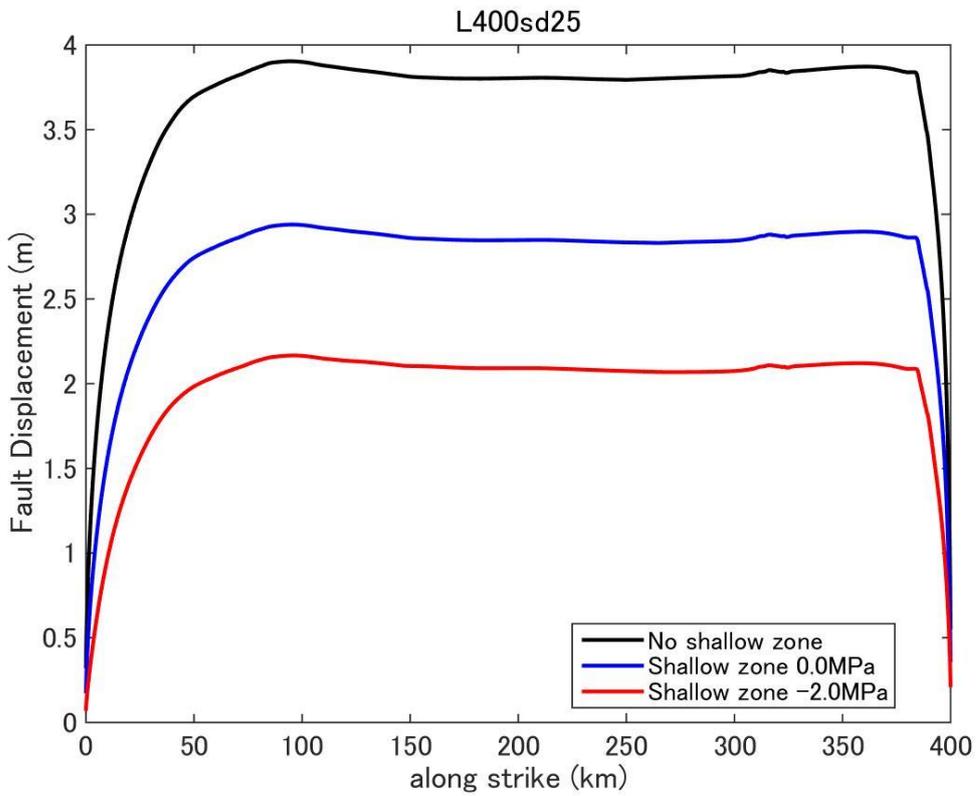

Figure D52. Fault displacement (surface rupture slip) distribution predicted by dynamic rupture model for a fault with fault length 400km and stress drop 2.5MPa.
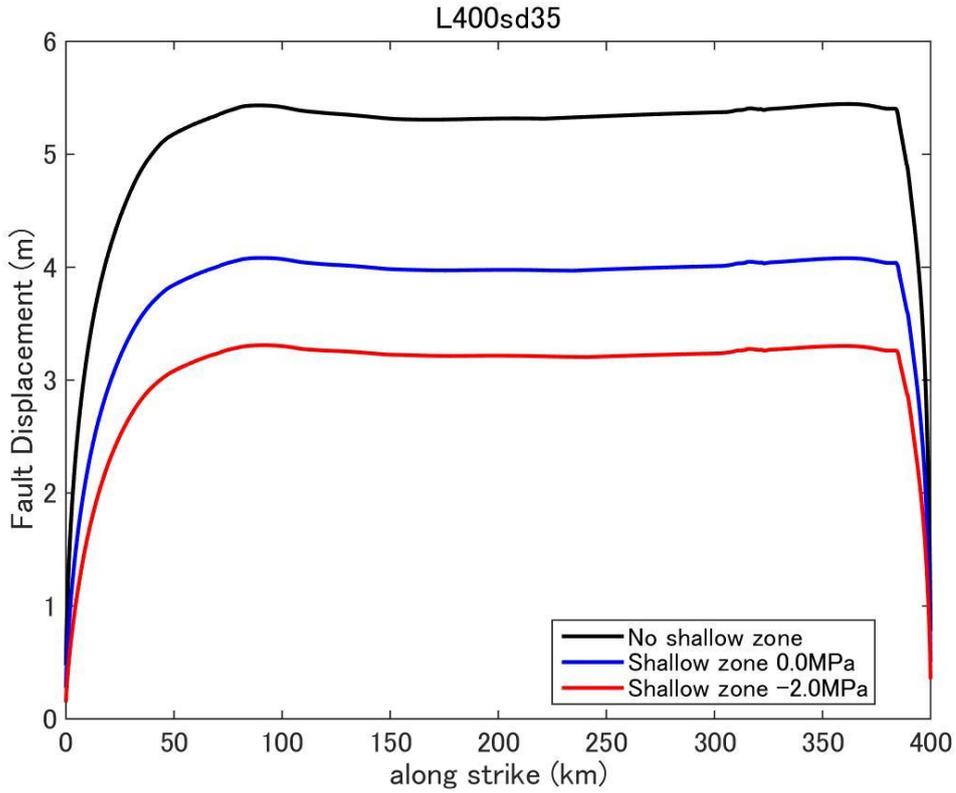
Figure D53. Fault displacement (surface rupture slip) distribution predicted by dynamic rupture model for a fault with fault length 400km and stress drop 3.5MPa.

Figure D54. Fault displacement (surface rupture slip) distribution predicted by dynamic rupture model for a fault with fault length 400km and stres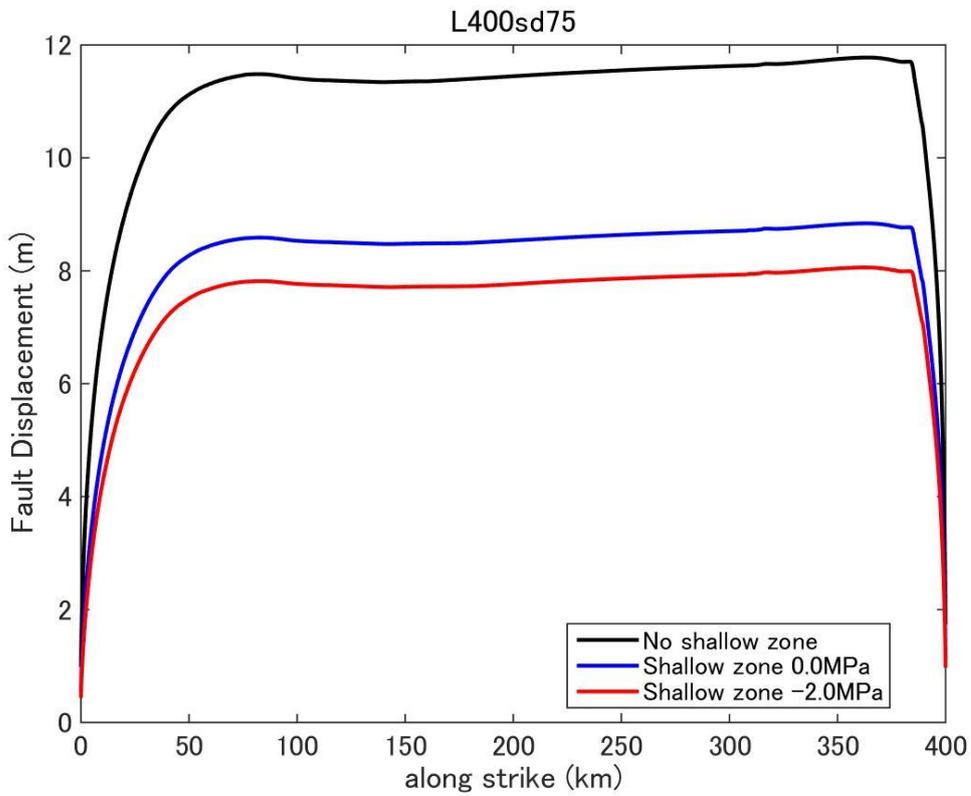s drop 7.5MPa.